RECENT VELOCITY FIELD IN WESTERN ANATOLIA FROM CONTINUOUS GPS DATA

by

Tayfun Kaynarca

B.S., Geodesy and Photogrammetry, Yıldız Technical University, 2008

Submitted to Kandilli Observatory and Earthquake
Research Institute in partial fulfilment of
the requirements for the degree of
Master of Science

Graduate Program in Geodesy

Boğaziçi University

2019

RECENT VELOCITY FIELD IN WESTERN ANATOLIA FROM CONTINUOUS GPS DATA

APPROVED BY:

Prof. Dr. Haluk Özener .....
(Thesis Supervisor)

Assoc. Prof. Dr. Aslı Doğru .....

Prof. Dr. Bahadır Aktuğ .....

DATE OF APPROVAL: 17.09.2019

ACKNOWLEDGEMENTS

Foremost, I would like to express my sincere gratitude to my advisor Prof. Dr. Haluk Özener for his continuous support of my graduation thesis and research for his motivation, enthusiasm, and immense knowledge. His guidance helped me in all time of research and writing of this thesis.

Besides my advisor, I would like to thank the rest of my thesis committee for their support, interest, encouragement and insightful comments.

My sincere thanks also goes to Prof. Dr. Uğur Şanlı, Prof. Dr. Semih Ergintav, Prof. Dr. Bahadır Aktuğ, Assoc. Prof. Dr. Aslı Doğru, Assoc. Prof. Dr. Fatih Bulut, Assoc. Prof. Dr. H. Hakan Yavaşoğlu, Dr. Soner Özdemir, and Res. Assist. Bengisu Gelin.

I send my special thanks to Ahmet Karakoç, İsmail Gümüşlü, Aytekin Dülger, Faruk Bayır, Orhan Küçük, Mehmet Kanpalta, Sinem Ceylan and Merve Aktaş for their continuous motivating support.

Last but not the least, I would like to send my special thanks to my parents who have supported me throughout entire process.

ABSTRACT

RECENT VELOCITY FIELD IN WESTERN ANATOLIA FROM CONTINUOUS GPS DATA

Aegean Region is one of the most deforming parts of Alpine-Himalayan orogenic belt. The region is intensely under pure shear stress which is caused by an internally deforming counter-clock rotation of the Anatolian plate relative to Eurasian plate. The counter-clockwise motion caused by the compression of the Arabian plate through Anatolian plate eventuate in north-south extension and formation of east-west trending active grabens.

Many seismological studies were carried out in Western Anatolia and its surroundings due to remarkable seismic activity in the area. In this study, GPS data from 16 of CORS-TR stations which measured in 2015, 2016, 2017 and 2018 were used by considering the seasonal effects.

The obtained velocities of selected CORS-TR stations were combined with the velocity fields of Reilinger et al., (2006) and Aktuğ et al., (2009) for better understanding of the dynamic mechanism of the region. 14 mutual IGS stations in the studies were utilized for the transformation process. Combined velocity values vary between 10.66 ± 1.22 mm/yr and 32.71 ± 0.54 mm/yr.

The obtained velocity field demonstrates that Western Anatolia is characterized by predominantly north-south extension and experiencing rapid internal deformation. Western Anatolia's internal mechanism supports graben formation in the east-west direction and results are consistent with the characteristics of the Western Anatolia extensional mechanism.

ÖZET

SÜREKLİ GÖZLEM YAPAN GPS İSTASYONLARI VERİLERİ İLE BATI ANADOLU'NUN GÜNCEL HIZ ALANININ BELİRLENMESİ

Ege Bölgesi, Alp-Himalaya orojenik deprem kuşağının en çok deformasyona uğrayan bölümlerinden birisidir. Bölge, Anadolu plakasının Avrasya plakasına göre saat yönünün tersi yönde dönmesi sonucu oluşan iç deformasyona bağlı olarak yoğun bir kesme gerilimi altındadır. Arap plakasının Anadolu bloğunu sıkıştırması sonucu oluşan saat yönünün tersine hareket kuzey-güney yönlü genişleme ve doğu-batı eğilimli aktif grabenlerin oluşmasına sebep olmaktadır.

Batı Anadolu ve çevresindeki sismik aktiviteden dolayı bölgede birçok sismolojik çalışma yapılmıştır. Bu çalışmada, sürekli gözlem yapan 16 CORS-TR istasyonunda 2015, 2016, 2017 ve 2018 yıllarının GPS verileri, mevsimsel etkiler de dikkate alınarak kullanılmıştır. GPS verileri, çalışma bölgesinin hız alanını elde etmek için GAMIT/GLOBK akademik yazılımı ile değerlendirilmiştir. Seçilen CORS-TR istasyonlarının elde edilen hızları, Reilinger et al., (2006) ve Aktuğ et al., (2009) hızları ile birleştirilmiştir. Dönüşüm, çalışmalarda ortak kullanılan 14 IGS istasyonu verileri kullanılarak yapılmıştır. Birleştirilmiş hızlar incelendiğinde, elde edilen hızların 10,66 ± 1,22 mm/yıl ve 32,71 ± 0,54 mm/yıl arasında değiştiği gözlemlenmektedir.

Elde edilen GPS hızları, Batı Anadolu'nun genişlemeli tektonik rejimi ile tutarlıdır. Çalışma sonucu elde edilen hız vektörleri incelendiğinde Batı Anadolu bölgesinin saat yönünün tersine bir harekete sahip olduğu ve kuzey-güney yönde genişleme, doğu-batı yönde graben oluşumunu destekleyecek bir mekanizmaya sahip olduğu gözlemlenmiştir.

TABLE OF CONTENTS

ACKNOWLEDGEMENTS iii
ABSTRACT iv
ÖZET v
LIST OF FIGURES viii
LIST OF TABLES xi
LIST OF SYMBOLS xiii
LIST OF ACRONYMS/ABBREVIATIONS xiv
1. INTRODUCTION 1
2. TECTONIC STRUCTURE OF TURKEY AND WESTERN ANATOLIA . 4
2.1. Active Tectonics of the Study Area (Western Anatolia) 5
3. GNSS, CORS (CONTINUOUSLY OPERATING REFERENCE STATION) AND CORS-TR SYSTEM 10
3.1. GNSS (Global Navigation Satellite System) 10
3.1.1. GPS (Global Positioning System) 10
3.1.2. GLONASS (Global Navigation Satellite System) 11
3.1.3. Galileo Satellite Positioning System 12
3.1.4. BeiDou Satellite Positioning Systems 12
3.1.5. IRNSS (Indian Regional Navigation Satellite System) 12
3.1.6. Quasi-Zenith Satellite System(QZSS) 12
3.2. Continuously Operating Reference Station (CORS) 13
3.3. CORS-TR (TUSAGA-Aktif) 15
3.3.1. CORS-TR Working Principle 17
3.3.2. Control Centers 18
3.3.3. Reference Stations 19
3.3.4. CORS-TR Users 20
3.4. GPS Data Used in Case Study 20
3.5. GNSS Processing Softwares 22
3.5.1. GAMIT/GLOBK 23
3.5.2. Processing of the GPS DATA 24

3.5.3. Kalman Filter 26
4. DATA PROCESSING AND ANALYSIS 30
4.1. Combined Velocity Field 31
4.2. 2017 Midilli Earthquake and 2017 Gokova Earthquake 34
5. DISCUSSION AND CONCLUSION 43
REFERENCES 47
APPENDIX A: PROCESS.DEFAULTS 60
APPENDIX B: SITES DEFAULTS 64
APPENDIX C: SESSION TABLE 66
APPENDIX D: CORS-TR 73

LIST OF FIGURES

Figure 1.1. Tectonic Settings of Turkey. KTJ, Karliova Triple Junction (Özdemir, 2019). 2

Figure 1.2. CORS-TR reference stations used in the study. 3

Figure 2.1. Significant tectonic structures of Western Anatolia (Firuzan, 2008). 6

Figure 2.2. Recorded earthquake data by RETMC- KOERI since 1900. 7

Figure 2.3. The seismic activity in Western Anatolia and its vicinity since 1900. 9

Figure 3.1. GPS Block IIIA satellite in orbit. 11

Figure 3.2. GLONASS-M series satellite. 11

Figure 3.3. Rendition of Japan's QZSS. 13

Figure 3.4. IGS Netwok Map (igs.org, 2019). 15

Figure 3.5. CORS-TR stations and simplified tectonic setting in Anatolia (Major tectonic structures are adapted from McClusky et al., 2000 and Emre et al., 2013). 16

Figure 3.6. Simplified CORS-TR System Design (İlbey, 2015). 17

Figure 3.7. Zephyr Geodetic Antenna and Trimble NETR5 GNSS receiver. . . 18

Figure 3.8. CORS-TR Reference Stations. 19

Figure 3.9. IGS Stations used in this study. 26

Figure 3.10. Filtrering, Smoothing and Temporal Relations (İnce, 1999). 27

Figure 4.1. GPS velocity vectors of CORS-TR stations in Eurasia-fixed reference frame. 31

Figure 4.2. The locations of the stations used in Combine Velocity Field. . . . 33

Figure 4.3. The combined GPS velocity vectors in the Eurasia-fixed reference frame. 42

Figure D.1. AFYN station coordinate-time series. 74

Figure D.2. AYD1 station coordinate-time series. 75

Figure D.3. AYVL station coordinate-time series. 76

Figure D.4. BALK station coordinate-time series. 77

Figure D.5. CAV1 station coordinate-time series. 78

Figure D.6. CESM station coordinate-time series. 79

Figure D.7. DIDI station coordinate-time series. 80

Figure D.8. DINA station coordinate-time series. 81

Figure D.9. FETH station coordinate-time series. 82

Figure D.10. HARC station coordinate-time series. 83

Figure D.11. ISPT station coordinate-time series. 84

Figure D.12. IZMI station coordinate-time series. 85

Figure D.13. KIKA station coordinate-time series. 86

Figure D.14. KUTA station coordinate-time series. 87

Figure D.15. SALH station coordinate-time series. 88

Figure D.16. USAK station coordinate-time series. 89

LIST OF TABLES

Table 2.1. Regional seismicity between 1904 and 2019 with magnitude 6.0 or larger (data provided by RETMC-KOERI) in Western Anatolia and surrounding areas. 8

Table 3.1. The coordinates of the CORS-TR stations used in this study. . . . 21

Table 3.2. The observation days and observation duration of CORS-TR reference stations. 21

Table 3.3. Commercial Softwares and Manifacturers. 22

Table 3.4. Scientific Softwares and Developer Institution. 23

Table 3.5. IGS Stations used in this study. 25

Table 4.1. Velocity estimates in Eurasia-fixed reference frame (EURA_I08) of CORS-TR stations. 30

Table 4.2. The common IGS sites used in the transformation. 32

Table 4.3. Euler Pole parameters (estimated in geographic units). 33

Table 4.4. Euler Pole parameters (estimated in angular vector units). 33

Table 4.5. Earthquakes with magnitudes over 6.0 during the analysis period. . 34

Table 4.6. Estimated velocities of CORS-TR Stations after Euler Pole Rotation. 34

Table 4.7. The velocity parameters from Reilinger et al., (2006). 35

Table 4.8. The velocity parameters from Aktuğ et al., (2009). 36

Table 4.9. The combined velocities. 38

Table 5.1. Velocity vector values. 44

LIST OF SYMBOLS

Mw	Earthquake Moment Magnitude
Ma	Mega-Annum (million years)
MHz	MegaHertz

LIST OF ACRONYMS/ABBREVIATIONS

CORS	Continuously Operating Reference Stations
DGPS	Differential Global Positioning System
EAF	East Anatolian Fault
EAFZ	East Anatolian Fault Zone
ED-50	European Datum 1950
ERP	Earth Rotation Parameters
EU	European Union
FIG	International Federation of Surveyors
FKP	Flachen Korrectur Parameter
GCM	General Command of Mapping
GDLRC	General Directorate of Land Registry and Cadastre
GEO	Geosynchronous Earth Orbit
GIS	Geographic Information System
GLONASS	Global'naya Navigatsionnaya Sputnikovaya Sistema
GNSS	Global Navigation Satellite System
GPS	Global Positioning System
HEO	Highly Elliptical Orbit
IAG	International Association of Geodesy
IGS	International GPS Service for Geodynamics
IGSO	Inclined Geosynchronous Orbit
IKU	Istanbul Kültür University
IRNSS	Indian Regional Navigation Satellite System
ISRO	Indian Space Research Organisation
ITRF	International Terrestrial Reference Frame
IUGG	International Union of Geodesy and Geophysics
JAXA	Japan Aerospace Exploration Agency
KTJ	Karlıova Triple Junction
MAC	Master Auxiliary Concept
MEO	Medium Earth Orbit

MIT	Massachusetts Institute of Technology
NAF	North Anatolian Fault
NAFZ	North Anatolian Fault Zone
NEMC-KOERI	National Earthquake Monitoring Center of Kandilli Observatory and Earthquake Research Institute
NGS	The National Geodetic Survey
NTRIP	Networked Transport of RTCM via Internet Protocol
QZSS	Quasi-Zenith Satellite System
RINEX	Receiver Independent Exchange
RMS	Root Mean Square
RTCA	Radio Technical Commission for Aeronautics
RTCM	Radio Technical Commission for Marine
RTK	Real Time Kinematic
SLR	Satellite Laser Ranging
SOPAC	Scripps Orbit and Permanent Array Center
TUBİTAK	Turkish Scientific and Technical Research Council of Turkey
USGS	United States Geological Survey
USNO	United States Naval Observatory Bulletin
VRS	Virtual Reference Station
WGS84	World Geodetic System 1984

1. INTRODUCTION

Plate tectonics is one of the Earth's most prominent dynamic systems in point of its impact on man and civilization. Geodesists, geologists and geophysicists have always been interested in the studies on the deformation analysis and velocity vectors of tectonic plates. In the past the measurements made with classical measuring instruments were difficult, laborious, and also were not sensitive enough. Satellite technology which started to be developed in 1960s has made great contributions to geodetic research.

In 1994 "International GPS Service for Geodynamics" (IGS) was founded to establish permanent IGS network which consisting of fixed GPS stations positioned to all over the world. Technically, these GPS stations are called as Continuous Operating Reference Stations (CORS). With the contribution of CORS networks, tectonic plate movements and deformation rates are calculated very accurate, sensitive and periodical.

The tectonic framework of Turkey is the physical expression of international collisional interactions and tectonic escape associated deformation since Early Pliocene (5 Ma) (Bozkurt, 2001). The tectonic structure of Anatolia and its vicinity are closely affiliated with the convergence of Eurasian plate, African plate and Arabian plate (Reilinger et al., 2006).

The African plate is subduction under the Anatolian and the Aegean plates by composing Hellenic Arc (Le Pichon et al., 1988). The Arabian plate is moving northward into the southern side of the Eurasian plate and the African plate is moving counter-clockwise direction relative to the Eurasian plate. The Anatolian plate moves to the west and south-west direction due to the compression of these plates. The block is rotating counter-clockwise as it escapes westwards from the collision zone between the Arabian and Eurasian plates.

Three major fault systems effect the seismic activity of Turkey excessively: (1) North Anatolian Fault Zone (NAFZ), (2) East Anatolian Fault Zone (EAFZ) and (3) Aegean Graben System. Approximately 1500 km length NAFZ is one of the most prominent right lateral strike-slip fault zone due to its extraordinary active seismicity. The EAFZ has approximately 580 km length and constitutes left lateral strike slip fault zone among the Arabian plate and Anatolian plate (Arpat 1971; McKenzie 1978, Duman and Emre 2013).

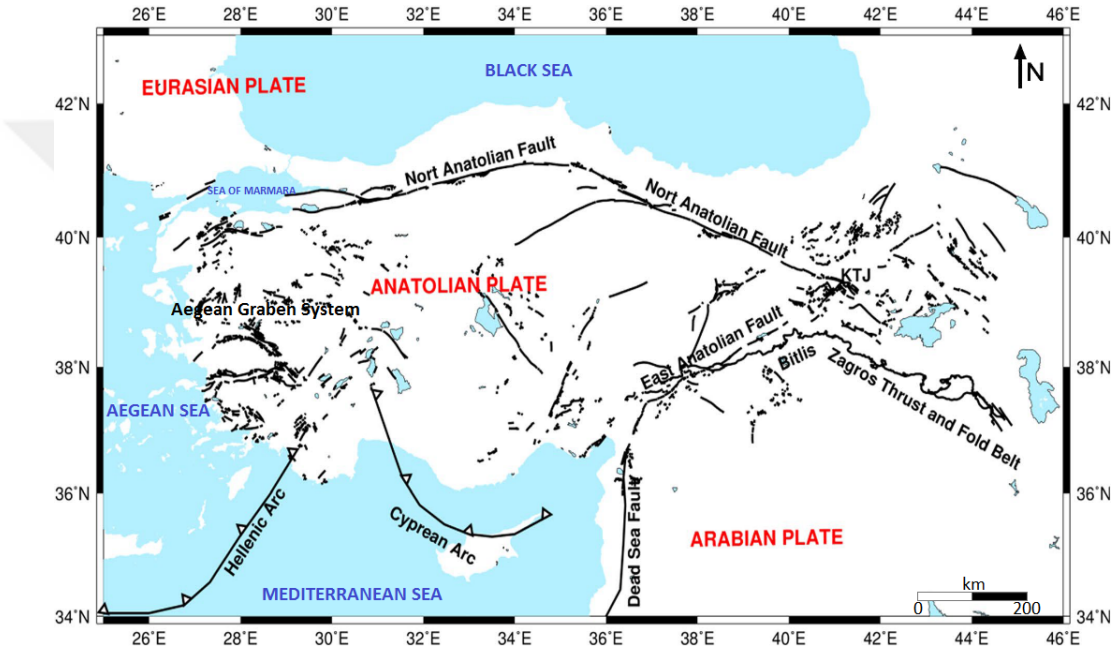


Figure 1.1. Tectonic Settings of Turkey. KTJ, Karliova Triple Junction (Özdemir, 2019).

Western Anatolia which is the study area of this study, is a region in the "Aegean Extensional Province". The most characteristic neotectonic structures of Western Anatolia can be shown as normal faults, strike-slip faults and E-W directed grabens (Bozkurt 2001).

Turkey is one of the most active countries with remarkable seismic activity. With the establishment of CORS-TR project, tectonic plate motions and deformation rates have been monitored regularly in the country. The aim of this thesis is to combine the velocities derived from CORS-TR stations and previous GPS campaigns. Thus, we

have important results about tectonic plate motions in Western Anatolia.

The second chapter of this study explains the tectonic structure and seismicity of Turkey and Western Anatolia. Additionally, the significant faults and grabens were denoted with maps and their seismicity described in terms of seismicity.

The third chapter of this study gives the technical details about GNSS CORS and CORS-TR (TUSAGA-AKTİF) systems. Furthermore, GAMIT/GLOBK scientific software was described with the aspects of GPS data processing.

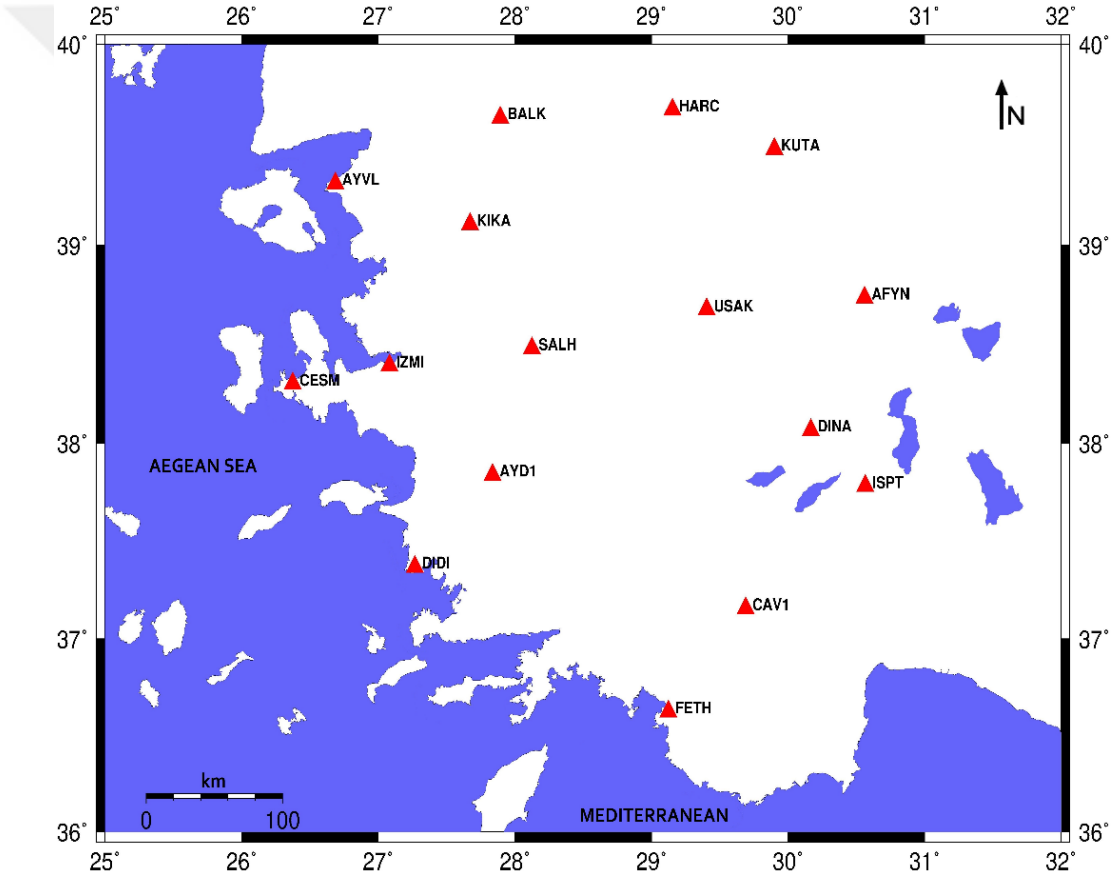


Figure 1.2. CORS-TR reference stations used in the study.

The last chapter explains the results of this study with the comparison and the conclusion with previous GPS studies.

2. TECTONIC STRUCTURE OF TURKEY AND WESTERN ANATOLIA

The tectonic structure of Turkey has been shaped by the formation of the collisional intracontinental convergence of Arabia, Africa and Eurasia lithospheric plates.

The African Plate has ± 10 mm/yr movement in a northern direction and the Arabian Plate has ± 15 mm/yr motion in a north-northeast direction related to the Eurasian Plate (Reilinger et al., 2006, Kremer and Le Pichon 2010; Walters et al., 2014).

Jackson (1994) points out two prominent plate motions in Anatolia: the westward motions of Anatolia and the southwestern movement of the Aegean, both relative to Eurasia. This southwest movement ends at the subduction of the African plate throughout the Hellenic Trench (Jackson 1994). In addition, Doutsos and Kokkolas (2001) hypothesized that central Aegean is expanding southwestward perhaps due to the motion of the Anatolian plate.

The NAFZ with its famous component North Anatolian Fault (NAF) extends approximately 1500 km from Karlıova Triple Junction in eastern Anatolia to the Marmara Sea (Şengör et al., 2005). NAFZ participates in the East Anatolian Fault Zone (EAFZ) at Karlıova Bingöl. McClusky et al., (2000) claimed that NAFZ has a 22-24±1 mm/year mean linear velocity.

The East Anatolian Fault Zone (EAFZ) is a NE-trending mega shear fault zone. The EAFZ has approximately 580 km length. The slip rate of the zone is about 10 mm/yr (Özener et al., 2010).

The Western Anatolia and Aegean Sea have significant seismic activity and rapidly deforming areas. Many large scale and catastrophic earthquakes occurred in the Aegean region. Westernmost Anatolia deflects the motion of Anatolia southward

through N-S extension across E-W trending grabens (Aktug and Kılıçoğlu, 2006).

The eastern part of Central Anatolia is featured with strike-slip tectonic regime and associated structures. On the other hand, the western part of Central Anatolia is featured with series of horst and graben structures bounded by active oblique-slip normal faults (Pasquare et al., 1988; Koçyiğit and Beyhan 1998).

The Dead Sea Transform Fault System, Cyprus Arc and Hellenic Trench are the other prominent neotectonic structural elements Turkey and its surrounding areas.

2.1. Active Tectonics of the Study Area (Western Anatolia)

The Western Anatolia region is bordered with the Eskişehir-Tuzgölü fault zone to the east (Barka et al., 1995), Simav Fault along the north and the Hellenic-Cyprus arc to the south.

The interactions of African plate, Arabian plate and Hellenic Subduction with each other has been shaped the neotectonic structures of Western Anatolia. According to previous GPS studies, the Anatolian plate has westward motion with annual velocity of 15-30 mm/year with anticlockwise rotation (McClusky et al., 2000; Reilinger et al., 2010). Aktuğ et al., 2009 claimed that the horst-graben system of Western Anatolia has 20 mm/yr GPS derived annual velocity. In addition, Çırmık and Pamukçu (2017) claimed that the velocity estimation of Western Anatolia was found as approximately 25 mm/year towards south westward with respect to the Eurasian plate. Nevertheless, the barrier effect of the Hellenic Subduction Zone to Aegean Sea and south of Greece generated N-S oriented tensional forces in the Western Anatolia and this resulted in the shaping of E-W trending grabens (Reilinger et al., 1997; Şengör et al., 1985).

Westward movement of the Anatolian Plate and Western Anatolia's north-south extensional regime are the two major forces that dominate the tectonics of the Aegean region. Extensional tectonic regime of the region can be expressed as the outcome of the rotational westward escape of Anatolian Plate (Emre et al., 2005).

The current N-S extension rate of the region is 30-40 mm/yr according to Oral et al., (1995) and McKenzie (1978). Since Early Miocene, much of it has been experienced N-S directed deformation. In the region, the crust has been deformed under the dominance of normal faults and strike-slip faults since Miocene (Erkül 2010). The most prominent structures in the region are the horst-grabens in the east-west direction due to the north-south prolonging of the region and sedimentary basins.

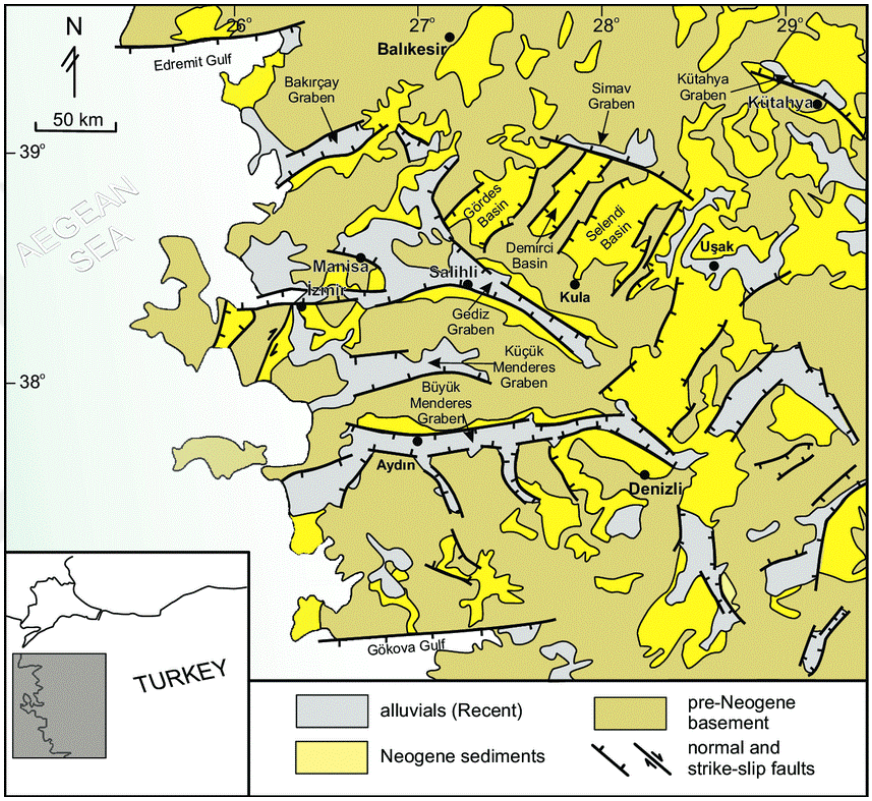


Figure 2.1. Significant tectonic structures of Western Anatolia (Firuzan, 2008). Thick lines with hachures represent normal fault: hachures point out down-thrown side, other thick lines indicates strike-slips faults and the arrows along them show the relative direction of movement (simplified and modified from Bingöl 1989, Bozkurt 2001, Bozkurt and Sözbilir 2004, Yılmaz et al., 2000, Seyitoglu 1997).

Thinned crust and large active grabens are the indications for notable stretching of the crust in an approximately north-south direction. The grabens in the region are bounded by normal fault zones which are east-west trending and have generally 100-150 km average length. In general, these normal fault zones are segmented and each segment has average 8-10 km extension (Yilmaz, 2000). In terms of prolongation,

Büyük Menderes, Küçük Menderes, Gediz, Gokova, Edremit, Bakırçak, Kütahya and Simah grabens are the most significant neotectonic elements in the region (Emre and Sözbilir, 2007).

The Western Anatolia region has been subjected to many disastrous earthquakes. Hence, earthquake researches in the region, which includes many big cities such as İzmir, the third largest city with a population of approximately 3.5 million, has become very important.

Since the beginning of the 1900s, a number of catastrophic earthquakes have occurred in Western Anatolia during the period of Instrumental Period. Some of these earthquakes have resulted in the death of many people and major material damage in the region.

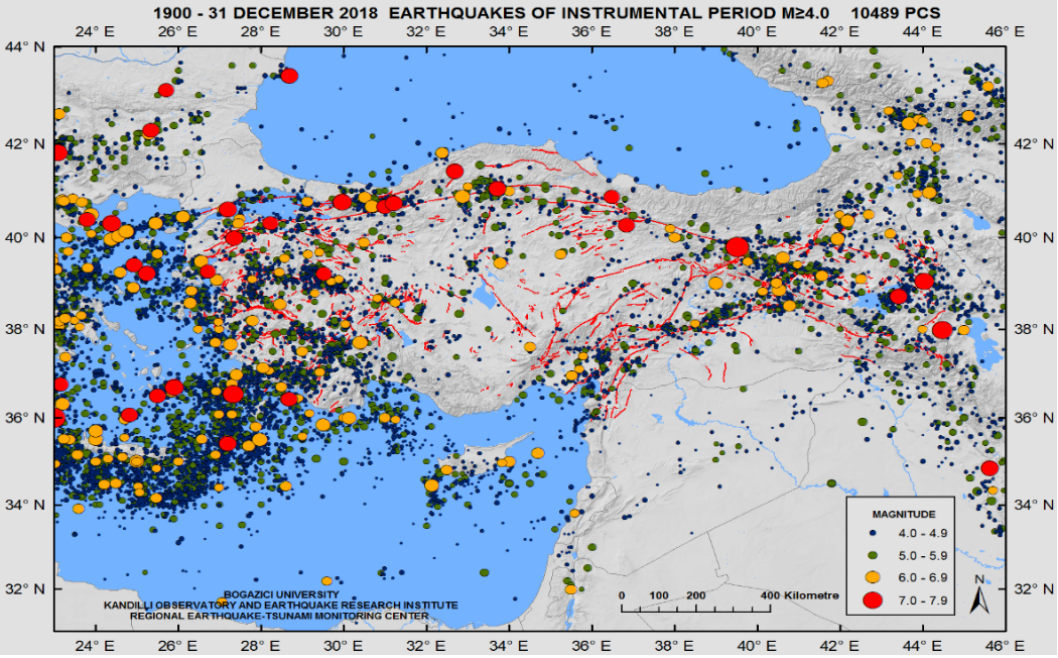


Figure 2.2. Recorded earthquake data by RETMC-KOERI since 1900. (http://www.koeri.boun.edu.tr/sismo/2/wp- content/uploads/2014/08/turkiye_aletsel.png).

Table 2.1. Regional seismicity between 1904 and 2019 with magnitude 6.0 or larger (data provided by RETMC-KOERI) in Western Anatolia and surrounding areas.

Date	**Latitude (deg)**	**Longitude (deg)**	**Depth (km)**	**Magnitude (Mw)**	**Location**
20.07.2017	36.97	27.71	7	6.6	GOKOVA GULF
06.12.2017	38.85	26.33	14.4	6.3	MIDILLI OFFSHORE
01.08.2013	39.65	25.50	8	6.2	DODECANESE OFFSHORE
06.10.2012	36.45	28.92	21.3	6.0	OLUDENIZ OFFSHORE
03.02.2002	38.68	30.82	5	6.0	COBANLAR-AFYONKARAHISAR
03.02.2002	38.58	31.25	10	6.0	TASKOPRU-SULTANDAGI
01.10.1995	38.11	30.05	5	6.0	BELENPINAR-DINAR
06.11.1992	38.16	26.99	17	6.0	ORHANLI-SEFERIHISAR
19.12.1981	39.22	25.25	10	7.2	AEGEAN SEA
13.07.1978	39.10	29.90	10	6.0	YAGCILAR-ASLANAPA
08.07.1978	39.68	29.42	0	6.0	BOZBELEN-TAVSANLI
25.05.1971	39.05	29.71	16	6.0	TOKUL-ASLANAPA
28.03.1970	39.21	29.51	18	6.2	KIZIK-CAVDARHISAR
28.03.1969	38.55	28.46	4	6.1	SOGANLI-ALASEHIR
23.05.1961	36.70	28.49	70	6.2	DALYAN OFFSHORE
25.04.1957	36.42	28.68	80	6.7	DALAMAN OFFSHORE
24.04.1957	36.43	28.63	80	6.5	DALAMAN OFFSHORE
09.07.1956	36.59	25.86	40	6.3	DODECANESE OFFSHORE
09.07.1956	36.69	25.92	10	7.0	DODECANESE OFFSHORE
20.02.1956	39.89	30.49	40	6.2	SULUKARAAGAC-TEPEBASI
16.07.1955	37.65	27.26	40	6.5	YUVACA-SOKE
18.03.1953	39.99	27.36	10	6.8	SOGUCAK-YENICE
23.07.1949	38.57	26.29	10	6.4	KUCUKBAHCE OFFSHORE
06.10.1944	39.48	26.56	40	6.5	EDREMIT GULF
25.06.1944	38.79	29.31	40	6.0	GOKCEDAL-USAK
15.11.1942	39.55	28.58	10	6.0	CATALCAM-DURSUNBEY
28.10.1942	39.10	27.80	50	6.0	KARAKURT-KIRKAGAC
13.12.1941	37.13	28.06	30	6.3	DAGPINAR-MUGLA
23.05.1941	37.07	28.21	40	6.0	KIRAN-MUGLA
22.09.1939	39.07	26.94	10	6.4	KIZILCUKUR-DIKILI
18.03.1935	36.08	27.30	83	6.0	DODECANESE OFFSHORE
23.04.1933	36.77	27.29	30	6.2	DODECANESE OFFSHORE
02.05.1928	39.64	29.14	10	6.0	ISHAKLAR-HARMANCIK
31.03.1928	38.18	27.80	10	6.3	DEREBASI-TIRE
05.06.1927	36.00	31.00	5	6.2	ANTALYA OFFSHORE
26.06.1926	36.54	27.33	100	7.2	DODECANESE OFFSHORE
16.03.1926	37.50	29.00	15	6.3	MEDET-TAVAS

Table 2.1. (continued).

Date	Lat. (°)	Lon. (°)	Depth (km)	Magnitude (Mw)	Location
01.03.1926	37.03	29.43	50	6.0	AYVACIK-CAMELI
18.11.1919	39.26	26.71	10	6.7	KUCUKKOY-AYVALIK
16.07.1918	36.08	26.99	70	6.0	DODECANESE OFFSHORE
03.10.1914	37.70	30.40	14	6.6	HALICILAR-BURDUR
30.04.1911	36.00	30.00	180	6.0	KALE OFFSHORE-ANTALYA
04.04.1911	36.50	25.50	140	6.7	DODECANESE OFFSHORE
19.01.1909	38.00	26.50	60	6.0	AEGEAN SEA
18.08.1904	38.00	27.00	30	6.0	KUSADASI GULF
11.08.1904	37.70	26.90	6	6.1	SISAM ISLAND

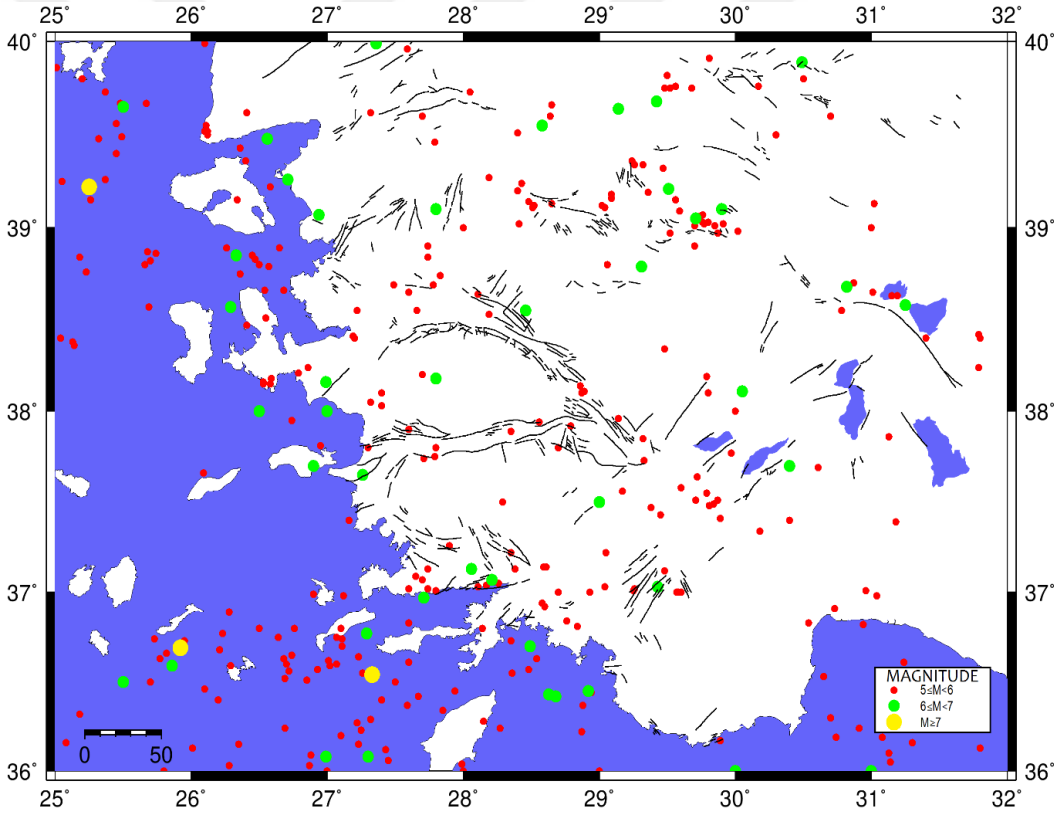


Figure 2.3. The seismic activity in Western Anatolia and its vicinity since 1900.

3. GNSS, CORS (CONTINUOUSLY OPERATING REFERENCE STATION) AND CORS-TR SYSTEM

3.1. GNSS (Global Navigation Satellite System)

Positioning techniques with satellite technology is widely used in the present day by researchers and civil users. Global Navigation Satellite System is prominent positioning technology which provides users high accurate position information, Cadastral measurements, navigation applications, engineering measurements, hydrographic measurements, vehicle tracking systems, development of Geographic Information System (GIS) databases can be shown as the main applications of GNSS systems.

The GNSS system consists of GPS (Global Positioning System) operated by the United States. GLONASS (Global Navigation Satellite System) operated by the Russian Federation. GALILEO satellite positioning systems being installed and managed by the European Union countries. BeiDou, the satellite positioning system of People's Republic of China. IRNSS (Indian Regional Navigation Satellite System) by Indian Space Research Organisation and QZSS (Quasi-Zenith Satellite System) by JAXA (Japan Aerospace Exploration Agency).

3.1.1. GPS (Global Positioning System)

The Global Positioning System is owned by the United States government. The system has been operated since February 1978 and full constellation of global activation and installation was completed in 1994 (NovAtel Inc., 2015).

There are 31 satellites in the GPS constellation. 27 of which are in use at a given time with the rest allocated as back up.



Figure 3.1. GPS Block IIIA satellite in orbit.
(https://www.lockheedmartin.com/en-us/products/gps.html).

3.1.2. GLONASS (Global Navigation Satellite System)

GLONASS is currently operated by the Russian Federal Space Agency. The current space segment of GLONASS is composed of 26 satellites. 24 satellites belong to GLONASS-M series, while other two satellites are of GLONASS K-1 series.



Figure 3.2. GLONASS-M series satellite. (image by https://www.gpsworld.com).

3.1.3. Galileo Satellite Positioning System

GALILEO Satellite Positioning Systems is designed and owned by European Union countries. The system went live in 2016. Currently 22 satellites in use at 23,222 km orbital altitude.

3.1.4. BeiDou Satellite Positioning Systems

BeiDou is managed by China National Space Administration. Last generation BeiDou satellites (BeiDou-3) launched in 2018 with intended global coverage is under development and is expected to complete with 35 fully operational satellites in its constellation by 2020.

3.1.5. IRNSS (Indian Regional Navigation Satellite System)

The system was created and managed by Indian Space Research Organisation (ISRO). The Space Segment consists of seven 7 operational satellites. 4 of them positioned in at orbital altitude of 35,786 km and 3 of them positioned at approximately 24,000 km.

3.1.6. Quasi-Zenith Satellite System(QZSS)

QZSS has been developed and managed by JAXA (Japan Aerospace Exploration Agency). The first Quasi-Zenith Satellite - QZS-1 (Michibiki-1) was launched on September 11, 2010.

The space segment of QZSS architected as; Total 7 satellites positioned in Highly Elliptical Orbit (HEO) and Geo-Stationary (GEO) orbit. Satellites transmit 6 signals with 4 different frequencies.

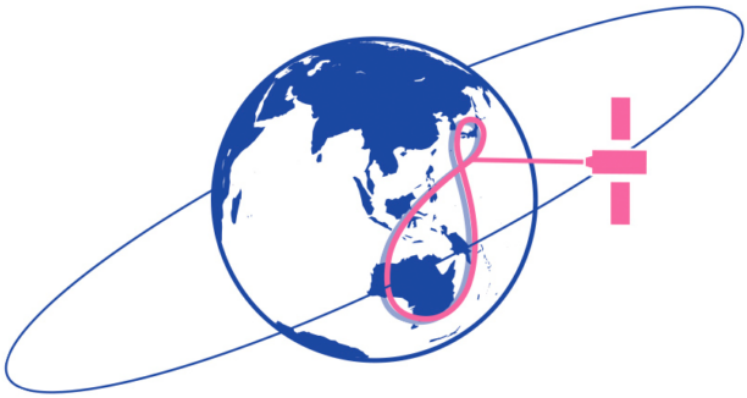


Figure 3.3. Rendition of Japan's QZSS.
(https://qzss.go.jp/en/technical/technology/orbit.html).

3.2. Continuously Operating Reference Station (CORS)

In Continuously Operating Reference Station (CORS) concept, the GNSS Reference Stations are operating continuously on fixed sites. Researchers and civil users can obtain geodetic longitude, geodetic latitude, orthometric height, acceleration of gravity, crustal velocity and geopotential data through CORS technology. The development and operation of CORS has been managed by NGS (National Geodetic Survey) since 1994. The CORS networks supply three-dimensional centimeter-level GPS positioning.

CORS Network was designed for continuous measurements supplied by GNSS satellites and transfer this data to GPS rover receivers.

IGS is the most famous CORS network in the world with its hundreds of worldwide geodetic quality reference sites and more than 200 agencies.

Precise point positions needed to be known in detail survey, application survey and engineering measurements. For this purpose. Classic RTK (Real Time Kinematic) method has been developed to determine point positions in centimeter-level (Arslanoğlu. 2002). However, this method requires a reference station with highly accurate coordinates and one or more rover receivers at a distance of 15-20 km to this station.

Since the late 1980s, the CORS system has been implemented to contribute geodetic measurements which requiring high accuracy (Mekik et al., 2011).

In the concept of CORS system the dependence on a single reference station was eliminated, and the possibility of performing atmospheric modeling for a particular region was also made possible by utilizing data of large number of permanent reference stations. As a result of this modelling, ionospheric and tropospheric errors, which affecting GNSS measurements, are minimized for positioning.

Advantages of CORS Network;

- Reliable, accurate, economic and robust positioning,
- The distance dependent errors are tremendously decreased,
- No second GNSS receiver required for RTK applications,
- Covering wider area with a small number of reference stations (70 km apart),
- Point coordinates are determined in a homogeneous coordinate system in CORS RTK.

High quality results are obtained and the necessary corrections for the measurement point can be calculated by interpolation utilizing the atmospheric model created for the whole network (Kahveci. 2009).

The most widely used, the most well-known and operable network is International GNSS Service (IGS) network.

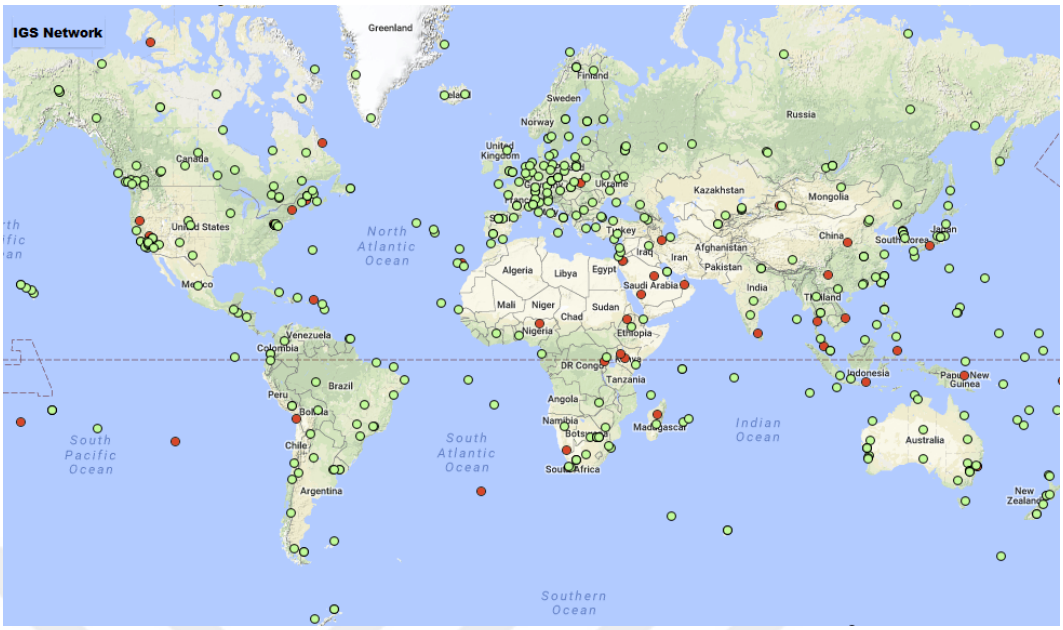


Figure 3.4. IGS Netwok Map (igs.org, 2019).

3.3. CORS-TR (TUSAGA-Aktif)

CORS-TR with a national name TUSAGA-AKTIF is a research and development project, which was signed on May 2006, supported by TUBITAK (Turkish Scientific and Technical Research Council of Turkey).

CORS-TR project consists of 2 powerful control centers and 158 permanent GPS base stations. 154 of the reference stations are located in Turkey and other four are positioned in the Turkish Republic of Northern Cyprus (Figure 3.5.).

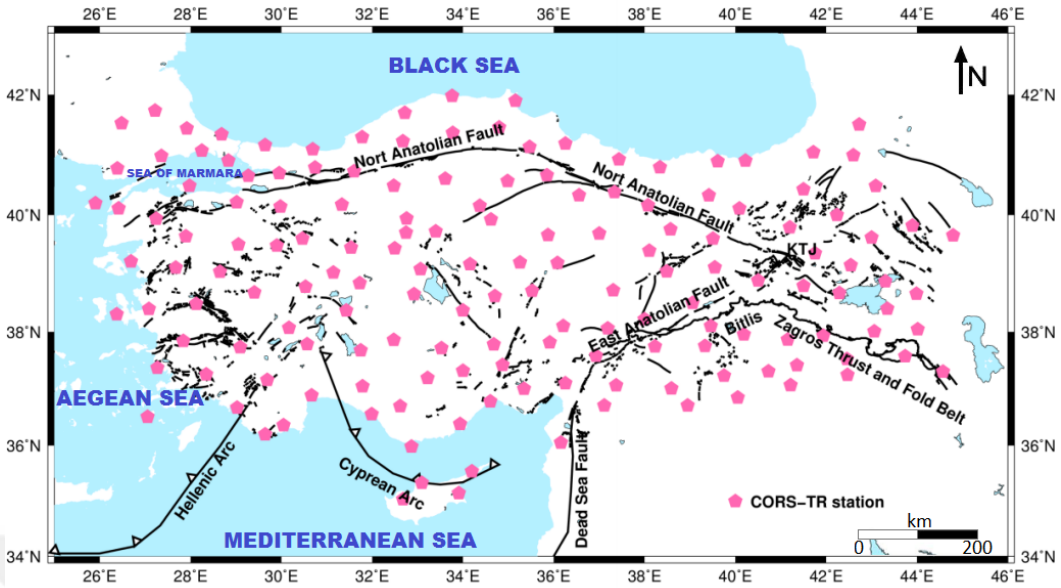


Figure 3.5. CORS-TR stations and simplified tectonic setting in Anatolia (Major tectonic structures are adapted from McClusky et al., 2000 and Emre et al., 2013).

Primary missions of CORS-TR project;

- Determining geographical locations fast and economic, both in real-time kinematic (RTK) and post-processing methods,
- Providing real-time and cm-level precise positioning,
- Determining precise conversion parameters between different coordinate systems (ITRF-ED50),
- Providing position information for military, nationwide cadastral, cartographic and geodetic tasks,
- Modeling atmosphere (troposphere and ionosphere) and thus contributing to signal and communication issues with more accurate meteorological estimation,
- Continuously monitoring tectonic plate motions in mm-level accuracy thus contributing to the early prediction of earthquakes (Brownjohn et al., 2004).

3.3.1. CORS-TR Working Principle

The observations of GPS receivers are transferred to master control center via VPN and GPRS/EDGE technologies. Ionospheric and tropospheric errors are modeled in the control center and the corrections of RTK/DGPS methods are computed instant and delivered to rovers with the GPRS/EDGE technology (Figure 3.6).

The main features of the CORS-TR receivers are;

- Dual frequency with choke-ring antenna,
- Capable to operate with GPS, GLONASS and GALILEO signals,
- Web-based infrastructure,
- Many communication techniques (Radio, GSM/GPRS, Thuraya, NTRIP, Internet).

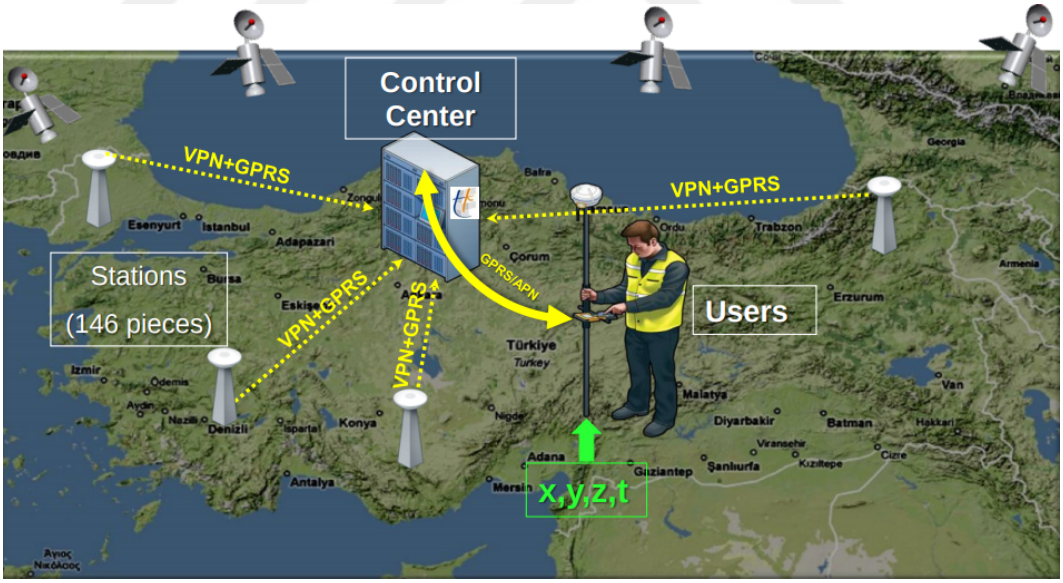


Figure 3.6. Simplified CORS-TR System Design (İlbey, 2015).

The users of a CORS-TR system with a single-frequency rover receivers using the DGPS data can determine the position at sub-meter accuracy and user with a dual-frequency rover receivers using the RTK data can obtain 1-10 centimeter-level position accuracy.



Figure 3.7. Zephyr Geodetic Antenna and Trimble NETR5 GNSS receiver.

3.3.2. Control Centers

In CORS-TR Project. 2 powerful control centers were designed and constructed as the master and the auxiliary. CORS-TR network calculations and corrections are computed and sent to all system users from these centers via internet (Mekik et al., 2011).

The control centers robust software were commanded to calculate ionosphere, troposphere, multipath, orbit corrections, and deliver corrections for RTK positioning.

The main missions of the software;

- Connecting of the all NetR5 reference stations in the system,
- Capable of operating with GPS, GLONASS and GALILEO signals,
- Transferring observations,

- Calculation of the coordinates of stations,
- Modeling errors. correction calculation,
- Monitoring rovers,
- RTK services.

The control center broadcasts VRS CMR+, VRS RTCM 3.1., SAPOS FKP 2.3., RTCM3Net (MAC) and DGPS corrections. In case of data cuts that may occur in ADSL line, a router and GPRS modem is activated and data transmission is provided by GPRS / EDGE (Mekik et al., 2011).

3.3.3. Reference Stations

Ground structure, electricity, telephone, internet availability, security, logistic support criteria were taken into consideration for selection of the location of reference stations. The stations were positioned within 70 km and 100 km. Based on these criteria, concrete pillars were preferred for ground stations and steel pillars were manufactured for terraces.



Figure 3.8. CORS-TR Reference Stations.

3.3.4. CORS-TR Users

CORS-TR users can utilize from different product services including coordinate and velocity information of RTK, DGPS, 1-second RINEX and 30-second RINEX data. CORS-TR Project provide important contributions to civil users, public and scientific institutions.

Some civil and scientific applications contributed by CORS-TR project as follows;

- Geodetic measurements,
- Infrastructure measurements and project applications,
- Precise navigation and vehicle tracking,
- Monitoring of engineering structures,
- Planning and environmental studies,
- E-government, e-municipality, e-commerce applications,
- Geographic Information Service (GIS),
- Meterological institutions,
- Geophysics departments of the universities,
- Seismology departments of the universities,
- Institutions working on space and earth sciences.

3.4. GPS Data Used in Case Study

The permanent network approach on the study of the crustal deformations and tectonic plate motions has been continuously developing since the early 1990s. The continuous developments in GPS technology have led to a rapid change in the observation methodology.

The movements of Western Anatolia were investigated by using GPS data from 16 of CORS-TR stations in Western Anatolia which measured in 2015, 2016, 2017 and 2018 were used by considering the seasonal effects in this study.

Table 3.1. The coordinates of the CORS-TR stations used in this study.

Station	**Station ID**	**Lat. (°)**	**Lon. (°)**
Afyon	AFYN	30.561	38.738
Aydın	AYD1	27.838	37.841
Ayvalık	AYVL	26.686	39.311
Balıkesir	BALK	27.894	39.639
Çavdır	CAV1	29.689	37.159
Çeşme	CESM	26.373	38.304
Dinar	DINA	30.166	38.069
Didim	DIDI	27.269	37.372
Fethiye	FETH	29.124	36.626
Harmancık	HARC	29.153	39.678
Isparta	ISPT	30.567	37.785
İzmir	IZMI	27.082	38.395
Kırkağaç	KIKA	27.672	39.106
Kütahya	KUTA	29.899	39.481
Salihli	SALH	28.124	38.483
Uşak	USAK	29.405	38.679

Table 3.2. The observation days and observation duration of CORS-TR reference stations.

YEAR	**Days of Year**	**Observation Duration**	**Data Rate (sec)**
2015	160-161-162	24h	30
2016	161-162-163	24h	30
2017	160-161-162	24h	30
2018	160-161-162	24h	30

*Considering the post-seismic deformations of 12.06.2017 Midilli Earthquake with 6.3 magnitude and 21.07.2017 Gokova Earthquake with 6.3 magnitude, the velocity

calculations for stations of AYD1, AYVL, CESM and DIDI were determined using pre-earthquake data.

3.5. GNSS Processing Softwares

GNSS data processing softwares are classified into two categories according to their purposes as commercial and scientific. Commercial softwares are generally used for common engineering works such as ground mapping, transportation and construction works.

Table 3.3. Commercial Softwares and Manifacturers.

SOFTWARE	**MANUFACTURERS**
TRIMBLE GEOMATICS OFFICE	TRIMBLE
ASTECH SOLUTION	ASTECH (FORMERLY MAGELLAN)
TOPCON TOOLS	TOPCON
LEICA GEO OFFICE	LEICA
PINNACLE	TOPCON

On the other hand, scientific softwares are used in the studies which require very precise results such as determination of crustal movement, establishment of fundamental GNSS networks and development of the terrestrial reference systems. Scientific softwares are more complicated if compare with the commercial softwares. A list of scientific software and developer institutions are given in Table 3.4 (Havazlı, 2012).

Table 3.4. Scientific Softwares and Developer Institution.

SOFTWARE	DEVELOPER INSTITUTION
GAMIT/GLOBK	MIT, SIO, HU
BERNESE	AIUB
GIPSY/OASIS II	JPL (NASA)
PAGE5	NOAA
GEONAP	UNIVERSITY of HANNOVER
MURO.COSM	UNIVERSITY of TEXAS - VAN MARTIN SYSTEM
DIPOP	UNIVERSITY of NEW BRUNSWICK

3.5.1. GAMIT/GLOBK

GAMIT and GLOBK are comprehensive tools of the collection of programs for processing and analyzing GPS measurement data for the monitoring of the crustal deformation.

GAMIT ("GNSS at MIT") runs under UNIX operating system used for estimation of relative positions of ground stations in three dimensions, earth orientation parameters, atmospheric Zenit delays and satellite orbits (Tetteyfio, 2007). GAMIT applies double differencing technique in order to produce positions of the stations. Since the functional (mathematical) model associated with the observations and parameters is non-linear GAMIT generates two solutions.

- The first to achieve station coordinates within a few decimeters.
- The second to acquire the final estimates.

GAMIT results are not generally used directly to obtain the final station coordinates. GAMIT is used to generate final estimates, associated covariance matrix of station positions, earth orientation parameters and orbital parameters. These outcome data are used as input for GLOBK to estimate velocities and positions.

GLOBK ("Global Kalman filter") is a Kalman filter which was developed primarily to integrate diverse geodetic solutions from space geodetic or terrestrial observations such as GPS, SLR and VLBI experiments. GLOBK estimates precise station coordinates and time series. Orbital parameters, earth-rotation parameters, associated covariance matrices, estimates for station coordinates and source positions composed from analyses of the primary observations are accepted as data for GLOBK. The primary solutions are accomplished with loose a priori ambiguities appointed to the global parameters, thus constraints can be implemented consistently in the combined solution.

GLOBK can be used for combining solution files produced by other GPS softwares such as GIPSY/OASIS II, Bernes and besides that terrestrial measurements and SLR observations.

3.5.2. Processing of the GPS DATA

The data used in this study is 24 hour RINEX (Receiver Independent Exchange Format) format and 30 second recording intervals, obtained from permanent CORS-TR stations. 16 IGS (International GNSS Service) stations were chosen around the network area to estimate station coordinates and velocities. These IGS stations were AJAC, BOR1, BSHM, BUCU, GRAS, GRAZ, MADR, MATE, NICO, NOT1, ORID, RAMO, POTS, WTZR, ZECK and ZWE2 (Figure 3.9.).

Following steps were applied during the processing;

- Precise final orbits by IGS were provided from SOPAC (Scripps Orbit and Permanent Array Center) in SP3 (Standard Product 3) format,
- Earth Rotation Parameters (ERP) obtained from USNO bull b (United States Naval Observatory bulletin b),
- For pressure and radiation effects. Berne model (9-parameter) was chosen,
- Scherneck model was utilized for ocean tide loading effects and solid earth tide impacts,
- The Saastamoinen a priori troposphere model (2-h intervals) was used to calculate

Zenith Delay unknowns,

- Process results were defined in the ITRF2008 (International Terrestrial Reference Frame 2008).

Table 3.5. IGS Stations used in this study.

Station Name	**Location**
AJAC	Ajaccio, France
BOR1	Borowiec, Poland
BSHM	Haifa, Israel
BUCU	Bucharest, Romania
GRAS	Caussols, France
GRAZ	Graz, Austria
MADR	Robledo, Spain
MATE	Matera, Italy
NICO	Nicosia, Cyprus
NOT1	Noto, Italy
ORID	Ohrid, Macedonia
POTS	Potsdam, Germany
RAMO	Mitzpe Ramon, Israel
WTZR	Bad Koetzting, Germany
ZECK	Zelenchukskaya, Russian Federation
ZWE2	Zwenigorod, Russian Federation

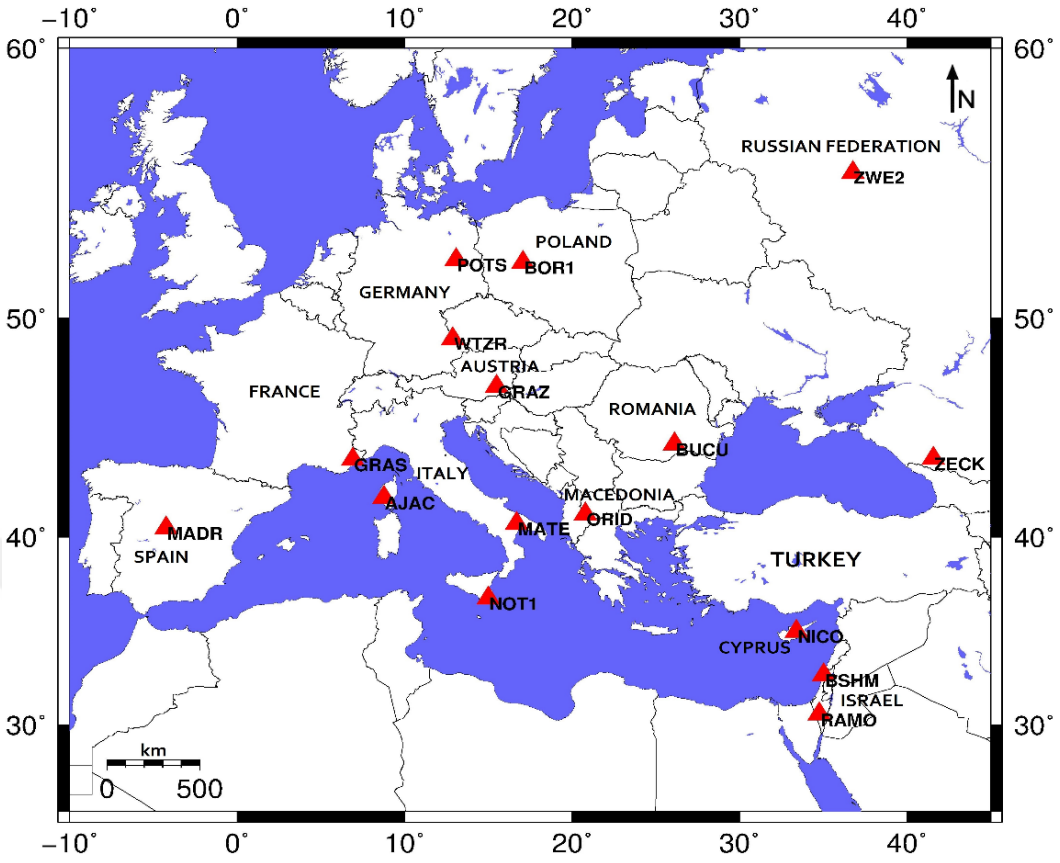


Figure 3.9. IGS Stations used in this study.

3.5.3. Kalman Filter

Kalman Filtering method is an estimation technique for instant phase estimation of linear and nonlinear dynamic systems analysis of estimation results (İnce, 1999).

Kalman filtering technique was developed to figure out mathematical equations by utilizing the computational capability of the least squares method. The estimates of the prior, present and oncoming states can be implemented using Kalman filtering (Welch and Bishop 2002).

Kalman Filter technique comprises prediction (extrapolation), filtering and smoothing steps. The Kalman Filter is used in time depended applications which unknown parameters are estimated according to the least square methods (Cross, 1990; Doğan. 2002).

(a) **Prediction (extrapolation):** In the case of t<tk. state variable values of the dynamic system at the moment of tk are calculated by using the state variable values at the moment of system t.

(b) **Filtering:** In the case of t=tk, the phase computation of the state variable values at the moment of t, using the measurements of tk is called filtering. The filtering part is the adjustment of the classical least squares method.

(c) **Smoothing:** In the case of t>tk, the variable of the dynamic system at the moment of tk are calculated together with the measurements made until the moment of ti (İnce, 1999).

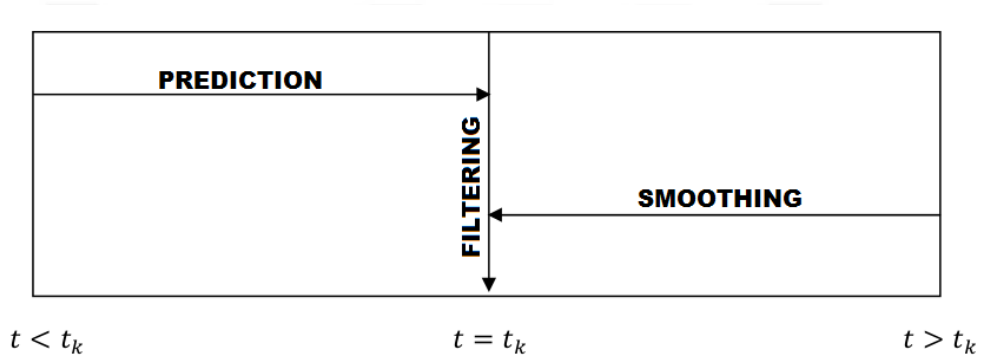


Figure 3.10. Filtrering, Smoothing and Temporal Relations (İnce, 1999).

The mathematical formation of Kalman Filter consist of two models; measurement update equations and time update equations.

$$x_k = \phi_{k.k-1} x_{k-1} + w_k \tag{3.1}$$

$$l_k = A_{k.k-1} + V_k \tag{3.2}$$

Where;

x_k: the state vector at the time of t_k,

x_{k-1}: the state vector at the time of t_{k-1},

$\phi_{k.k-1}$: the transition matrix from time of t_{k-1} to t_k,

w_k: the noise vector symbolizing the dynamic model at time of t_k,

l_k: the observation vector at time of t_k,

A_k: the design matrix for the measurement model,

V_k: the noise vector representing the measurement model at time of t_k.

The prediction and filtering equations of the Kalman filtering technique can be summarized as;

$$\bar{x}_{\bar{k}} = \phi_{k.k-1}\bar{x}_{k-1} \tag{3.3}$$

$$Q_{\bar{k}} = \phi_{k.k-1}Q_{k-1}{\phi_{k.k-1}}^T + Q_w \tag{3.4}$$

$$Q_w = {\alpha^2}_a w_k w_k^T \tag{3.5}$$

The mathematical equations of filtering:

$$\bar{x}_k = \bar{x}_{\bar{k}} K_k \left(l_k - A_k \bar{x}_{\bar{k}}\right) \tag{3.6}$$

$$Q_k = \left(I - K_k A_k\right) {Q_k}^{-T} \tag{3.7}$$

$$K_k = Q_k - {A_k}^T (A_k Q_k - {A_k}^T + Q_l)^{-1} \tag{3.8}$$

where;

$\bar{x}_{\bar{k}}$: the predicted estimation of the state vector at time t_k,

$\bar{x}_{k-1}$: the filtered estimation of the state vector at time t_{k-1},

$Q_{\bar{k}}$: the covariance matrix of the predicted state vector,

Q_w: the covariance matrix of the dynamic model noise,

σ_a^2: the variance of the non-deterministic variable in the dynamic model,

Q_k: the covariance matrix of the filtered state vector,

K_k: the gain matrix.

Probable outliers should be detected performing deformation analysis. The sequence is the most important criteria to detect outliers in Kalman Filter (Salzmann. 1990):

$$v_k = l_k – A_k \bar{x}_{\bar{k}} \tag{3.9}$$

4. DATA PROCESSING AND ANALYSIS

In this study, GPS data collected in the years of 2015 between 2018 of 16 CORS-TR stations in Western Anatolia. Table 4.1. shows the longitude and latitude values, eastward velocities, northward velocities, uncertainties of eastward volicities, uncertainties of northward velocities, and correlation coefficient between eastward and northward components (RHO) in Eurasia fixed reference frame. Figure 4.1. shows GPS velocity vectors of CORS-TR stations in Eurasia-fixed reference frame.

Table 4.1. Velocity estimates in Eurasia-fixed reference frame (EURA_I08) of CORS-TR stations.

Site	**Lon (°)**	**Lat (°)**	**Ve (mm/yr)**	**Vn (mm/yr)**	σ_{Ve} **(mm/yr)**	σ_{Vn} **(mm/yr)**	**RHO**
AFYN	30.561	38.738	-19.87	-2.00	0.72	0.72	-0.212
AYD1	27.838	37.841	-20.31	-14.95	1.15	1.23	-0.062
AYVL	26.686	39.311	-20.37	-10.62	0.72	0.77	-0.130
BALK	27.894	39.639	-21.42	-6.00	0.54	0.53	-0.213
CAV1	29.689	37.159	-16.91	-10.85	0.64	0.64	-0.317
CESM	26.373	38.304	-19.84	-22.05	0.85	0.93	-0.097
DIDI	27.269	37.372	-19.22	-24.62	0.74	0.79	-0.162
DINA	30.166	38.069	-20.83	-5.45	0.63	0.60	-0.302
FETH	29.124	36.626	-14.53	-15.69	0.71	0.74	-0.241
HARC	29.153	39.678	-22.07	-3.67	0.61	0.59	-0.201
ISPT	30.567	37.785	-18.28	-5.19	0.69	0.68	-0.275
IZMI	27.082	38.395	-21.86	-16.52	0.65	0.68	-0.155
KIKA	27.672	39.106	-22.60	-10.75	0.60	0.59	-0.212
KUTA	29.899	39.481	-23.13	-4.13	0.61	0.58	-0.237
SALH	28.124	38.483	-22.54	-10.56	0.65	0.66	-0.157
USAK	29.405	38.679	-23.66	-3.97	0.66	0.65	-0.215

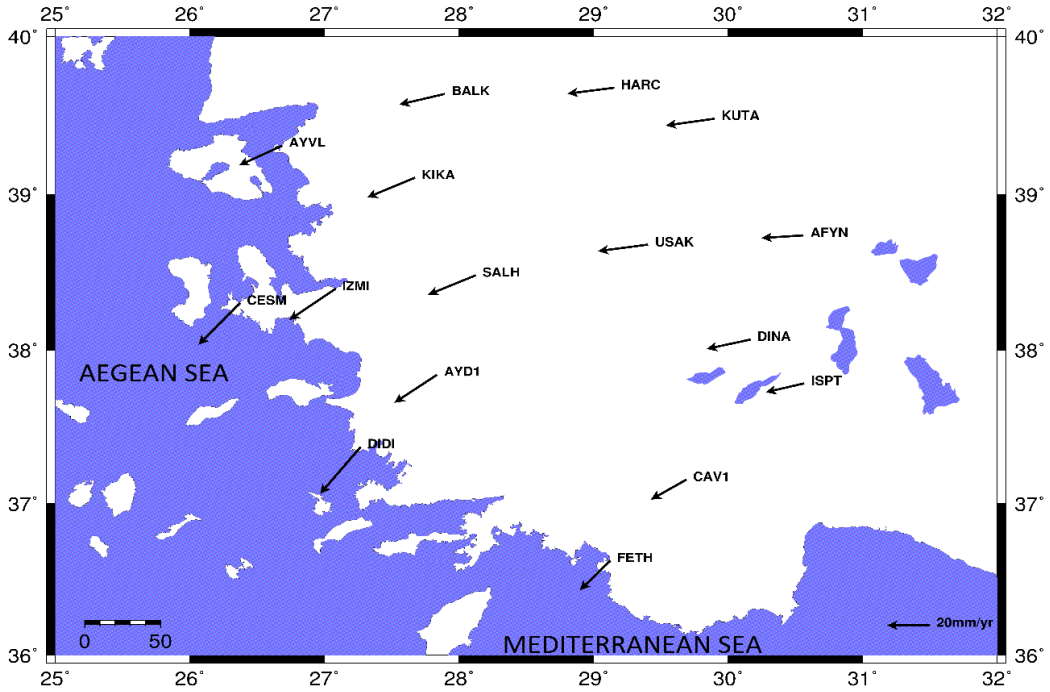


Figure 4.1. GPS velocity vectors of CORS-TR stations in Eurasia-fixed reference frame.

4.1. Combined Velocity Field

After the estimation of the velocity values of the stations, our velocity field was combined with the velocity field from the Reilinger et al., in 2006 and Aktuğ et al., in 2009. Our velocity field is maintained from 16 continuously recording CORS-TR stations in Western Anatolia in the period of 2015 and 2018. Beside our CORS-TR network, the data of 16 IGS sites surrounding Western Turkey were used. IGS sites were utilized for reference frame definition and determination of our site coordinates in ITRF system.

Because the velocity fields from previous works expressed in the same reference as Eurasia fixed (EURA I08), our velocity field is also transformed and expressed in the Eurasia fixed reference frame. The transformation was realized with the help of 14 common IGS sites used in the projects.

Table 4.2. The common IGS sites used in the transformation.

Site-Site	**Lon (°)**	**Lat (°)**	**r_{V_e} (mm/yr)**	**r_{V_n} (mm/yr)**	**re (mm/yr)**	**rn (mm/yr)**
BOR1-BOR1	17.073	52.277	-0.95	-2.84	0.120	0.200
BSHM-BSHM	35.023	32.779	-5.50	8.19	-0.353	0.857
BUCU-BUCU	26.126	44.464	-0.50	-0.69	0.720	-1.360
GRAS-GRAS	6.921	43.755	1.38	0.47	0.710	0.200
GRAZ-GRAZ	15.493	47.067	2.08	0.74	0.780	0.500
MATE-MATE	16.704	40.649	2.79	3.55	1.430	.4500
NICO-NICO	33.396	35.141	-6.92	42461	-0.624	0.311
NOT1-NOT1	14.990	36.876	-0.32	4.25	-2.180	4.030
ORID-ORID	20.794	41.127	0.48	-2.26	0.440	-2.780
POTS-POTS	13.066	52.379	0.59	-0.17	0.120	-0.010
RAMO-RAMO	34.763	30.598	-3.25	8.72	0.470	0.864
WTZR-WTZR	12.879	49.144	0.47	-0.33	0.330	0.470
ZECK-ZECK	41.565	43.788	-1.36	0.64	0.780	1.230
ZWE2-ZWE2	36.758	55.699	0.45	-1.37	0.590	-1.100

The velocity fields were combined using the equations below;

$$\nu_2 = \nu_1 + R\,(\Omega x r) \tag{4.1}$$

Where;

ν_2: The velocity vector expressed in the individual reference frame,

ν_1: The estimated combined velocity vector of site,

R: The transformation matrix from cartesian coordinates to local coordinates at site,

Ω: Euler rotation vector,

r: The position vector of each site.

Table 4.3. Euler Pole parameters (estimated in geographic units).

Lon (°)	**Lat (°)**	**Ω (°/Ma)**
-45.6856	1.7774	0.0000000027

Table 4.4. Euler Pole parameters (estimated in angular vector units).

X (mas/Myr)	**Y (mas/Myr)**	**Z (mas/Myr)**
-0.0067615	-0.0002098	-0.0069286

The rms value after transformation process is calculated as 1.3102.

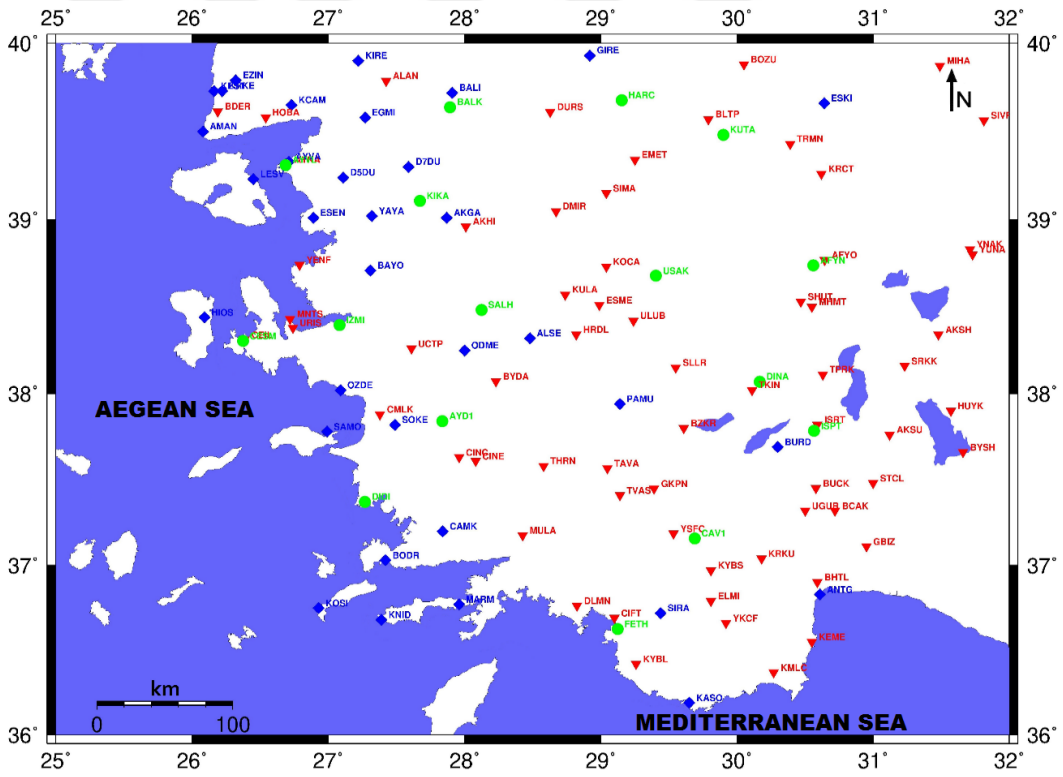


Figure 4.2. The locations of the stations used in Combine Velocity Field. Red points: stations of Reilinger et al., 2006, blue points: stations of Aktug et al., 2009, and green points : CORS-TR stations used in this study.

4.2. 2017 Midilli Earthquake and 2017 Gokova Earthquake

According to long permanent GPS observations (more than 9 years time span) of Ozdemir and Karslioglu (2019), when the time series of the local sites were examined attentively, it was noticed that 2017 Midilli Earthquake and 2017 Gokova Earthquake caused the coseismic displacements on the stations of AYD1, AYVL, CESM and DIDI.

Table 4.5. Earthquakes with magnitudes over 6.0 during the analysis period.

Earthquake	Epicenter				
	Lon (o)	Lat (o)	Date	M	Affected CORS- TR site
Midilli	26.37	38.93	12.06.2017	6.3	AYVL, CESM
Gokova	27.41	36.93	20.07.2019	6.6	AYDI, DIDI
* Earthquake information is from USGS eartquake catalog					

Since we have only 1 year GPS data after these earthquakes, post-earthquake data were not used for these 4 stations considering post-seismic deformations. Instead, pre-earthhquake velocities estimated from 3 years of data, are used for these CORS-TR stations.

Table 4.6. Estimated velocities of CORS-TR Stations after Euler Pole Rotation.

Site	**Lon (°)**	**Lat (°)**	V_e **(mm/yr)**	V_n **(mm/yr)**	σ_{Ve} **(mm/yr)**	σ_{Vn} **(mm/yr)**	**RHO**
AFYN	30.561	38.738	-19.53	-1.36	0.72	0.72	-0.212
AYD1	27.838	37.841	-19.96	-14.37	1.15	1.23	-0.062
AYVL	26.686	39.311	-20.08	-10.06	0.72	0.77	-0.130
BALK	27.894	39.639	-21.13	-5.41	0.54	0.53	-0.213
CAV1	29.689	37.159	-16.53	-10.23	0.64	0.64	-0.317
CESM	26.373	38.304	-19.51	-21.50	0.85	0.93	-0.097
DIDI	27.269	37.372	-18.86	-24.05	0.74	0.79	-0.162
DINA	30.166	38.069	-20.47	-4.81	0.63	0.60	-0.302
FETH	29.124	36.626	-14.14	-15.08	0.71	0.74	-0.241
HARC	29.153	39.678	-21.77	-3.06	0.61	0.59	-0.201
ISPT	30.567	37.785	-17.91	-4.55	0.69	0.68	-0.275
IZMI	27.082	38.395	-21.53	-15.95	0.65	0.68	-0.155
KIKA	27.672	39.106	-22.29	-10.17	0.60	0.59	-0.212
KUTA	29.899	39.481	-22.82	-3.50	0.61	0.58	-0.237
SALH	28.124	38.483	-22.21	-9.97	0.65	0.66	-0.157
USAK	29.405	38.679	-23.33	-3.35	0.66	0.65	-0.215

Table 4.7. The velocity parameters from Reilinger et al., (2006).

Site	**Lon (°)**	**Lat (°)**	V_e **(mm/yr)**	V_n **(mm/yr)**	σ_{Ve} **(mm/yr)**	σ_{Vn} **(mm/yr)**	**RHO**
AKGA	27.873	39.006	-21.02	-10.31	0.68	0.66	0.014
ALSE	28.483	38.315	-22.61	-13.18	0.96	0.89	0.004
AMAN	26.082	39.501	-20.82	-9.08	0.96	0.97	-0.017
ANTG	30.610	39.330	-12.20	-8.20	0.60	0.60	-0.004
AYVA	26.707	39.326	-21.06	-9.80	0.73	0.71	-0.009
BALI	27.906	39.722	-21.20	-4.53	0.71	0.63	0.003
BAYO	27.308	38.711	-17.44	-14.74	0.77	0.72	0.004
BODR	27.423	37.032	-15.96	-26.08	0.67	0.58	-0.048
BURD	30.297	37.689	-19.20	-8.63	0.56	0.51	-0.030
CAMK	27.836	37.196	-17.58	-24.98	0.63	0.58	-0.055
D5DU	27.112	39.244	-19.64	-12.11	1.67	1.72	-0.004
D7DU	27.590	39.295	-16.75	-12.25	1.64	1.66	-0.011
EGMI	27.269	39.577	-20.77	-6.40	0.95	0.94	0.043
ESEN	26.885	39.010	-21.06	-13.52	1.78	1.75	-0.019
ESKI	30.637	39.658	-24.01	-1.74	0.97	0.90	0.015
EZIN	26.317	39.785	-20.05	-9.19	0.95	0.99	0.001
GIRE	28.923	39.930	-23.43	-0.54	0.96	0.95	0.057
HIOS	26.085	38.443	-19.07	-22.96	0.72	0.65	0.066
KASO	29.650	36.190	-10.00	-8.80	0.50	0.70	-0.006
KATV	27.781	35.952	-8.21	-28.82	0.44	0.42	0.037
KCAM	26.732	39.653	-22.65	-7.26	0.94	0.93	0.023
KEST	26.157	39.731	-20.86	-9.16	0.93	0.95	-0.018
KIRE	27.217	39.897	-19.62	-8.40	0.61	0.60	0.017
KNID	27.394	36.681	-11.85	-29.90	0.64	0.60	-0.031
KOSI	26.929	36.752	-15.88	-26.53	0.72	0.62	0.079
KRKE	26.216	39.726	-21.11	-9.61	0.95	0.96	0.001
KYNS	24.410	37.363	-17.29	-25.79	0.68	0.60	0.090
LESV	26.451	39.234	-19.47	-12.68	0.74	0.65	0.048
MARM	27.963	36.772	-14.23	-25.98	0.59	0.53	-0.036
MILO	24.521	36.747	-16.36	-24.64	0.66	0.59	0.082
NSKR	24.543	38.887	-12.15	-23.82	0.73	0.65	0.061
ODME	28.000	38.248	-20.62	-12.62	0.93	0.87	-0.009
OZDE	27.085	38.019	-20.01	-19.68	0.69	0.61	-0.070
PAMU	29.136	37.941	-21.80	-7.82	0.67	0.63	-0.008
SAMO	26.989	37.780	-18.97	-23.89	0.70	0.61	0.074
SEVA	24.392	38.086	-15.23	-25.88	0.65	0.60	0.058
SIRA	29.439	36.720	-15.12	-11.57	0.68	0.62	-0.047
SOKE	27.486	37.818	-19.66	-18.98	0.91	0.87	-0.018
YAYA	27.316	39.024	-20.63	-13.31	0.76	0.71	0.013

Table 4.8. The velocity parameters from Aktuğ et al., (2009).

Site	**Lon (°)**	**Lat (°)**	V_e **(mm/yr)**	V_n **(mm/yr)**	σ_{Ve} **(mm/yr)**	σ_{Vn} **(mm/yr)**	**RHO**
AFYO	30.644	38.769	-21.42	-2.98	0.51	0.51	0.000
AKHI	28.010	38.960	-22.89	-8.96	0.77	0.74	0.000
AKSH	31.480	38.340	-22.44	-1.70	1.40	1.82	-0.050
AKSU	31.121	37.762	-16.19	-5.10	0.56	0.54	-0.020
ALAN	27.420	39.780	-22.95	-8.51	0.73	0.72	0.022
AYKA	26.700	39.311	-19.93	-12.87	0.45	0.45	-0.010
BCAK	30.720	37.320	-18.24	-5.23	2.55	2.61	0.000
BDER	26.189	39.614	-19.04	-11.04	0.52	0.49	-0.010
BLTP	29.790	3.9570	-25.62	-5.60	0.76	0.89	-0.070
BHTL	30.590	36.900	-12.01	-4.73	0.53	0.55	0.000
BOZU	30.050	39.880	-23.90	-3.49	1.13	1.22	-0.030
BUCK	30.580	37.450	-16.17	-6.24	0.59	0.64	0.010
BYDA	28.230	38.070	-21.41	-13.97	0.62	0.66	0.000
BYSH	31.660	37.660	-14.69	-2.88	0.73	0.87	-0.010
BZKR	29.610	37.800	-20.46	-9.84	0.70	0.83	-0.010
CEIL	26.385	38.311	-18.32	-22.88	0.48	0.48	-0.010
CIFT	29.100	36.690	-14.83	-16.22	0.56	0.58	0.000
CINC	27.960	37.630	-20.45	-21.60	0.67	0.69	0.000
CINE	28.081	37.609	-20.64	-21.16	0.43	0.40	-0.010
CMLK	27.380	37.880	-21.32	-20.00	0.67	0.69	0.010
DION	23.933	38.079	-15.87	-25.48	0.42	0.40	0.000
DLMN	28.826	36.762	-15.44	-20.07	0.60	0.56	-0.020
DMIR	28.671	39.046	-20.96	-6.51	0.57	0.54	0.020
DURS	28.630	39.610	-23.66	-6.02	0.84	0.95	-0.110
ELMI	29.810	36.790	-11.94	-13.60	2.37	2.42	-0.060
EMET	29.250	39.340	-23.06	-7.82	0.77	0.89	-0.070
ESME	28.990	38.510	-22.64	-7.49	0.55	0.55	0.000
GBIZ	30.950	37.110	-19.34	-8.96	0.71	0.84	0.010
GKPN	29.392	37.448	-20.03	-12.24	0.53	0.55	-0.010
HOBA	26.540	39.580	-21.13	-13.45	0.68	0.75	-0.020
HRDL	28.820	38.340	-24.12	-10.71	0.58	0.62	0.000
HUYK	31.570	37.900	-16.14	-3.44	0.58	0.62	0.000
ISRT	30.590	37.820	-18.52	-7.23	0.64	0.72	0.000
KEME	30.550	36.550	-10.26	-5.66	0.56	0.58	-0.010
KMLC	30.270	36.370	-8.60	-6.30	0.79	0.93	0.020
KOCA	29.040	38.730	-26.05	-10.49	0.53	0.55	0.000
KRCT	30.620	39.260	-23.79	-6.30	1.83	2.16	-0.910
KRKU	30.180	37.040	-14.30	-6.53	0.56	0.59	0.010
KRPT	27.224	35.493	-12.00	-30.43	0.39	0.37	0.000
KULA	28.740	38.570	-23.31	-9.68	0.64	0.64	-0.010
KYBL	29.260	36.420	-12.55	-15.06	0.62	0.62	0.000
KYBS	29.810	36.971	-20.07	-8.73	0.52	0.55	-0.020

Table 4.8. The velocity parameters from Aktuğ et al., (2009) (continued).

Site	**Lon(°)**	**Lat (°)**	V_e **(mm/yr)**	V_n **(mm/yr)**	σ_{Ve} **(mm/yr)**	σ_{Vn} **(mm/yr)**	**RHO**
MHMT	30.550	38.500	-20.20	-5.23	0.79	0.89	-0.030
MIHA	31.490	39.870	-24.06	-1.59	0.89	0.87	-0.020
MNTS	26.720	38.430	-19.35	-12.86	1.01	1.01	-0.020
MULA	28.427	37.175	-17.91	-20.94	0.51	0.51	-0.010
SHUT	30.470	38.530	-22.25	-4.86	3.11	3.36	-0.100
SIMA	29.040	39.150	-23.01	-8.72	1.11	1.37	-0.270
SIVR	31.814	39.564	-20.43	-2.31	0.71	0.61	0.010
SLLR	29.550	38.150	-21.86	-8.06	0.53	0.56	0.000
SRKK	31.230	38.160	-18.13	-5.98	0.90	1.14	-0.060
STCL	31.000	37.480	-15.71	-5.93	0.70	0.81	0.020
TAVA	29.048	37.566	-20.76	-15.86	0.59	0.63	0.000
THRN	28.580	37.580	-22.53	-17.56	0.59	0.62	0.000
TKIN	30.110	38.020	-21.70	-8.00	0.55	0.56	0.000
TPRK	30.630	38.110	-20.52	-5.69	1.16	1.62	-0.150
TRMN	30.390	39.430	-22.64	-1.16	1.35	1.67	-0.400
TUC2	24.070	35.530	-16.81	-24.04	1.27	1.23	0.000
TVAS	29.140	37.410	-20.31	-14.33	3.29	3.51	-0.350
UCTP	27.610	38.260	-22.15	-17.16	0.59	0.62	0.000
UGUR	30.500	37.320	-18.56	-8.36	0.73	0.86	0.020
ULUB	29.240	38.420	-25.08	-10.18	0.55	0.59	0.010
URIS	26.740	38.380	-22.92	-20.31	0.67	0.75	0.000
YENF	26.790	38.740	-23.26	-17.48	0.77	0.92	-0.010
YKCF	29.920	36.660	-14.35	-9.26	0.58	0.61	0.000
YNAK	31.710	38.830	-21.02	-0.69	0.70	0.72	0.000
YSFC	29.535	37.185	-18.97	-13.55	0.51	0.54	-0.010
YUNA	31.730	38.800	-21.02	-0.68	0.70	0.72	0.000

Table 4.9. The combined velocities.

Site	**Lon (°)**	**Lat (°)**	V_e **(mm/yr)**	V_n **(mm/yr)**	σ_{Ve} **(mm/yr)**	σ_{Vn} **(mm/yr)**	**RHO**
AFYN	30.561	38.738	-19.53	-1.36	0.72	0.72	-0.212
BHTL	30.590	36.900	-12.01	-4.73	0.53	0.55	0.000
AFYO	30.644	38.769	-21.42	-2.98	0.51	0.51	0.000
AKGA	27.873	39.006	-21.02	-10.31	0.68	0.66	0.014
AKHI	28.010	38.960	-22.89	-8.96	0.77	0.74	0.000
AKSH	31.480	38.340	-22.44	-1.70	1.40	1.82	-0.050
AKSU	31.121	37.762	-16.19	-5.10	0.56	0.54	-0.020
ALAN	27.420	39.780	-22.95	-8.51	0.73	0.72	0.022
ALSE	28.483	38.315	-22.61	-13.18	0.96	0.89	0.004
AMAN	26.082	39.501	-20.82	-9.08	0.96	0.97	-0.017
ANTG	30.610	39.330	-12.20	-8.20	0.60	0.60	-0.004
AYD1	27.838	37.841	-19.96	-14.37	1.15	1.23	-0.062
AYKA	26.700	39.311	-19.93	-12.87	0.45	0.45	-0.010
AYVA	26.707	39.326	-21.06	-9.80	0.73	0.71	-0.009
AYVL	26.686	39.311	-20.08	-10.06	0.72	0.77	-0.130
ANTG	30.610	39.330	-12.20	-8.20	0.60	0.60	-0.004
BALI	27.906	39.722	-21.20	-4.53	0.71	0.63	0.003
BALK	27.894	39.639	-21.13	-5.41	0.54	0.53	-0.213
BAYO	27.308	38.711	-17.44	-14.74	0.77	0.72	0.004
BCAK	30.720	37.320	-18.24	-5.23	2.55	2.61	0.000
BDER	26.189	39.614	-19.04	-11.04	0.52	0.49	-0.010
BLTP	29.790	39.570	-25.62	-5.60	0.76	0.89	-0.070
BODR	27.423	37.032	-15.96	-26.08	0.67	0.58	-0.048
BOZU	30.050	39.880	-23.90	-3.49	1.13	1.22	-0.030
BUCK	30.580	37.450	-16.17	-6.24	0.59	0.64	0.010
BURD	30.297	37.689	-19.20	-8.63	0.56	0.51	-0.030
BYDA	28.230	38.070	-21.41	-13.97	0.62	0.66	0.000
BYSH	31.660	37.660	-14.69	-2.88	0.73	0.87	-0.010
BZKR	29.610	37.800	-20.46	-9.84	0.70	0.83	-0.010
CAMK	27.836	37.196	-17.58	-24.98	0.63	0.58	-0.055
CAV1	29.689	37.159	-16.53	-10.23	0.64	0.64	-0.317
CEIL	26.385	38.311	-18.32	-22.88	0.48	0.48	-0.010
CESM	26.373	38.304	-19.51	-21.50	0.85	0.93	-0.097
CIFT	29.100	36.690	-14.83	-16.22	0.56	0.58	0.000
CINC	27.960	37.630	-20.45	-21.60	0.67	0.69	0.000
CINE	28.081	37.609	-20.64	-21.16	0.43	0.40	-0.010
CMLK	27.380	37.880	-21.32	-20.00	0.67	0.69	0.010
D5DU	27.112	39.244	-19.64	-12.11	1.67	1.72	-0.004
D7DU	27.590	39.295	-16.75	-12.25	1.64	1.66	-0.011
DIDI	27.269	37.372	-18.86	-24.05	0.74	0.79	-0.162
DINA	30.166	38.069	-20.47	-4.81	0.63	0.60	-0.302
DION	23.933	38.079	-15.87	-25.48	0.42	0.40	0.000
DLMN	28.826	36.762	-15.44	-20.07	0.60	0.56	-0.020
DMIR	28.671	39.046	-20.96	-6.51	0.57	0.54	0.020

Table 4.9. The combined velocities (continued).

Site	**Lon (°)**	**Lat (°)**	V_e **(mm/yr)**	V_n **(mm/yr)**	σ_{Ve} **(mm/yr)**	σ_{Vn} **(mm/yr)**	**RHO**
DURS	28.630	39.610	-23.66	-6.02	0.84	0.95	-0.110
EGMI	27.269	39.577	-20.77	-6.40	0.95	0.94	0.043
ELMI	29.810	36.790	-11.94	-13.60	2.37	2.42	-0.060
EMET	29.250	39.340	-23.06	-7.82	0.77	0.89	-0.070
ESEN	26.885	39.010	-21.06	-13.52	1.78	1.75	-0.019
ESKI	30.637	39.658	-24.01	-1.74	0.97	0.90	0.015
ESME	28.990	38.510	-22.64	-7.49	0.55	0.55	0.000
EZIN	26.317	39.785	-20.05	-9.19	0.95	0.99	0.001
FETH	29.124	36.626	-14.14	-15.08	0.71	0.74	-0.241
GBIZ	30.950	37.110	-19.34	-8.96	0.71	0.84	0.010
GIRE	28.923	39.930	-23.43	-0.54	0.96	0.95	0.057
GKPN	29.392	37.448	-20.03	-12.24	0.53	0.55	-0.010
HARC	29.153	39.678	-21.77	-3.06	0.61	0.59	-0.201
HIOS	26.085	38.443	-19.07	-22.96	0.72	0.65	0.066
HOBA	26.540	39.580	-21.13	-13.45	0.68	0.75	-0.020
HRDL	28.820	38.340	-24.12	-10.71	0.58	0.62	0.000
HUYK	31.570	37.900	-16.14	-3.44	0.58	0.62	0.000
ISPT	30.567	37.785	-17.91	-4.55	0.69	0.68	-0.275
ISRT	30.590	37.820	-18.52	-7.23	0.64	0.72	0.000
IZMI	27.082	38.395	-21.53	-15.95	0.65	0.68	-0.155
KASO	29.650	36.190	-10.00	-8.80	0.50	0.70	-0.006
KATV	27.781	35.952	-8.21	-28.82	0.44	0.42	0.037
KCAM	26.732	39.653	-22.65	-7.26	0.94	0.93	0.023
KEME	30.550	36.550	-10.26	-5.66	0.56	0.58	-0.010
KEST	26.157	39.731	-20.86	-9.16	0.93	0.95	-0.018
KIKA	27.672	39.106	-22.29	-10.17	0.60	0.59	-0.212
KIRE	27.217	39.897	-19.62	-8.40	0.61	0.60	0.017
KMLC	30.270	36.370	-8.60	-6.30	0.79	0.93	0.020
KNID	27.394	36.681	-11.85	-29.90	0.64	0.60	-0.031
KOCA	29.040	38.730	-26.05	-10.49	0.53	0.55	0.000
KOSI	26.929	36.752	-15.88	-26.53	0.72	0.62	0.079
KRCT	30.620	39.260	-23.79	-6.30	1.83	2.16	-0.910

Table 4.9. The combined velocities (continued).

Site	**Lon (°)**	**Lat (°)**	V_e **(mm/yr)**	V_n **(mm/yr)**	σ_{Ve} **(mm/yr)**	σ_{Vn} **(mm/yr)**	**RHO**
KRKE	26.216	39.726	-21.11	-9.61	0.95	0.96	0.001
KRKU	30.180	37.040	-14.30	-6.53	0.56	0.59	0.010
KRPT	27.224	35.493	-12.00	-30.43	0.39	0.37	0.000
KULA	28.740	38.570	-23.31	-9.68	0.64	0.64	-0.010
KUTA	29.899	39.481	-22.82	-3.50	0.61	0.58	-0.237
KYBL	29.260	36.420	-12.55	-15.06	0.62	0.62	0.000
KYBS	29.810	36.971	-20.07	-8.73	0.52	0.55	-0.020
KRKU	30.180	37.040	-14.30	-6.53	0.56	0.59	0.010
KYNS	24.410	37.363	-17.29	-25.79	0.68	0.60	0.090
LESV	26.451	39.234	-19.47	-12.68	0.74	0.65	0.048
MARM	27.963	36.772	-14.23	-25.98	0.59	0.53	-0.036
MHMT	30.550	38.500	-20.20	-5.23	0.79	0.89	-0.030
MIHA	31.490	39.870	-24.06	-1.59	0.89	0.87	-0.020
MILO	24.521	36.747	-16.36	-24.64	0.66	0.59	0.082
MNTS	26.720	38.430	-19.35	-12.86	1.01	1.01	-0.020
MULA	28.427	37.175	-17.91	-20.94	0.51	0.51	-0.010
NSKR	24.543	38.887	-12.15	-23.82	0.73	0.65	0.061
ODME	28.000	38.248	-20.62	-12.62	0.93	0.87	-0.009
OZDE	27.085	38.019	-20.01	-19.68	0.69	0.61	-0.070
PAMU	29.136	37.941	-21.80	-7.82	0.67	0.63	-0.008
SALH	28.124	38.483	-22.21	-9.97	0.65	0.66	-0.157
SAMO	26.989	37.780	-18.97	-23.89	0.70	0.61	0.074
SEVA	24.392	38.086	-15.23	-25.88	0.65	0.60	0.058
SHUT	30.470	38.530	-22.25	-4.86	3.11	3.36	-0.100
SIMA	29.040	39.150	-23.01	-8.72	1.11	1.37	-0.270
SIRA	29.439	36.720	-15.12	-11.57	0.68	0.62	-0.047
SIVR	31.814	39.564	-20.43	-2.31	0.71	0.61	0.010
SLLR	29.550	38.150	-21.86	-8.06	0.53	0.56	0.000
SOKE	27.486	37.818	-19.66	-18.98	0.91	0.87	-0.018
SRKK	31.230	38.160	-18.13	-5.98	0.90	1.14	-0.060
STCL	31.000	37.480	-15.71	-5.93	0.70	0.81	0.020

Table 4.9. The combined velocities (continued).

Site	**Lon(°)**	**Lat (°)**	V_e **(mm/yr)**	V_n **(mm/yr)**	σ_{Ve} **(mm/yr)**	σ_{Vn} **(mm/yr)**	**RHO**
TAVA	29.048	37.566	-20.76	-15.86	0.59	0.63	0.000
THRN	28.580	37.580	-22.53	-17.56	0.59	0.62	0.000
TKIN	30.110	38.020	-21.70	-8.00	0.55	0.56	0.000
TPRK	30.630	38.110	-20.52	-5.69	1.16	1.62	-0.150
TRMN	30.390	39.430	-22.64	-1.16	1.35	1.67	-0.400
TUC2	24.070	35.530	-16.81	-24.04	1.27	1.23	0.000
TVAS	29.140	37.410	-20.31	-14.33	3.29	3.51	-0.350
UCTP	27.610	38.260	-22.15	-17.16	0.59	0.62	0.000
UGUR	30.500	37.320	-18.56	-8.36	0.73	0.86	0.020
ULUB	29.240	38.420	-25.08	-10.18	0.55	0.59	0.010
URIS	26.740	38.380	-22.92	-20.31	0.67	0.75	0.000
USAK	29.405	38.679	-23.33	-3.35	0.66	0.65	-0.215
YAYA	27.316	39.024	-20.63	-13.31	0.76	0.71	0.013
YENF	26.790	38.740	-23.26	-17.48	0.77	0.92	-0.010
YKCF	29.920	36.660	-14.35	-9.26	0.58	0.61	0.000
YNAK	31.710	38.830	-21.02	-0.69	0.70	0.72	0.000
YSFC	29.535	37.185	-18.97	-13.55	0.51	0.54	-0.010
YUNA	31.730	38.800	-21.02	-0.68	0.70	0.72	0.000

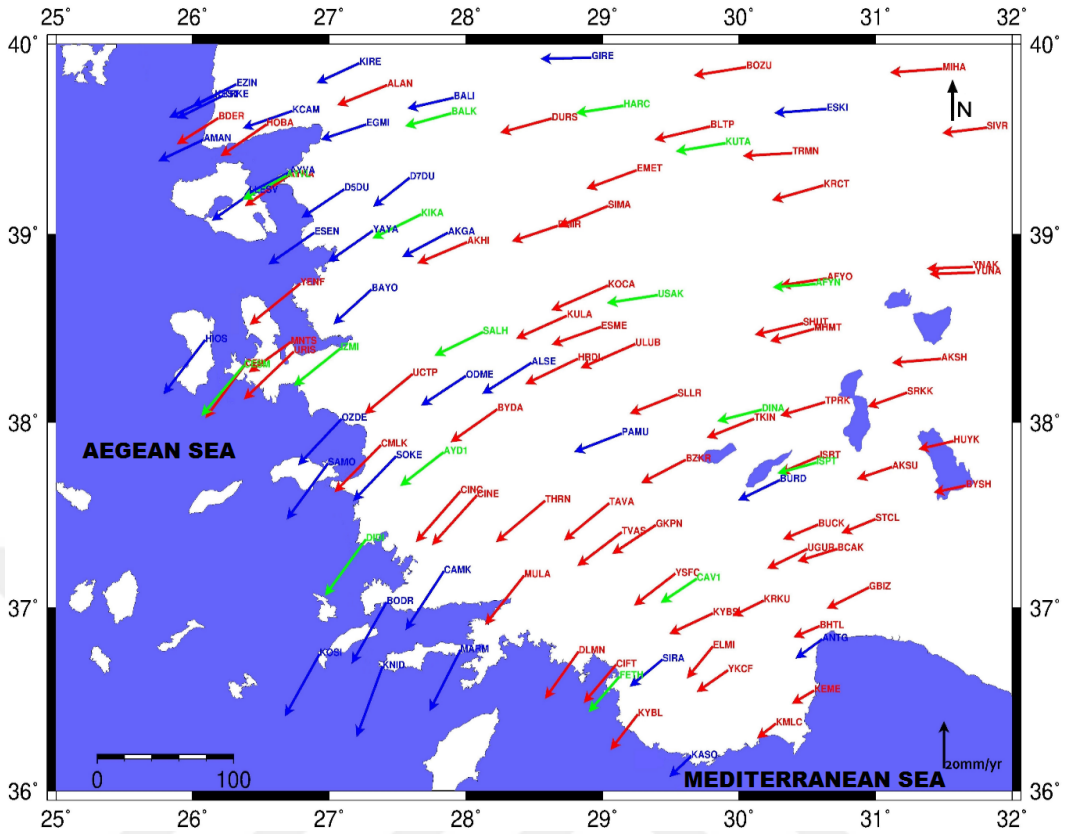


Figure 4.3. The combined GPS velocity vectors in the Eurasia-fixed reference frame. Reilinger et al., (2006) are represented by red vectors, Aktuğ et al., (2013) are shown by blue vectors and CORS-TR vectors are represented in green.

It is clearly seen that, the stations in the map have displacements in the direction of west and south-west relative to Eurasia. The stations near the Aegean coasts have almost the direction of south. However, the stations near the Central Anatolia have approximately west direction. The combined velocity values indicates that velocities are vary between 10.72 ± 1.22 mm/year and 32.71 ± 0.54 mm/year in the direction of SW with respect to Eurasia.

5. DISCUSSION AND CONCLUSION

GPS velocities have been used for many years to determine crustal movements and velocity fields in seismically active zones to analyze the characteristics of the deformation effectively. It is possible to monitor position changes with few mm level for the horizontal component and obtain high precision geodetic velocity field through long span of data provided by homogenic permanent GPS networks. In order to investigate the displacements due to tectonic motions, it is necessary to determine the amount of change in coordinates by calculating the velocity field and deformation.

The Western Anatolia region is located into the Aegean Extensional Province which is seismically very active part of the Alpine-Himalayan orogenic system. The intensity of the seismic activities in the region made it obligatory to reveal that more data should be obtained from the region to observe the recent kinematics of the region. Western Anatolia has experienced many devastating earthquakes, therefore monitoring, recording, and scientific investigation of the seismicity of the region has great importance. In the light of these purposes, many scientific studies have been carried out in the region.

The aim of this study is to investigate recent crustal motions and relative displacements in the Western Anatolia region. In this aim, the GPS data of 16 CORS-TR stations which are positioned in Western Anatolia were used. CORS-TR network provides reliable data to be used in earthquake surveys with its services throughout the country and providing 24 hours of data. The GPS data used in this study is 24 hour RINEX format and 30 second recording intervals. The date of the collection of data were selected attentively to minimize seasonal effects.

As mentioned previous chapters, GPS data measured in 2015, 2016, 2017 and 2018 were used for 12 of CORS-TR stations. Considering the post-seismic effects of 2017 Midilli Earthquake (Mw=6.3) and 2017 Gokova Earthquake (Mw=6.6), the velocity parameters of AYD1, AYVL, CESM and DIDI stations were estimated using

pre-earthquake data as 2015. 2016 and 2017 measurements.

In this study, in order to define the coordinates of stations, velocity estimations, datum definition and to associate our local network to global network, 16 stations (AJAC, BOR1, BSHM, BUCU, GRAS, GRAZ, MADR, MATE, NICO, NOT1, ORID, RAMO, POTS, WTZR, ZECK, ZWE2) selected from IGS network as reference, considering the repeatabilities and the geographic coverage. These stations are reliable, homogeneously distributed and that have been collecting data for many years. The processing were carried out in ITRF2008 reference frame with the help of GAMIT/GLOBK.

In the first step, the horizontal velocity values of CORS-TR stations were calculated in ITRF2008 reference system relative to Eurasia-fixed frame and these values were used to define the inter-seismic velocity field of the region. The velocities with respect to Eurasian plate vary between 19.00 ± 0.97 mm/yr and 31.23 ± 1.08 mm/yr after processing.

Table 5.1. Velocity vector values.

Station	**Velocity (mm/yr)**
ISPT	19.00 ± 0.97
AFYN	19.97 ± 1.02
CAV1	20.09 ± 0.91
FETH	21.38 ± 1.03
DINA	21.53 ± 0.87
BALK	22.24 ± 0.76
HARC	22.37 ± 0.85
AYVL	22.97 ± 1.05
KUTA	23.50 ± 0.84
USAK	23.99 ± 0.93
SALH	24.89 ± 0.93
KIKA	25.03 ± 0.84
AYD1	25.22 ± 1.68
IZMI	27.40 ± 0.94
CESM	29.66 ± 1.26
DIDI	31.23 ± 1.08

For better understanding of the dynamic mechanism of the region, we decided to increase the spatial resolution of our velocity field. Accordingly, we densified our

velocity field with the previously published velocities from Reilinger et al., (2006) and Aktuğ et al., (2009). Longer observation time span and widespread additional GPS data were needed for comprehensive research in the region. The combined velocity field in this study comprises 123 GPS stations (including our stations).

After the transformation processes, obtained combined velocity field provided us dense and more dependable results. The present study represents the utilization of combining GPS data to improve seismic hazard assessment throughout the Western Anatolia. The combined velocity values of this study indicates that velocities are vary between 10.66 ± 1.22 mm/year and 32.71 ± 0.54 mm/year in the direction of SW with respect to Eurasia.

According to previous GPS studies, the Anatolian plate has westward motion with an annual velocity between 15 mm/yr and 30 mm/yr (McClusky et al., 2000; Reilinger et al., 2010). Doğru et al., 2014 calculated the velocities of the stations around Izmir as 25 mm/yr and 28 mm/yr relative to the Eurasian plate from 3 years of survey-mode GPS data. According to the study of Çırmık and Pamukçu in 2017, Western Anatolia has 25 mm/yr movement towards south west relative to the Eurasian plate.

The results found in this study are consistent with the Reilinger et al., 2006, Aktuğ et al., 2009 and the previous studies done in the region. The velocity vectors indicates anti-clockwise rotation which is also consistent with the orientation of the geological structure of the region. According to the GPS derived velocities, ISPT station has the slowest velocity while DIDI has the fastest.

The combined velocity values specifie that Western Anatolia currently experiences active extension whose rate increases from the Central Anatolia to the Aegean coast due to a counter-clockwise rotation.

In conclusion, this study and previous studies indicate that Western Anatolia experiences extensional active deformation due to lithospheric interactions of Africa,

Arabia, Eurasian plates and the barrier effect of the Hellenic Subduction Zone. Under the influence of these forces, Anatolian plate moves westward and counter-clockwise rotation of the Anatolian plate occurs at a rate between 20 mm/yr and 25 mm/yr. 2017 Midilli Earthquake (Mw=6.3) and 2017 Gokova Earthquake (Mw=6.6) are the latest major earthquakes in the region. These indicates that Western Anatolia and its vicinity have high potential to create destructive earthquakes that can affect thousands of people and cause economic devastation.

This study was made using 4 years of GPS data. In order to examine the kinematics of the region in more detail, dense GPS data provided by survey-type GPS measurements with longer observation span can be combined with the data by continuously recording GPS stations.

REFERENCES

Aktuğ, B. and Kılıçoglu, A., 2006. Recent Crustal Deformation of Izmir, Western Anatolia and Surrounding Regions as Deduced From Repeated GPS Measurements and Strain Field, Journal of Geodynamics, 41, 471-484.

Aktuğ, B., Kılıçoğlu, A., Lenk, O., and Gürdal, M., 2009. Establishment of Regional Reference Frames for Quantifying Active Deformation Areas in Anatolia, Studia Geophysica et Geodaetica, Vol. 53 (2), pp. 169-183.

Aktuğ, B., et al. 2009. Deformation of Western Turkey from a combination of permanent and campaign GPS data: Limitsto block-like behavior, J. Geophys, Res., 114.

Aktuğ, B., Dikmen, U., Doğru, A., and Ozener, H., 2013. Seismicity and Strain Accumulation around Karlıova Triple Junction (Turkey), Journal of Geodynamics, Vol. 67, pp. 21-29.

Aldanmaz, E., 2002. Mantle source characteristics of alkali basalts and basanites in an extensional intra-continental plate setting, Western Anatolia, Turkey: Implication for multi-stage melting, International Geology Review 44, 440-57.

Ambraseys, N. N., and Jackson, J. A., 1998. Faulting Associated with Historical and Recent Earthquakes in the Eastern Mediterranean Region, Geophysical Journal International, Vol. 133, pp. 390-406.

Arpat, A. E., 1971. 22 Mayıs, 1974 Bingöl Depremi Ön Rapor, Institute of Mineral Research and Exploration Report 4697.

Arpat, E., and Şaroğlu, F., 1975. Türkiye'deki bazı önemli genç tektonik olaylar, TJK Bülteni, 18, 91-101.

Arslanoğlu, M., 2002. Investigating the Usability of the Real Time Kinematic GPS in Urban Information Systems, Master of Science Thesis, ZKÜ, FBE, Zonguldak.

Barka, A. A., Akyüz, H. S., Altunel, E., Sunal, G., Çakir, Z., Dikbaş, A., Yerli, B., Armijo, R., Meyer, B., De Chabalier, J. B., Rockwell, T., Dolan, J. R., Hartleb, R., Dawson, T., Christofferson, S., Tucker, A., Fumal, T., Langridge, R., Stenner, H., Lettis, W., Bachhuber, J., and Page, W., 2002. The Surface rupture and slip distribution of the 17 August 1999 İzmit earthquake (M 7.4), North Anatolian Fault, Bulletin of the Seismological Society of America, 92, 43-60.

Barka, A., Reilinger, R., Şaroğlu, F., and Şengör, A.M.C., 1995. The Isparta angle: Its importance in the neotectonics of the Eastern Mediterranean region in Pişkin, Ö., et al., Proceedings of the International Earth Science Colloquium on the Aegean Region: Izmir University of 9 Eylul, pp. 3-17.

Bayrak, T., 2003. Developing a dynamic deformation model and a dynamic movement surface model for landslides, PhD. Karadeniz Technical University, Graduate School of Natural and Applied Sciences, Trabzon, Turkey (in Turkish).

Bazarov, Y., Introduction to Global Navigation Satellite System. AGARD Lecture Series 207, s: 2/1-21, NATO yayını, Kanada 1996.

Bingöl, E., 1989. Geological map of Turkey (Scale: 1/2.000.000), General Directorate of Mineral Research and Exploration (MTA), Ankara.

Bozkurt, E., 2001. Neotectonics of Turkey-A Synthesis. Geodinamica Acta Vol. 14, pp. 3-30.

Bozkurt, E., and Sözbilir, H., 2004. Tectonic evolution of the Gediz Graben: field evidence for an episodic, two-stage extension in Western Turkey, Geological Magazine 141, 63-79.

Brownjohn, J.M.W., Hao, H., Chouw, N., 2004. Field measurement and analysis

of roadway filtering on traffic-induced ground vibrations. Proceedings the 11th International Conference on Soil Dynamics and Earthquake Engineering and the 3rd International Conference on Earthquake Geotechnical Engineering, pp 196-203.

Cross, P.A., 1990. Advanced Least Squares Applied to Position Fixing Working Papers, North East London Polytechnic, Dept. of Surveying, 205 pp.

Çırmık, A., and Pamukçu, O., 2017. Clarifying the interplate main tectonic elements of Western Anatolia. Turkey by using GNSS velocities and Bouguer gravity anomalies, J. Asian Earth Sci. 148:294-304.

Çırmık, A., Pamukçu, O., Gönenç, T., Kahveci, M., Şalk, M., Herring, T., 2017. Examination of the kinematic structures in Izmir (Western Anatolia) with repeated GPS observations (2009, 2010 and 2011), J. African Earth Sci., 126:1-12.

Dabove, P., Manzino, A.M., Agostino, M.D., 2012. Achievable Positioning Accuracies in a Network of GNSS Reference Stations, DOI: 10.5772/28666.

Delaney, D., Ward, T., 2004. A Java tool for exploring state estimation using the Kalman filter, ISSC 2004, Belfast, June 30 - July 2.

Dewey, J. F., and Şengör, A.M.C., 1979. Aegean and Surrounding Region: Complex Multiplate and Continuum Tectonics in a Convergent Zone, Geological Society of America Bulletin, Vol. 90 (1), pp. 84-92.

Dewey, J. F., Hempton, M.R., Kidd, W.S.F., Saroğlu, F., and Şengör, A.M.C., 1986. Shortening of Continental Lithosphere: The Neotectonics of Eastern Anatolia-A Young Collision Zone, In Collision Tectonics, Geological Society Special Publication Vol. 19 pp. 3-36.

Doğan U., 2002. 17 Ağustos 1999 İzmit Depreminden Kaynaklanan Deformasyonların Kinematik Modellerle Araştırılması, Doktora Tezi, Yıldız Teknik Üniversitesi, Fen

Bilimleri Enstitüsü, İstanbul.

Dogru, A., Ozener, H., Aktug, B., and Gorgun, E., 2014. Geodetic and seismological investigation of crustal deformation near Izmir (Western Anatolia), 1367-9120. http://dx.doi.org/10.1016/j.jseaes.2013.12.008.

Doganalp, S., Turgut, B., and Inal, C., 2005. Deformation analysis by Kalman Filtering and S transformation techniques for height networks in proceedings of Symposium on 2nd National Engineering measurements, Istanbul, Turkey, 23-35 November 2005, 28-40, 2005 (in Turkish).

Duman, T.Y., Emre, Ö., Doğan, A., Özalp, S., 2005. Step-Over and Bend Structures along the 1999 Duzce Earthquake Surface Rupture, North Anatolian Fault, Turkey. Bulletin of the Seismological Society of America, Vol. 95, No. 4:1250-1262, doi: 10.1785/0120040082.

Duman, T.Y., and Emre, Ö., 2013. The East Anatolian Fault: geometry, segmentation and jog characteristics, Geol. Soc. (Lond.) Spec. Publ. 372.

Doutsos, T., and Kokkalas, S., 2001. Stress and deformation patterns in the Aegean region, Journal of Structural Geology 23: 455-472.

Elitok, Ö., Dolmaz, M.N., 2008. Mantle flow-induced crustal thinning in the area between the easternmost part of the Anatolian plate and the Arabian Foreland (E Turkey) deduced from the geological and geophysical data, Gondwana Research 13.3.302- 318. doi: 10.1016/j.gr.2007.08.007.

Emre, O., Ozalp, S., Dogaz, A., Ozaksoy, V., Yildirim, C., Goktas, F., 2005. The Report on Faults of İzmir and its Vicinity and their Earthquake Potentials, General Directorate of Mineral Research and Exploration Report No: 10754.

Emre, T., and Sözbilir, H., 2007. Tectonic evolution of the Kiraz Basin. Küçük Menderes Graben: evidence for compression/uplift - related basin formation over-

printed by extensional tectonics in West Anatolia, Turkish Journal of Earth Sciences 16, 441-470.

EOP (Earth Observation Portal)2019. https://directory.eoportal.org/web/eoportal/satellite-missions/q/qzss#foot17%29.

Eren, K., and Uzel, T., Ulusal Cors Sisteminin Kurulması ve Datum Dönüşümü Projesi, TUSAGA Aktif (CORS-TR): 3. Çalıştay, 2008.

Ergintav, S., Reilinger, R.E., Çakmak, R., Floyd, M., Çakır, Z., Doğan, U., King, R.W., McClusky, S., Özener, H., 2014. Istanbul's earthquake hot spots: geodetic constraints on strain accumulation along faults in the Marmara seismic gap, Geophys. Res. Lett. 41 (16), 5783-5788.

Erkül, F., 2010. Tectonic significance of synextensional ductile shear zones within the Early Miocene Alaçamdağ granites, Northwestern Turkey, Geological Magazine, 147, 611-637.

Evans, A.G., Swift, E.R., Cunningham, J.P., Hill, R.W., Blewitt, G., Yunck, T.P., Lichten, S.M., Hatch, R.R., Malys, S., Bossler, J., 2002, The Global Positioning System Geodesy Odyssey, Navigation, 49(1), 7-34.

FIG Publication No. 49., 2010., Cost Effective GNSS Positioning Techniques., FIG Commission 5 Publication, Dr. Neil D. Weston, United States, Dr. Volker Schwieger, Germany.

Firuzan, E., 2008. Statistical Earthquake Frequency Analysis for Western Anatolia, Turkish Journal Of Earth Sciences, 17(4):741-762.

Gao, W., Gao, C., and Pan, S., 2017. A method of GPS/BDS/GLONASS combined RTK positioning for middle-long baseline with partial ambiguity resolution, Surv. Rev. 2017. 49. 212-220, doi:10.1179/1752270615Y.0000000047.

Glosdny, J., and Hetzel, R., 2007. Precise U-Pb ages of syn-extensional Miocene intru-

sions in the central Menderes Massif, Western Turkey, Geological Magazine 144, 235-246.

Grewal, M.S., and Andrews, A.P., 1993. Kalman Filtering Theory and Practice, Prentice Hall, USA.

Havazlı, 2012. Determination of Strain Accumulation Along Tuzla Fault, Ms Thesis.

Isik, V., Uysal, I.T., Caglayan, A., Seyitoglu, G., 2014. The evolution of intraplate fault systems in central Turkey: structural evidence and Ar-Ar and Rb-Sr age constraints for the Savcili Fault Zone, Tectonics, 33, 1875-1899, DOI: 10.1002/2014TC003565.

İlbey, A., 2015. World GIS Day Congress and Exhibition. General Directorate of Land Registry and Cadastre, Ankara.

İnce, C.D., 1999. Dinamik Sistemlerin GPS ve Kalman Filtresi ile Anlık Olarak İzlenmesi, Doktora Tezi, İstanbul Teknik Üniversitesi, İstanbul.

İnce, C.D., Sahin, M., 2000. Real-time deformation monitoring with GPS and Kalman Filter, Earth Planets and Space, 52(10): 837-840.

Jackson, J., 1994. Active tectonics of the Aegean region, Annual Review of Earth and Planetary Sciences, 22: 239-271.

Herring, T.A., King, R.W., McClusky, S.C., 2018. Introduction to GAMIT/GLOBK Release 10.7, Department of Earth Atmospheric and Planetary Sciences Massachusetts Institute of Technology.

Hollenstein, C., Müller, M.D., Geiger, A., Kahle, H.G., 2008, Crustal motion and deformation in Greece from a decade of GPS measurements, 1993-2003, Tectonophysics 449(1):17-40.

Kahveci, M., 2009. Kinematik GNNS ve RTK Cors Ağları, Zerpa Publisher, Ankara.

Kalman, R.E., 1960. A New Approach to Linear Filtering and Prediction Problems, Journal of Basic Engineering, pp. 35-45.

Koçbulut, F., Akpınar, Z., Tatar, O., Piper, J.D.A., Roberts, A.P., 2013. Palaeomagnetic study of the Karacadağ Volcanic Complex, SE Turkey: monitoring Neogene anticlockwise rotation of the Arabian Plate, Tectonophysics 608, 1007-1024.

Koçyiğit, Beyhan, B., 1998. A new intracontinental transcurrent structure: the Central Anatolian Fault Zone, Turkey, Tectonophysics, 284, 317-336.

Koçyiğit, A., and Özaçar, A., 2003. Extensional Neotectonic Regime through the NE Edge of the Outer Isparta Angle, SW Turkey, Turkish Journal of Earth Sciences, Vol. 12, pp. 67-90.

Kozacı, O., Dolan, J.F., Finkel, R., and Hartleb, R., 2007. Late Holocene Slip Rate for the North Anatolian Fault, Turkey from Cosmogenic 36Cl Geochronology: Implications for the Constancy of Fault Loading and Strain Release Rates, Geology, Vol. 35, pp. 867-870.

Landau, H., Vollath, U., and Chen, X., 2002. Virtual Reference Station Systems, Journal of Global Positioning Systems, Vol. 1, No. 2: pp. 137-143.

Le Pichon, X., Bergerat, F., and Roulet, M.J., 1988. Plate Kinematics and Tectonics Leading to the Alpine Belt Formation: A New Analysis, Geological Society of America, Vol. 218, pp. 111-131.

Le Pichon, X., Chamot-Rooke, N., Lallemant, S.L., Noomen, R., and Veis, G., 1995. Geodetic Determination of the Kinematics of Central Greece With Respect to Europe: implications for Eastern Mediterranean Tectonics, Journal of Geophysical Research, Vol. 100, pp. 12675-12690.

Le Pichon, X., and Kreemer, C., 2010. The miocene-to-present kinematic evolution of the Eastern Mediterranean and Middle East and its implications for dynamics,

Annu. Rev. Earth Planet. Sci. 38 (1), 323-351, 00046.

McClusky, S., Balassania, S., Barka, A., Demir, C., Ergintav, S., Georgiev I., Gürkan, O., Hamburger, M., Hurst, K., Kahle, H., Kastens, L., Kekelidze, G., King, R.W., Kotzev, V., Lenk, O., Mahmoud, S., Mishin, A., Nadariya, M., Ouzounis, A., Paradissis, D., Peter, Y., Prilepin, M., Reilinger R., Şanlı, I., Seeger, H., Taeleb, A., Toksoz, M.N., and Veis, G., 2000. GPS Constraints on Plate Motions and Deformation in the Eastern Mediterranean: Implications for Plate Dynamics, Journal of Geophysical Research, V. B105, No. B3, pp. 5695-5719.

McKenzie, D.P., 1970. Plate tectonics of the Mediterranean Region, Nature, 226, pp. 239-243.

McKenzie, D., 1978. Active Tectonics of the Alpine-Himalayan Belt: the Aegean Sea and Surrounding Regions, Geophysical Journal of the Royal Astronomical Society, Vol. 55, pp. 217-254.

Mekik, C., Yildirim, O., and Bakici, S., 2011. The Turkish Real Time Kinematic GPS Network (TUSAGA-Aktif) Infrastructure, Scientific research and essays 6 (19) DOI: 10.5897/SRE10.923.

NovAtel Inc, 2015. Introduction to GNSS, Second Edition. https://www.novatel.com/an-introduction-to-gnss/

Oral, M.B., Reilinger, R.E., Toksöz, M.N., King, R.W., Barka, A.A., Kınık, İ., et al., 1995. Global positioning system offers evidence of plate motions in eastern Mediterranean, EOS Transaction, 76, 9.

Öcalan, T., and Tunalıoğlu, N., 2010. Data communication for real-time positioning and navigation in global navigation satellite systems (GNSS)/continuously operating reference stations (CORS) networks, Scientific Research and Essays, Vol.5, Number:18.

Özdemir, S., 2019. Transient signal detection in continuous GPS coordinate time series using empirical mode decomposition and principal component analysis, PhD Thesis, July 2019.

Özdemir, S., and Karslıoğlu, M.O., 2019. Soft clustering of GPS velocities from a homogeneous network in Turkey, J Geodesy. https://doi.org/10.1007/s00190-019-01235-z.

Özener, H., Doğru, A., Turgut, B., Yılmaz, O., Ergintav, S., Çakmak, R., Doğan, U., and Arpat, E., 2010. Kinematics of the Eastern Part of the North Anatolian Fault Zone, Journal of Geodynamics, Vol. 49, pp. 141-150.

Pasquare, G., Poli, S., Vezzoli, L., and Zanchi, A., 1988. Continental arc volcanism and tectonic setting in Central Anatolia, Tectonophysics, 146, 217-230.

Piper, J.D.A., Gürsoy, H., Tatar, O., Beck, M.E., Rao, A., Koçbulut, F., and Mesci, B.L., 2010. Distributed neotectonic deformation in the Anatolides of Turkey: A palaeomagnetic analysis, Tectonophysics, 488(1), 31-50.

Povero, G., 2019. GNSS Signals Introduction. https://www.gsc-europa.eu/electronic-library.

Raquet, J.F., 1998. Development Of A Method For Kinematic GPS Carrier-Phase Ambiguity Resolution Using Multiple Reference Receivers, PhD Thesis, Dept. of Geomatics Engineering, University of Calgary, Canada.

Reilinger, R.E., McCLusky, S.C., Oral, M.B., King, R.W., and Toksöz, M.N., 1997. Global Positioning System Measurements of Present-Day Crustal Movements in the Arabia-Africa-Eurasia Plate Collision Zone, Journal of Geophysical Research, Vol. 102. pp. 9983-9999.

Reilinger, R., McClusky, S., Vernant, P., Lawrence, S., Ergintav, S., Cakmak, R., Özener, H., Kadirov, F., Guliev, I., Stepanyan, R., Nadariya, M., Hahubia, G.,

Mahmoud, S., Sakr, K., ArRajehi, A., Paradissis, D., Al-Aydrus, A., Prilepin, M., Guseva, T., Evren, E., Dmitrotsa, A., Filikov, S.V., Gomez, F., Al-Ghazzi, R., Karam, G., 2006. GPS constraints on continental deformation in the Africa-Arabia-Eurasia continental collision zone and implications for the dynamics of plate interactions, J. Geophys. Res., Solid Earth 111 (B5), B05411.

Reilinger, R., McClusky, S., Paradisis, D., Ergintav, S., Vernant, P., 2010. Geodetic constraints on the tectonic evolution of the Aegean region and strain accumulation along the Hellenic subduction zone, Tectonophysics 488, 22-30. https:// doi. org/ 10. 1016/j. tecto. 2009. 05. 027.

Seyitoğlu, G., Kazancı, N., Karakuş, K., Fodor, L., Araz, H., and Karadenizli, L., 1997. Does continuous compressive tectonic regime exist during Late Palaeogene to Late Neogene in NW Central Anatolia, Turkey' Preliminary observations, Turkish Journal of Earth Sciences 6, 77-83.

Şengör, A.M.C., Görür, N., and Saroğlu, F., 1985. Strike-Slip Faulting and Related Basin Formation in Zones of Tectonic Escape: Turkey as a Case Study, Society of Economic Paleontologists and Mineralogists, Special Publication, Tulsa, OK.

Şengör, A.M.C., Tüysüz, O., İmren, C., Sakınç, M., Eyidoğan, H., Görür, N., Le Pichon, X., and Rangin, C.C., 2005. The North Anatolian Fault: A New Look, Annual Review of Earth and Planetary Sciences, Vol. 33, pp. 1-75.

Taymaz, T., Jackson, J., and McKenzie, D., 1991. Active Tectonic of North and Central Agean Sea, Geophysical Journal International, Vol. 106, pp. 433-490.

Tetteyfio, I., GPS Technology, 2007. Analysis of Data From the GPS Reference Station at AAU Using GAMIT.

Tatar, O., et al., 2012. Crustal deformation and kinematics of the Eastern Part of the North Anatolian Fault Zone (Turkey) from GPS measurements, Tectonophysics 518-521, 55-62. http://dx.doi.org/10.1016/j.tecto.2011.11.010.

Taymaz, T., Jackson, J., and McKenzie, D., 1991. Active Tectonic of North and Central Agean Sea. Geophysical Journal International Vol. 106, pp. 433-490.

Tsai, C., Kurz, L., 1983. An adaptive robustifying approach to Kalman filtering, Automatica, 19:279-288.

Tonarini, S., Agostini, S., Innocenti, F., and Manetti, P., 2005. d11B as tracer of slab dehydration and mantle evolution in western Anatolia Cenozoic magmatizm, TerraNova, 17, 259-264.

Uzel, B., Sözbilir, H., Özkaymak, Ç., 2012. Neotectonic evolution of an actively growing superimposed basin in western Anatolia: the inner bay of Izmir, Turkey, Turk. J. Earth Sci. 22 (4), 439-471. http://dx.doi.org/10.3906/yer-0910-11.

Vollath, U., Buecherl, A., Landau, H., Pagels, C., Wager, B., 2000. Multi-base RTK positioning using virtual reference stations, Proc 13th Int. Tech. Meeting of the Satellite Division of the U.S. Inst. of Navigation, ION GPS-2000, Salt Lake City, September 19-22, 123-131.

Vollath U., Buecherl, A., and Landau, H., 2001. Long-Range RTK Positioning Using Virtual Reference Stations, Proceedings of the International Symposium on Kinematic Systems in Geodesy, Geomatics and Navigation, KIS 2001 (June 2001, Banff. Canada), Department of Geomatics Engineering, University of Calgary, 470-474.

Yıldırım, Ö., Bakıcı, S., Cingöz, A., Erkan, Y., Gülal, E., Dindar, A., 2007. TUSAGA-Aktif (CORS-TR) Projesi Ve Ülkemize Katkıları, TMMOB Harita ve Kadastro Mühendisleri Odası Ulusal Coğrafi Bilgi Sistemleri Kongresi, 30 Ekim-02 Kasım 2007, KTÜ, Trabzon.

Yılmaz, Y., Genç, S.C., Gürer, O.F., Bozu, M., Yılmaz, K., Karacık, Z., Altunkayak, and Elmas, A., 2000. When did the western Anatolian grabens begin to develop' In: Bozkurt, E., Winchester, J.A., and Piper, J.D.A., (eds), Tectonics and Mag-

matism in Turkey and the Surrounding Area, Geological Society, London, Special Publications 173, 353-384.

Yılmaz, Y., Şaroğlu, F., and Goner, Y., 1987. Initiation of the neomagmatism in East Anatolia, Tectonophysics, 134, 177-199.

Walters, R.J., Parsons, B., Wright, T.J., 2014. Constraining crustal velocity fields with InSAR for Eastern Turkey: limits to the block-like behavior of Eastern Anatolia, J. Geophys. Res., Solid Earth 119 (6), 5215-5234.

Welch, G., Bishop, G., 2001. An Introduction to the Kalman Filter, University of North Carolina at Chapel Hill, ACM Inc. Publication, Los Angeles.

Welch, G., Bishop, G., 2002. An Introduction to the Kalman Filter, Department of Computer Science, University of North Carolina at Chapel Hill.

Wessel, P., Smith, W.H.F., 1998. New, improved version of the generic mapping tools released, Geosci Union 79:579.

Westaway, R., 1994. Evidence for dynamic coupling of surface processes with isostatic compensation in the lower crust during active extension of western Turkey, Journal of Geophyical Research 99, 20203-20223.

Wübbena, G., Willgalis, S., 2001. State Space Approach for Precise Real Time Positioning in GPS Reference Networks, Presented at International Symposium on Kinematic Systems in Geodesy, Geomatics and Navigation, KIS-01, Banff. June 5-8, Canada.

Web Sites:

https://www.igs.org/about

https://www.gsa.europa.eu/gsa/organisation

http:/www.koeri.boun.edu.tr/sismo/2/wp-content/uploads/2014/08/turkiye_aletsel.png

https://www.lockheedmartin.com/en-us/products/gps.html

https://www.gpsworld.com

APPENDIX A: PROCESS.DEFAULTS

```
      # process.defaults
#
# Do not remove any of these entries. To by-pass a function. set the value to null: ""

## LOCAL DIRECTORIES
# Directory for translation of raw data set rawpth = "$procdir/raw"
# Directory path for raw archives (search all levels); e.g. /data18/simon
set rawfnd = ""
# Input files for RINEX translators
set mpth = "$procdir/mkrinex"
# RINEX files directory
set rpth = "$procdir/rinex"
# Directory path for RINEX archives (search all levels); e.g. /data18/simon set rnxfnd
= ""
# Broadcast orbit directory
set bpth = "$procdir/brdc"
# IGS files directory
set ipth = "$procdir/igs"
# G-files directory
set gpth = "$procdir/gfiles"
# GAMIT and GLOBK tables directory
set tpth = "$procdir/tables"
# Output directory for skyplots
set gifpth = "$procdir/figs"
# Globk solution directory
set glbpth = "$procdir/gsoln"
# Globk binary h-file directory
set glfpth = "$procdir/glbf"
# Directory path for other h-files (LA. LB. LC options; search all levels)
```

e.g. "/raid1/tah/SIO_GLL"; (/raid6/ftp/pub/MIT_GLL/H07 /raid2/simon/gps_analysis/cgps _hfiles)
set hfnd = ""
Template files
set templatepth = "$procdir/templates"
Place to store temporary control files
set cpth = "$procdir/control"
Archive root directory (cannot be null)
set archivepth = "$procdir/archive"

FTP INFO FOR REMOTE FILES
Raw data archive
set rawarchive = 'chandler.mit.edu'
set rawdir = 'pub/continuous/mitnet'
set rawlogin = "anonymous simon@chandler.mit.edu"
Addresses for CDDSI. SOPAC. IGSCB. UNAVCO. BKG. IGN. USNO are given in template/ftp_info

##GAMIT
Set sampling interval. number of epochs. and start time for processing
set sint = '30'

set nepc = '2880'
set stime = '0 0'
Variables for updating tables
set stinf_unique = "-u"
set stinf_nosort = "-nosort"
set stinf_slthgt = "2.00"
Set "Y" to use RINEX header coordinates not in lfile or apr file
set use_rxc = "N"
Broadcast orbits
set brdc = 'brdc'

Minimum x-file size to be processed (Def. 300 blocks; most OS use 1 Kb blocks)
set minxf = '300'
Set search window for RINEX files which might contain data for day - default check the previous day
set rx_doy_plus = 0
set rx_doy_minus = 1
Default globk .apr file
set aprf = igs14_comb.apr
Set compress (copts). delete (dopts) and archive (aopts) options. (Don't forget to set the archivepth.)
Possible d-. c-. and a- opts: D. H. ao. ac. as. b. c. d. e. g. h. i. j. k. l. m. o. p. q. t. x. ps. all"
set dopts = (c)
set copts = (x k ao)
set aopts = "
Set the rinex ftp archives (defined in ftp_info) you would like to look for data in.
(Default archives searched are: sopac. cddis and unavco).
set rinex_ftpsites = (cddis sopac unavco)

RESOURCES
Minimum raw disk space in Mbytes
set minraw = '100'
Minimum rinex disk space in Mbytes
set minrinex = '100'
Minimum archive disk space in Mbytes
set minarchive = '100'
Minimum working disk space in Mbytes
set minwork = '500'

SYSTEM-DEPENDENT SETTINGS
UNIX df command must be set to return the correct form
Most machines (

set udf = 'df -mk'

but note that if you have free > 1 Tb. you will need to change this to Mb

set udf = 'df -m'

HP

set udf = 'bdf'

UNIX mail command

Most machines

set umail = 'mail -s'

HP

set umail = 'mailx -s'

Mail address for sending the processing report (if " will default to 'whoami' in sh_gamit)

set mailto = "

Host name for email and anonymous ftp password use (if " will default to 'hostname' in sh_gamit)

set machine = "

Ghostscript path

set gspath = '/usr/bin'

ImageMagick path fir png conversion

set impath = '/usr/bin/X11'

set impath = '/usr/bin'

APPENDIX B: SITES DEFAULTS

```
     # File to control the use of stations in the processing
#
# Format: site expt keyword1 keyword2 ....
#
# where the first token is the 4- or 8-character site name (GAMIT uses only
# 4 characters. GLOBK allows only 4 unless there are earthquakes or renames).
# the second token is the 4-character experiment name. and the remaining
# tokens. read free-format. indicate how the site is to be used in the processing.
# All sites for which there are RINEX files in the local directory will be used
# automatically and do not need to be listed.
#
# ftprnx = sites to ftp from rinex data archives.
# ftpraw = sites to ftp from raw data archives.
# localrx = site names used to search for rinex files on your local system.
# (required in conjunction with rnxfnd path variable set in process.defaults).
# xstinfo = sites to exclude from automatic station.info updating.
# xsite = sites to exclude from processing. all days or specified days
#
# Replace 'expt' with your experiment name and edit the following to list sites needed
from external archive

#IGS stations
zeck_gps ders ftprnx xstinfo
nico_gps ders ftprnx xstinfo
orid_gps ders ftprnx xstinfo
bucu_gps ders ftprnx xstinfo
bshm_gps ders ftprnx xstinfo
mate_gps ders ftprnx xstinfo
pots_gps ders ftprnx xstinfo
```

not1_gps ders ftprnx xstinfo
graz_gps ders ftprnx xstinfo
gras_gps ders ftprnx xstinfo
bor1_gps ders ftprnx xstinfo
ajac_gps ders ftprnx xstinfo
wtzr_gps ders ftprnx xstinfo
madr_gps ders ftprnx xstinfo
zwe2_gps ders ftprnx xstinfo
ramo_gps ders ftprnx xstinfo

#Local stations
afyn_gps ders localrx xstinfo
ayd1_gps ders localrx xstinfo
ayvl_gps ders localrx xstinfo
balk_gps ders localrx xstinfo
cav1_gps ders localrx xstinfo
cesm_gps ders localrx xstinfo
dina_gps ders localrx xstinfo
didi_gps ders localrx xstinfo
feth_gps ders localrx xstinfo
harc_gps ders localrx xstinfo
ispt_gps ders localrx xstinfo
izmi_gps ders localrx xstinfo
kika_gps ders localrx xstinfo
kuta_gps ders localrx xstinfo
salh_gps ders localrx xstinfo
usak_gps ders localrx xstinfo

templates for removing sites
ttth_gps expt xsite:1999_256-1999_278 xsite:1999_300-1999_365

APPENDIX C: SESSION TABLE

Session Table

Processing Agency = MIT

Satellite Constraint = Y; Y/N (next two lines are free-format but 'all' must be present)
all a e i n w M rad1 rad2 rad3 rad4 rad5 rad6 rad7 rad8 rad9;
0.01 0.01 0.01 0.01 0.01 0.01 0.01 0.01 0.01 0.01 0.01 0.01 0.01 0.01 0.01

<< Controls must begin in column 1 >>

Choice of Experiment = BASELINE ; BASELINE/RELAX./ORBIT
Type of Analysis = 1-ITER ; 1-ITER(autcln prefit and conditional redo) / 0-ITER (no postfit autcln) / PREFIT
AUTCLN redo = Y ; Y/N; 3rd soln only if needed. assume 'Y' if 'Type of analysis = 1-ITER'
Choice of Observable = LC_AUTCLN ; LC_AUTCLN (default). LC_HELP (codeless L2). L1_ONLY (L1 soln from dual freq).
L2_ONLY (L2 soln from dual freq). L1.L2_INDEPENDENT (L1 + L2 from dual freq)
L1&L2 (same as L1.L2_INDEPENDENT but with ion constraint);
L1_RECEIVER (must add 'L1only' in autcln.cmd)
Station Error = ELEVATION 10 5 ; 1-way L1. a**2 + (b**2)/(sin(elev)**2) in mm. default = 10. 0.
AUTCLN reweight = Y ; Y/N; reweight data from autcln rms; replaces 'Use N-file' in releases < 10.32

AUTCLN Command File = autcln.cmd ; Filename; default none (use default options)
Decimation Factor = 4 ; FOR SOLVE. default = 1
Quick-pre decimation factor = 10 ; 1st iter or autcln pre. default same as Decimation Factor

Quick-pre observable = LC_ONLY ; for 1st soln. default same as Choice of observable

Ionospheric Constraints = 0.0 mm + 8.00 ppm
Ambiguity resolution WL = 0.15 0.15 1000. 99. 15000. ; for LC_HELP. ignored for LC_AUTCLN
Ambiguity resolution NL = 0.15 0.15 1000. 99. 15000. ; allow long baselines with LC_AUTCLN

Zenith Delay Estimation = Y ; Yes/No (default No)
Interval zen = 2 ; 2 hrs = 13 knots/day (default is 1 ZD per day)
Zenith Constraints = 0.50 ; zenith-delay a priori constraint in meters (default 0.5)
Zenith Variation = 0.02 100. ; zenith-delay variation. tau in meters/sqrt(hr). hrs (default .02 100.)
Elevation Cutoff = 0 ; default 0 to use value in autcln.cmd
Atmospheric gradients = Y ; Yes/Np (default No)
Number gradients = 2 ; number of gradient parameters per day (NS or ES); default 1
Gradient Constraints = 0.01 ; gradient at 10 deg elevation in meters; default 0.03 m

Update T/L files = L_ONLY ; T_AND_L (default). T_ONLY. L_ONLY. NONE
Update tolerance = .3 ; minimum adjustment for updating L-file coordinates. default .3 m

Met obs source = GPT 50 ; hierarchical list with humidity value at the end; e.g. RNX UFL GPT 50 ; default GTP 50
if [humid value] < 0. use RNX. UFL(VMF1). or GPT2 if available
Output met = N ; write the a priori met values to a z-file (Y/N)
Use met.list = N ; not yet supported
Use met.grid = N ; not yet supported
DMap = GMF ; GMF(default)/VMF1/NMFH; GMF now invokes GPT2 if gpt.grid is available (default)
WMap = GMF ; GMF(default)/VMF1/NMFW; GMF now invokes GPT2 if gpt.grid

is available (default)
Use map.list = N ; VMF1 list file with mapping functions. ZHD. ZWD. P. Pw. T. Ht
Use map.grid = N ; VMF1 grid file with mapping functions and ZHD
Yaw Model = Y ; Y/N default = Y
Radiation Model for ARC = BERNE ; BERNE/BERN2/UCLR1/UCLR2/NONE default = BERNE
Earth radiation model = NONE ; NCLE1/NCLE2/TUME1/TUME2/NONE default = NONE; MIT repro2 = NCLE1
Antenna thrust model = NONE ; ANTBK/NONE default = NONE; MIT repro2 = ANTBK
Inertial frame = J2000 ; J2000/B1950 default = J2000
Reference System for ARC = EGM08 ; WGS84/EGM96/EGM08/EGR08 default = EGM008; MIT repro2 = EGR08 (relativity)

Tides applied = 31 ; Binary coded: 1 earth 2 freq-dep 4 pole 8 ocean 16 remove mean for pole tide

; 32 atmosphere ; default = 31
Use otl.list = N ; Ocean tidal loading list file from OSO

Use otl.grid = Y ; Ocean tidal loading grid file. GAMIT-format converted from OSO
Etide model = IERS03 ; IERS96/IERS03
Earth Rotation = 11 ; Diurnal/Semidirunal terms: Binary coded: 1=pole 2=UT1 4=Ray model; 8=IERS2010 16=include libration terms; default=11
Apply atm loading = N ; Y/N for atmospheric loading
Use atml.list = N ; Atmospheric (non-tidal) loading list file from LU
Use atml.grid = N ; Atmospheric (non-tidal) loading grid file from LU. converted to GAMIT format
Use atl.list = N ; Atmospheric tides. list file. not yet available
Use atl.grid = N ; Atmospheric tides. grid file

Antenna Model = AZEL ; NONE/ELEV/AZEL default = ELEV Use AZEL for IGS

absolute ANTEX files
SV antenna model = ELEV ; NONE/ELEV default = NONE Use ELEV for IGS ANTEX files
SV antenna off = N ; Y/N to estimate satellite antenna offsets (default N)

Delete AUTCLN input C-files = Y ; Y/N ; default Y to force rerun of MODEL
Scratch directory = /tmp

<< List of additional controls not commonly - blank first column to indicate a comment >>

Simulation con : s-file name
Inertial frame = B1950 ; B1950/J2000 (default = J2000)

Initial ARC ; Y/N default = Yes
Final ARC ; Y/N default = No
Radiation Model for ARC ; SPHRC/BERNE/SRDYB/SVBDY default = SPHRC
Reference System for ARC ; WGS72/WGS84/MERIT/IGS92/EGM96/EGM08(incremental_updat
(default = EGM08)
Reference System for ARC = EGM08 ; WGS72/WGS84/MERIT/IGS92/EGM96/EGM08/EGR08
default = EGM008; MIT repro2 = EGR08 (relativity)

Tabular interval for ARC ; 900. seconds (new default). 1350. seconds (old default)
Stepsize for ARC ; 75. seconds (new default). 168.75 seconds (old default)
Arc debug flag : Turn on various print and test options (see arc.f) (default = 0)

Earth Rotation ; Diurnal/Semidirunal terms: Binary coded: 1=pole 2=UT1 4=Ray model; 8=IERS2010 ; default=11
Estimate EOP ; Binary coded: 1 wob 2 ut1 4 wob rate 8 ut1 rate

Wobble Constraint = 3. 0.3 ; Default 3. (arcsec) 0.3

(arcsec/day)
UT1 Constraint = 0.00002 0.02 ; Default .00002 (sec) 0.02 (sec/day)

Number Zen = 4 ; number of zenith-delay parameters (default 1)

Zenith Constraints = 0.50 ; zenith-delay a priori constraint in meters (default 0.5)
Zenith Model = PWL ; PWL (piecewise linear)/CON (step)
Zenith Variation = 0.02 100. ; zenith-delay variation. tau in meters/sqrt(hr). hrs (default .02 100.)
Gradient Constraints = 0.03 ; gradient at 10 deg elevation in meters
Gradient Variation = .01 100 ; gradient variation
Tropospheric Constraints = NO ; YES/NO (spatial constraint)

Ion model = NONE ; NONE/GMAP (default NONE) use 2nd/3rd order ionsopheric corrections
Mag field = IGRF12 : IGRF12/IGRF11/IGRF10/DIPOLE (default IGRF12)

Yaw Model ; YES/NO default = YES
I-file = N ; Use I-file (Y/N) (default Y)

AUTCLN Postfit = Y ; Assume 'Y' if 'Type of analysis = 1-ITER' (autcln.cmd.postfit file also)
Delete AUTCLN input C-files = Y ; YES/NO/Intermediate (default no)
AUTCLN Command File ; Filename; default none (use default options)
Delete eclipse data = POST ; ALL/NO/POST (Default = NO)
SCANDD control ; BOTH (default) /NONE/FIRST/FULL/IFBAD see manual sec. 5.2
Iteration ; CFILES / XFILES (default)
Edit AUTCLN Command File ; YES/NO; default = NO (For clocks. no longer needed)

Ambiguity resolution WL ; default = 0.15 0.15 1000. 10. 500.
Ambiguity resolution NL ; default = 0.15 0.15 1000. 10. 500.

Type of Biases : IMPLICIT (default for quick). EXPLICIT (default for full)
H-file solutions ; ALL ; LOOSE-ONLY
Skip loose : Y / N (default) sometimes necessary for short baselines
Station Error = BASELINE 10. 0. ; 1-way L1. a**2 + (b**2)(L**2) in mm. ppm. default = 10. 0.
Station Error = UNIFORM 10. ; 1-way L1 in mm. default = 10.
Station Error = ELEVATION 4.3 7.0 ; 1-way L1 . a**2 + b**2/sin(elev)**2 in mm. default = 4.3 7.0
Satellite Error = UNIFORM 0. ; 1-way L1 in mm (added quadratically to station error) default = 0.
Select Epochs ; Enter start and stop epoch number (applies only to SOLVE)
Decimation Factor ; FOR SOLVE. default = 1
Elevation Cutoff = 15. ; For SOLVE. overrides the MODEL or AUTCLN values if they are lower
Correlation print ; Threshhold for printing correlations (default 0.9999)

Export Orbits ; YES/NO default = NO

Orbit id ; 4-char code read only if Export Orbits = YES
Orbit Format ; SP1/SP3 (NGS Standard Products)
Orbit organization ; 3-char code read only if Export Orbits = YES
Reference System for Orbit = ITR93 ; ITR92/ITR91/ITR90/WGS84/MERIT (for SP3 header)

Reference System for ARC = EGM08 ; WGS84/EGM96/EGM08/EGR08 default = EGM008; MIT repro2 = EGR08 (relativity)

Lunar eclipses = Y ; Set = N to turn off lunar eclipses in ARC to match model of GAMIT < 10.2 (default Y)
(no longer supported: see arc_debug below)
Delete all input C-files ; YES/NO default = NO
Delete MODEL input C-files ; YES/NO default = NO

Delete AUTCLN input C-files ; YES/NO default = NO

Update T/L files ; T_AND_L (default). T_ONLY. L_ONLY. NONE

(Applies only to update for final solution after initial)

Update tolerance ; minimum adjustment for updating L-file coordinates. default .3 m

SOLVE-only = YES ; YES/NO default = NO

X-compress = YES ; Uncompress/compress X-files default = NO

SCANDD control ; FULL (default). FIRST. BOTH. IFBAD.NONE

Run CTOX = YES ; Make clean X-files from C-files default = NO

Bias apriori = 100. ; Optional constraint on biases for LC_AUTCLN (default 0 -> no constrint)

SOLVE print = Y ; Turn on SOLVE output to screen (default N)

Bias apriori = 1000. ; Optional constraint on biases for LC_AUTCLN (default 1000. 0 -> constraint)

Bias rcond = 10000. ; Condition number ratio for fixing dependent biases (default 10000.)

APPENDIX D: CORS-TR

In this chapter. long-term coordinate time series of 16 CORS-TR reference stations were demonstrated with three graphs for each station between the years of 2015 and 2018. Reference station velocities were acquired from trend analysis by time series which were generated by daily precise coordinates combined with Kalman analysis.

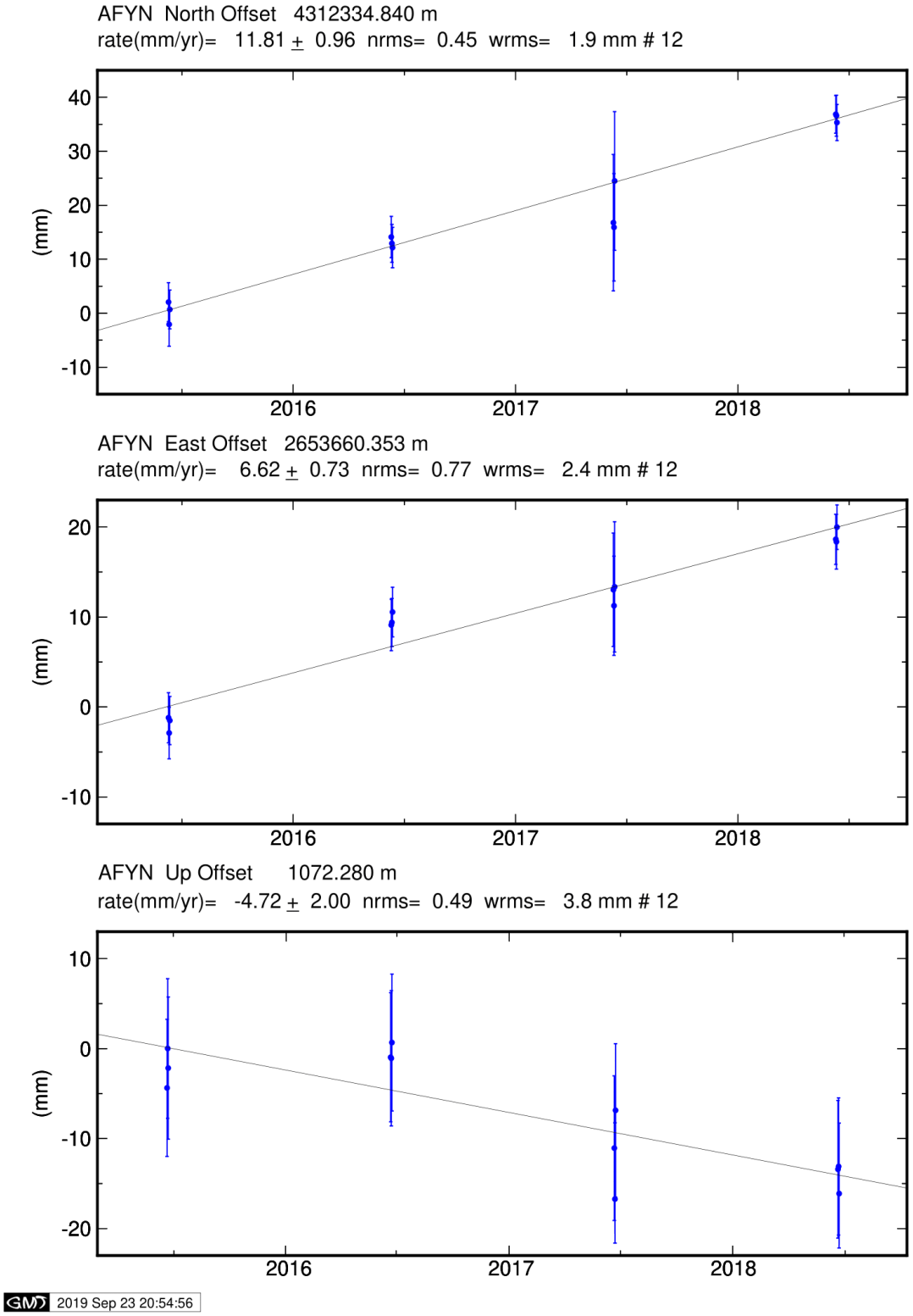


Figure D.1. AFYN station coordinate-time series.

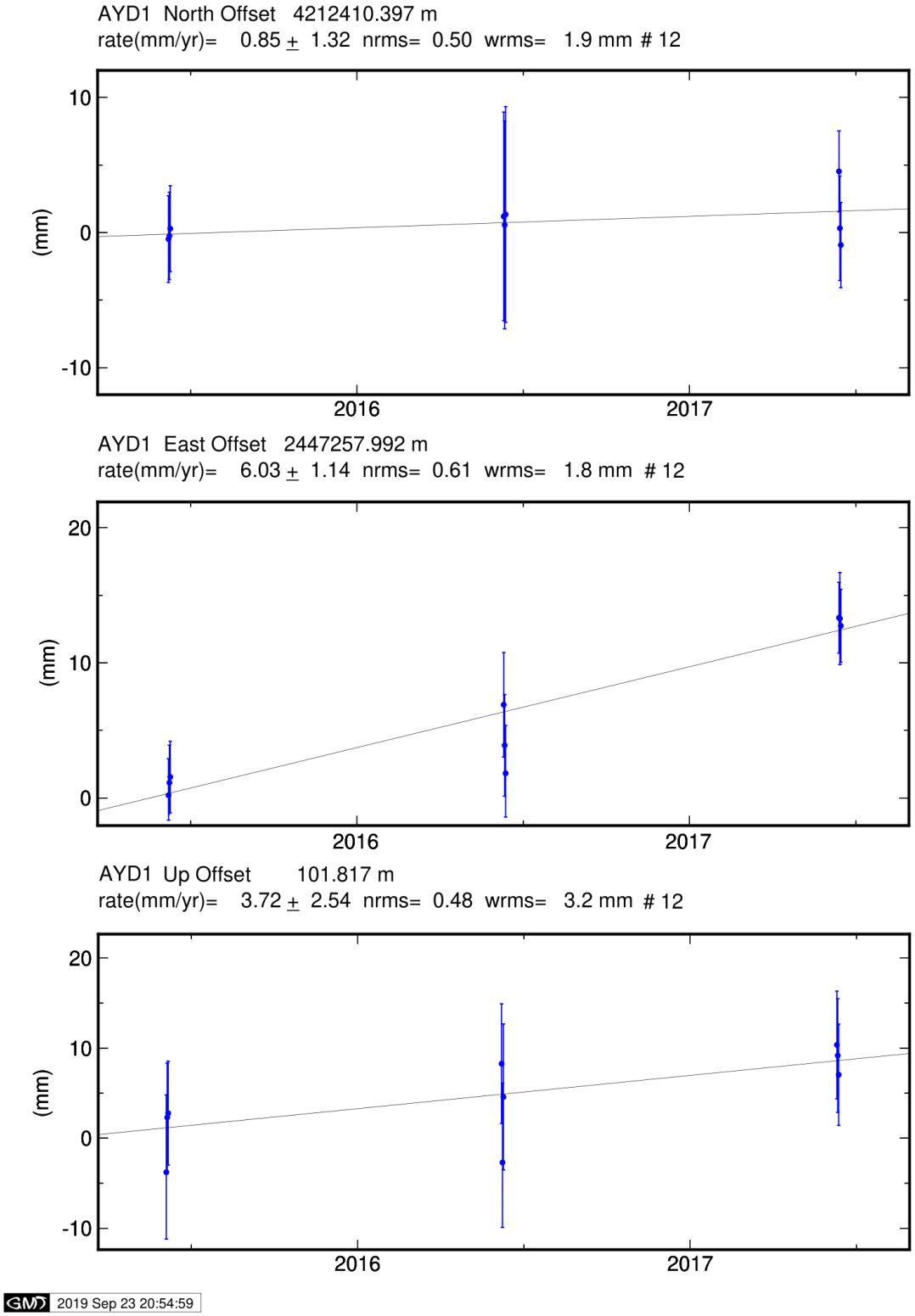


Figure D.2. AYD1 station coordinate-time series.

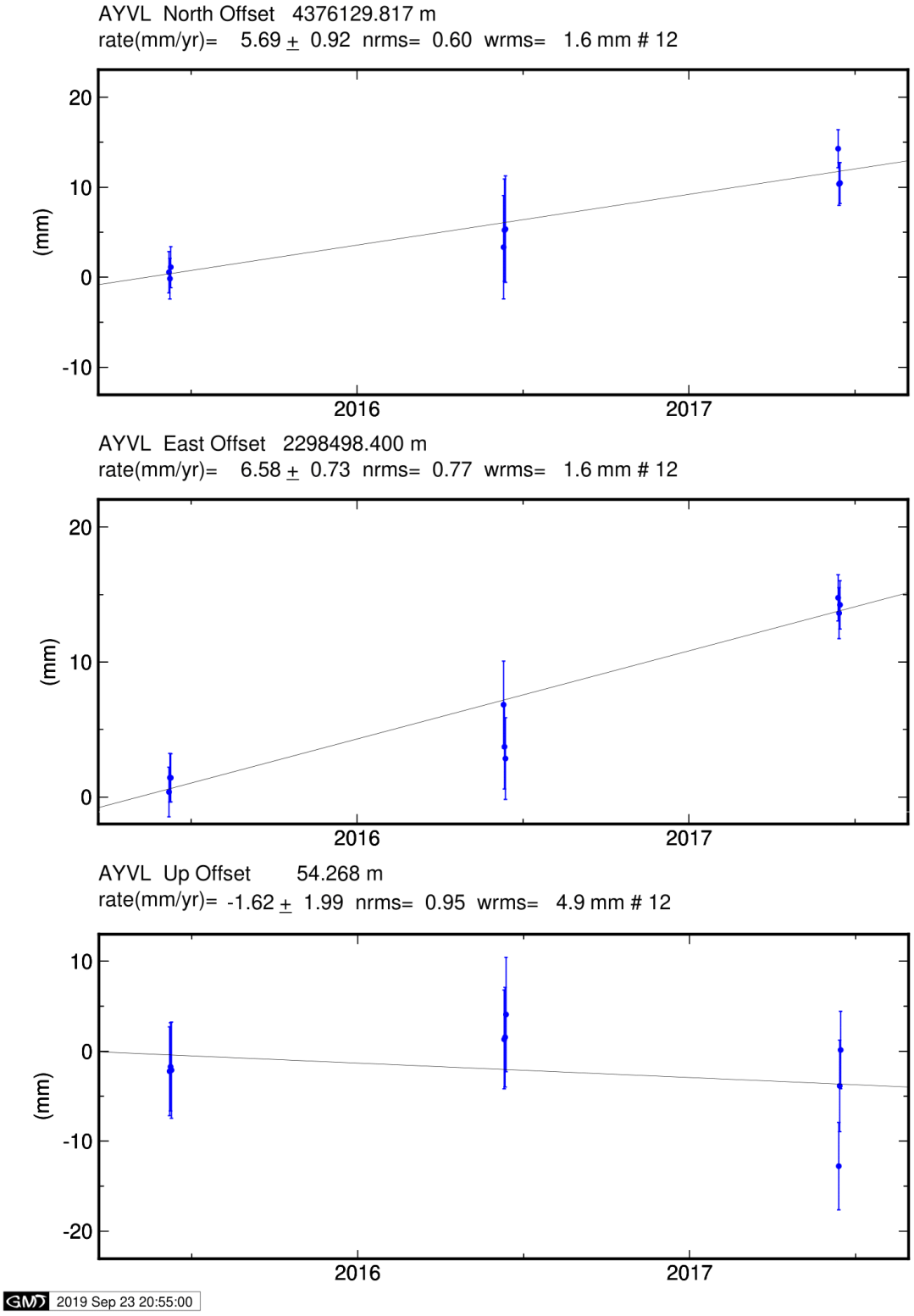


Figure D.3. AYVL station coordinate-time series.

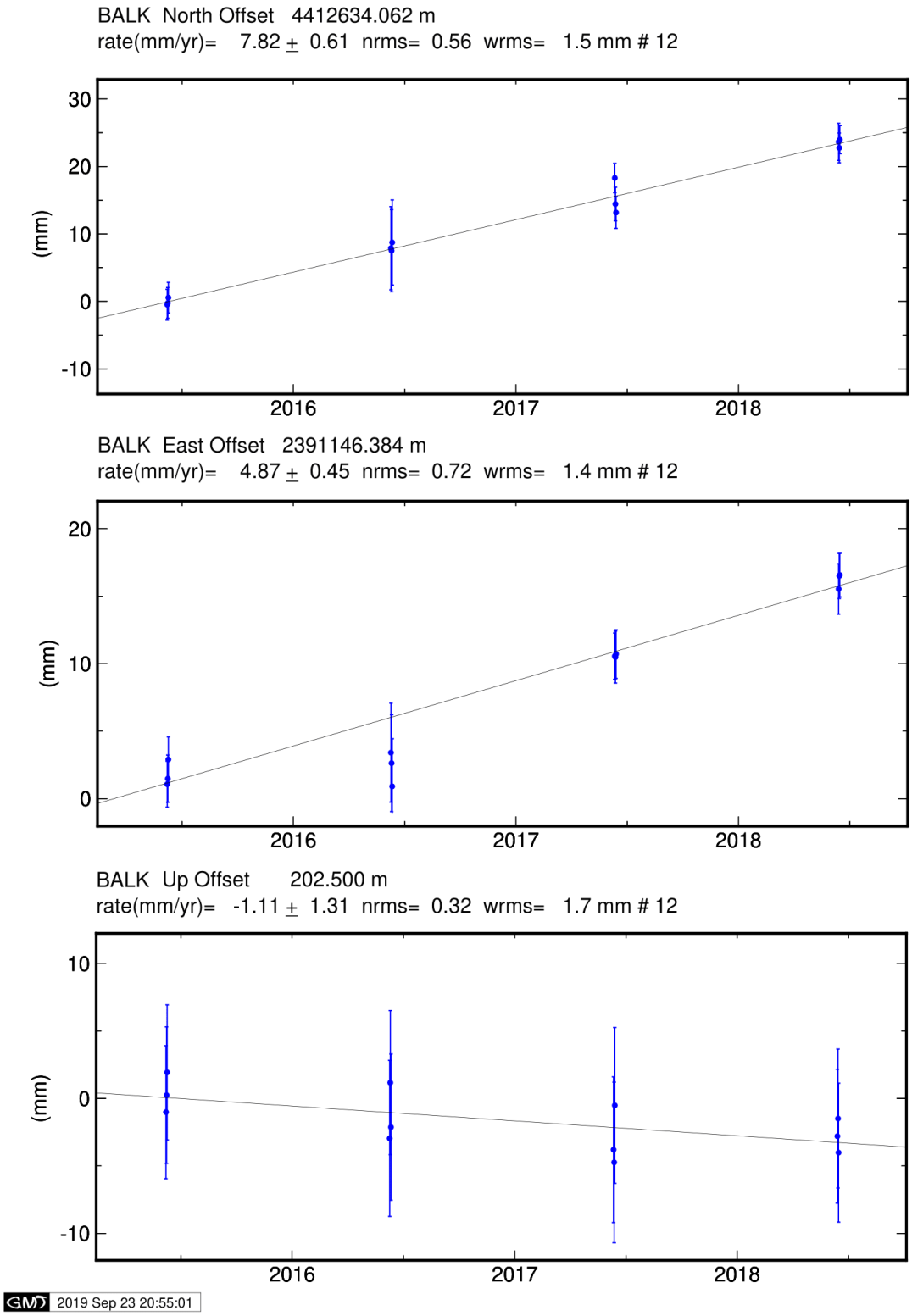


Figure D.4. BALK station coordinate-time series.

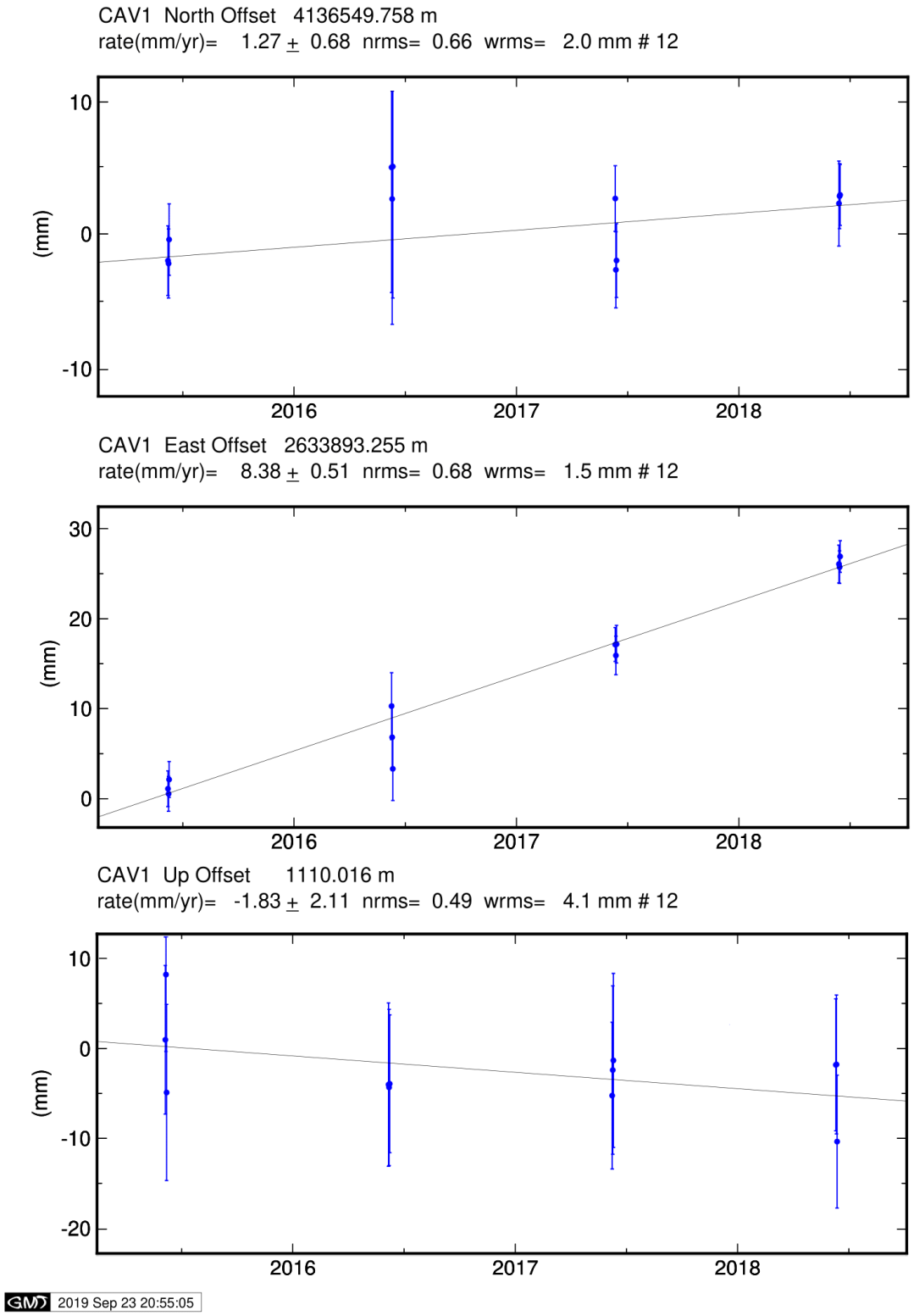


Figure D.5. CAV1 station coordinate-time series.

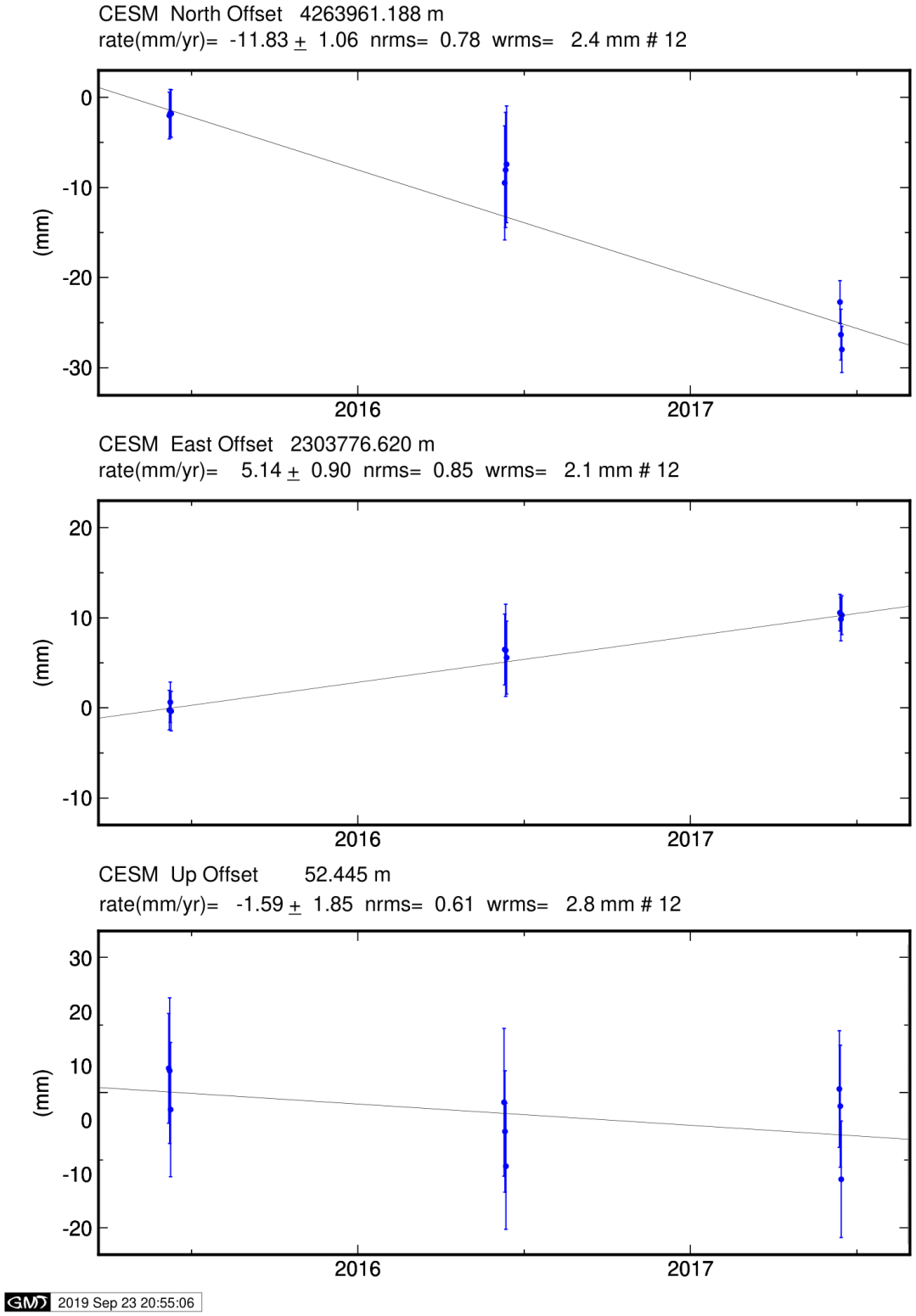


Figure D.6. CESM station coordinate-time series.

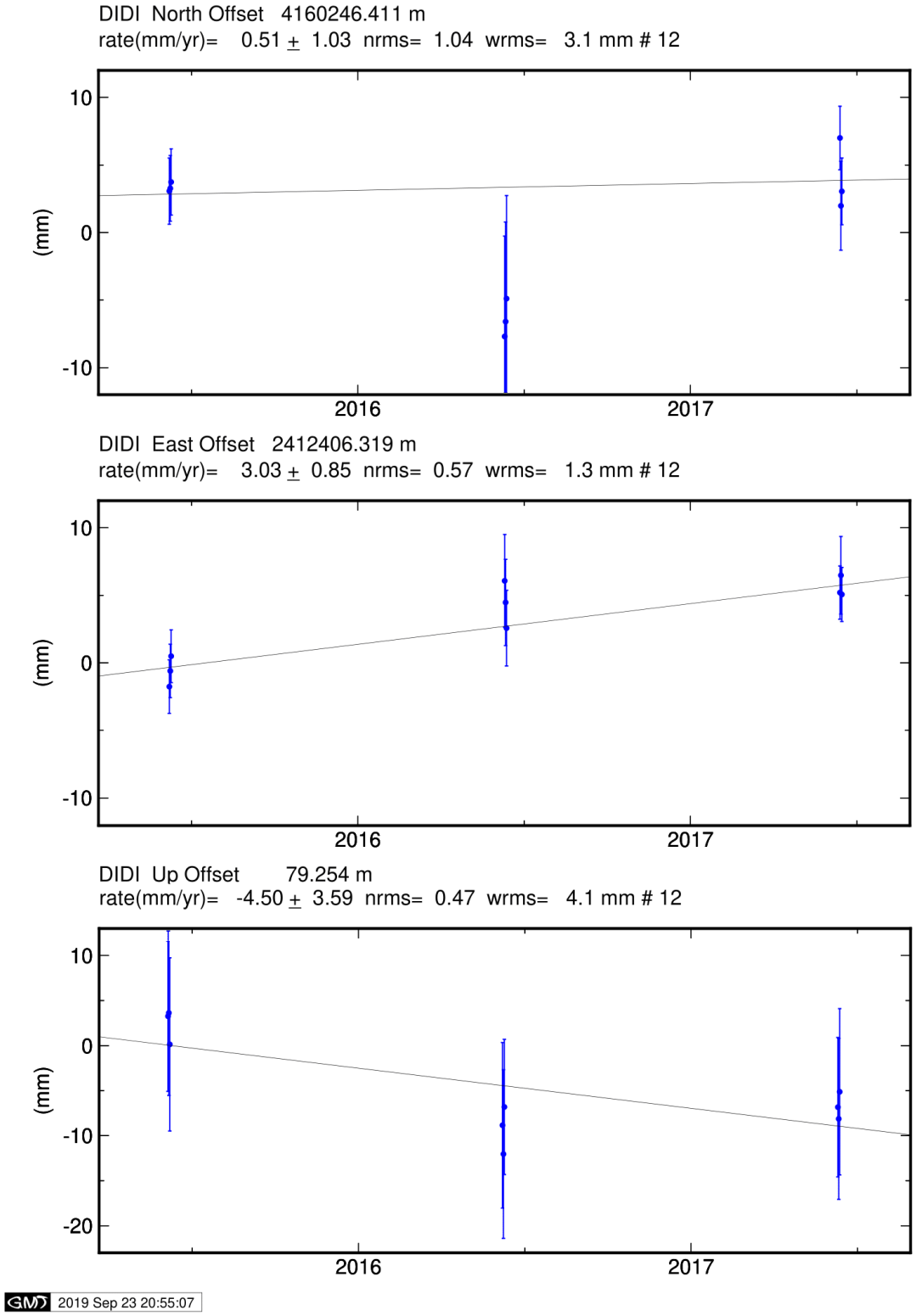


Figure D.7. DIDI station coordinate-time series.

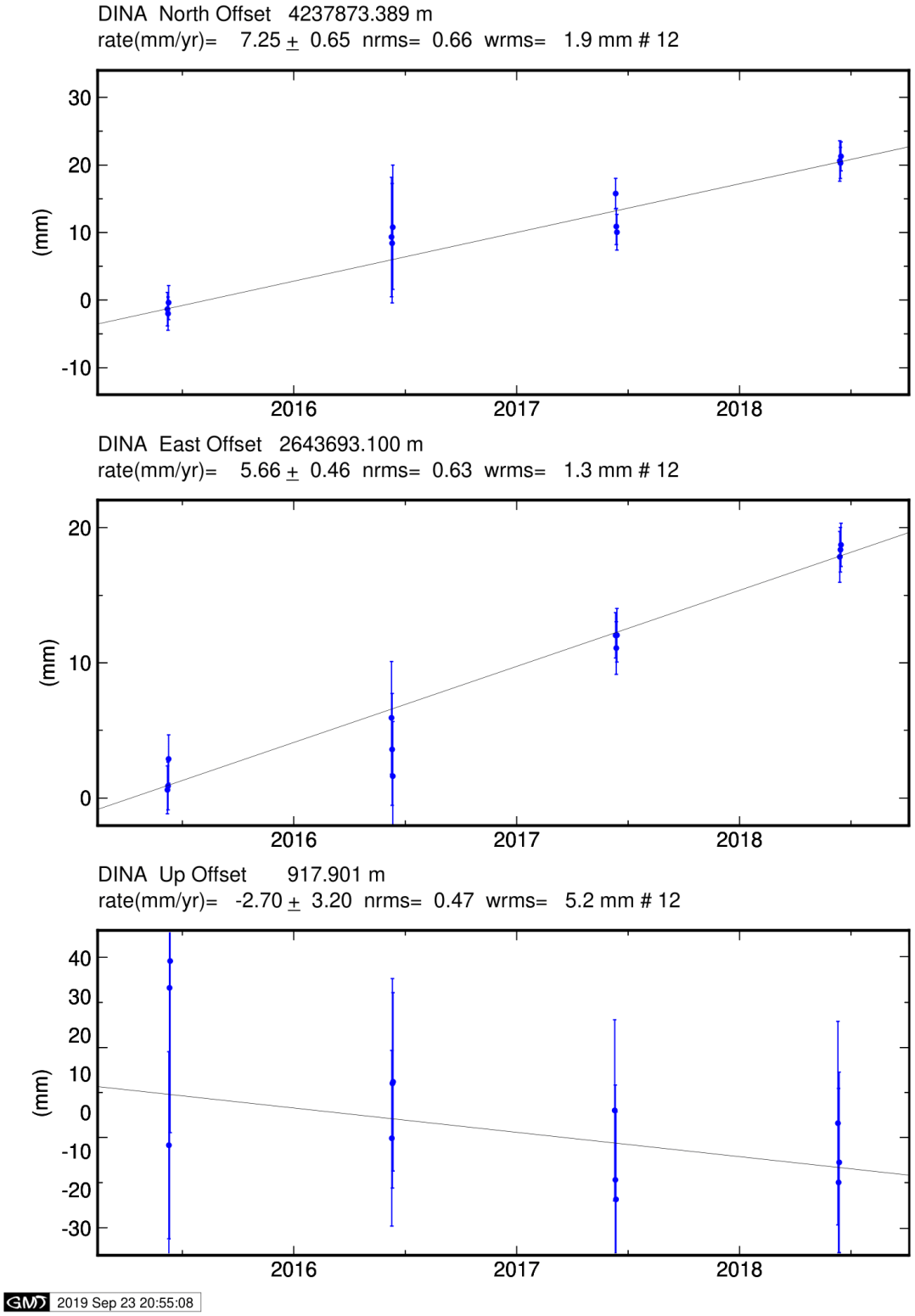


Figure D.8. DINA station coordinate-time series.

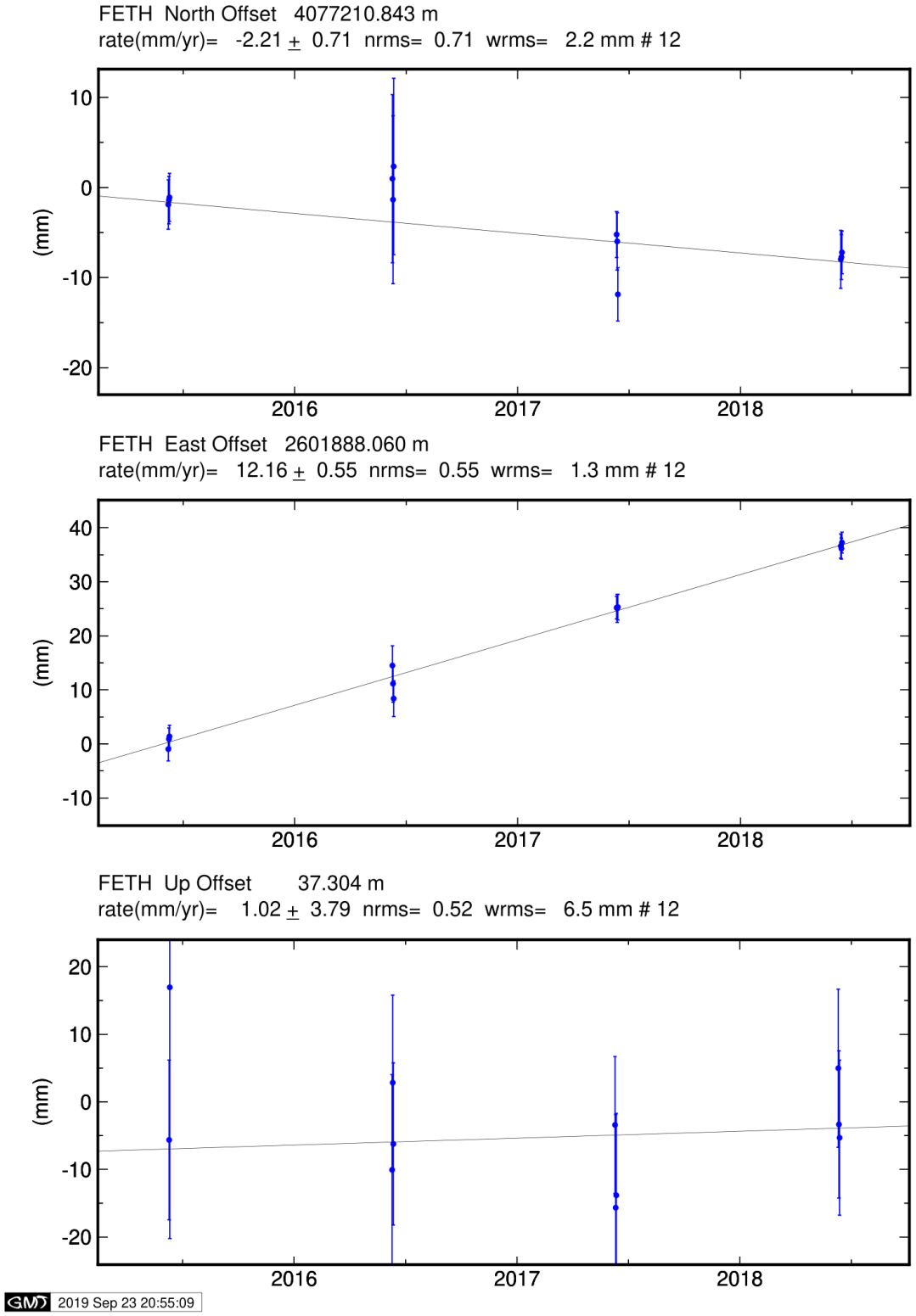


Figure D.9. FETH station coordinate-time series.

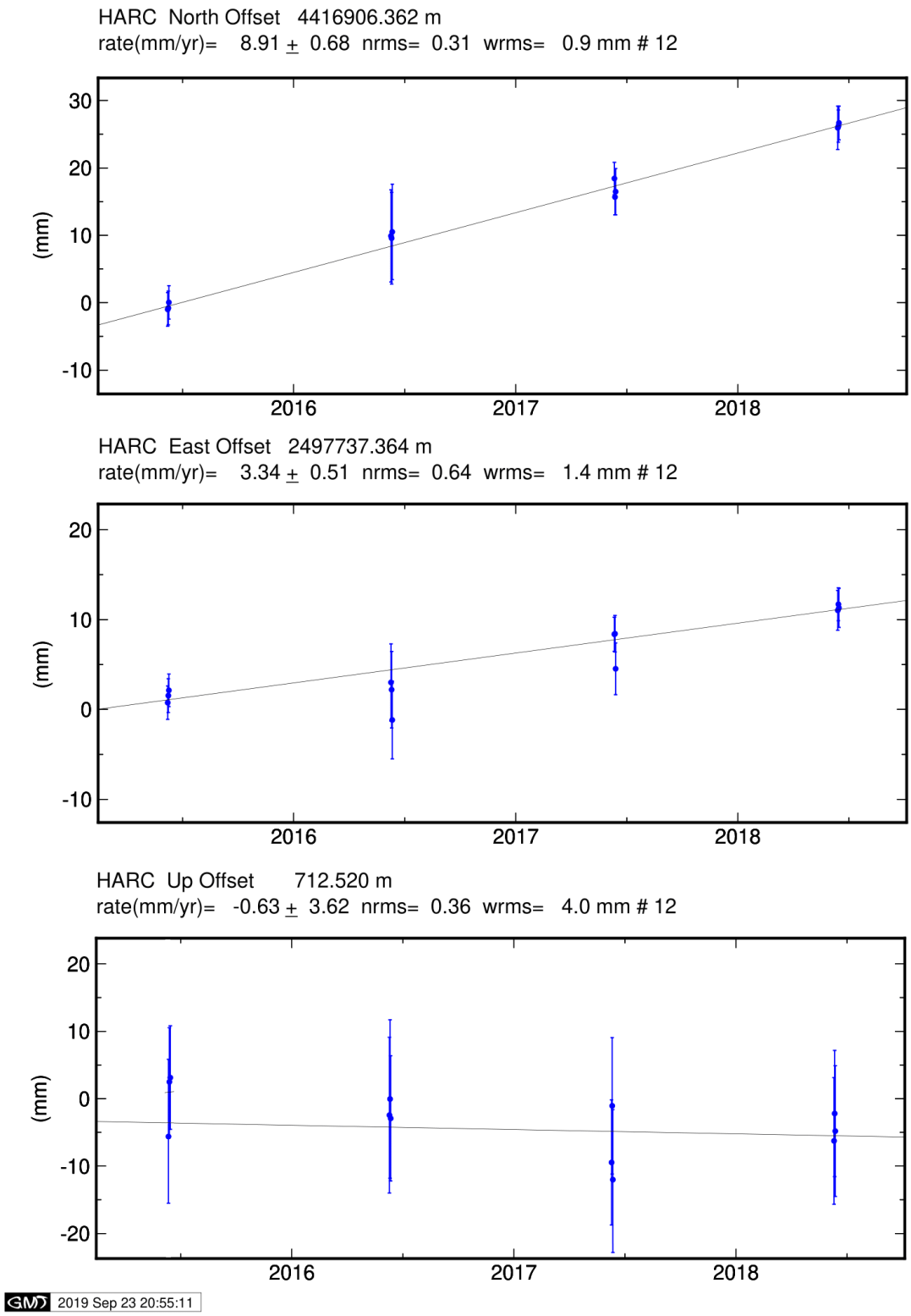


Figure D.10. HARC station coordinate-time series.

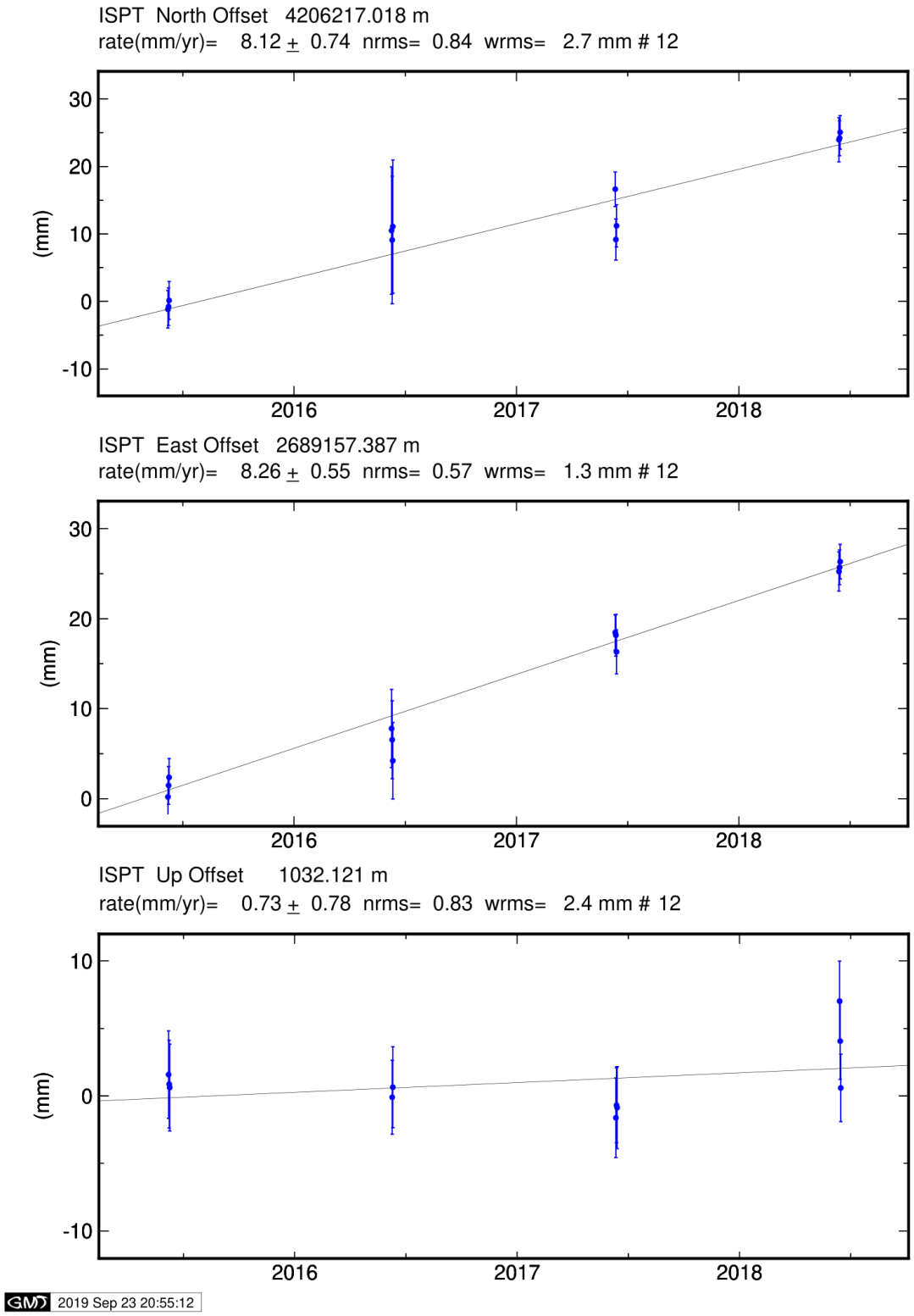


Figure D.11. ISPT station coordinate-time series.

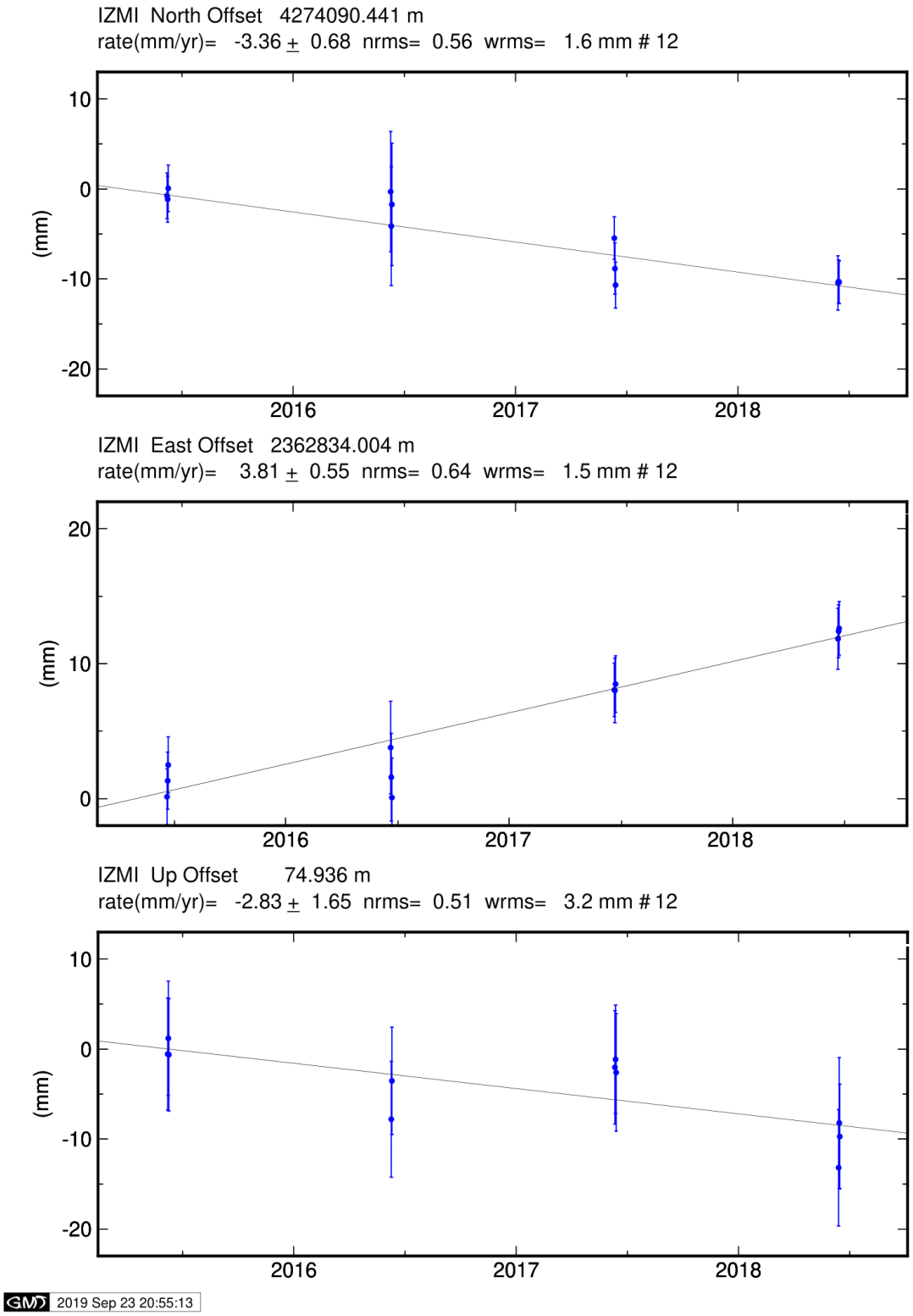


Figure D.12. IZMI station coordinate-time series.

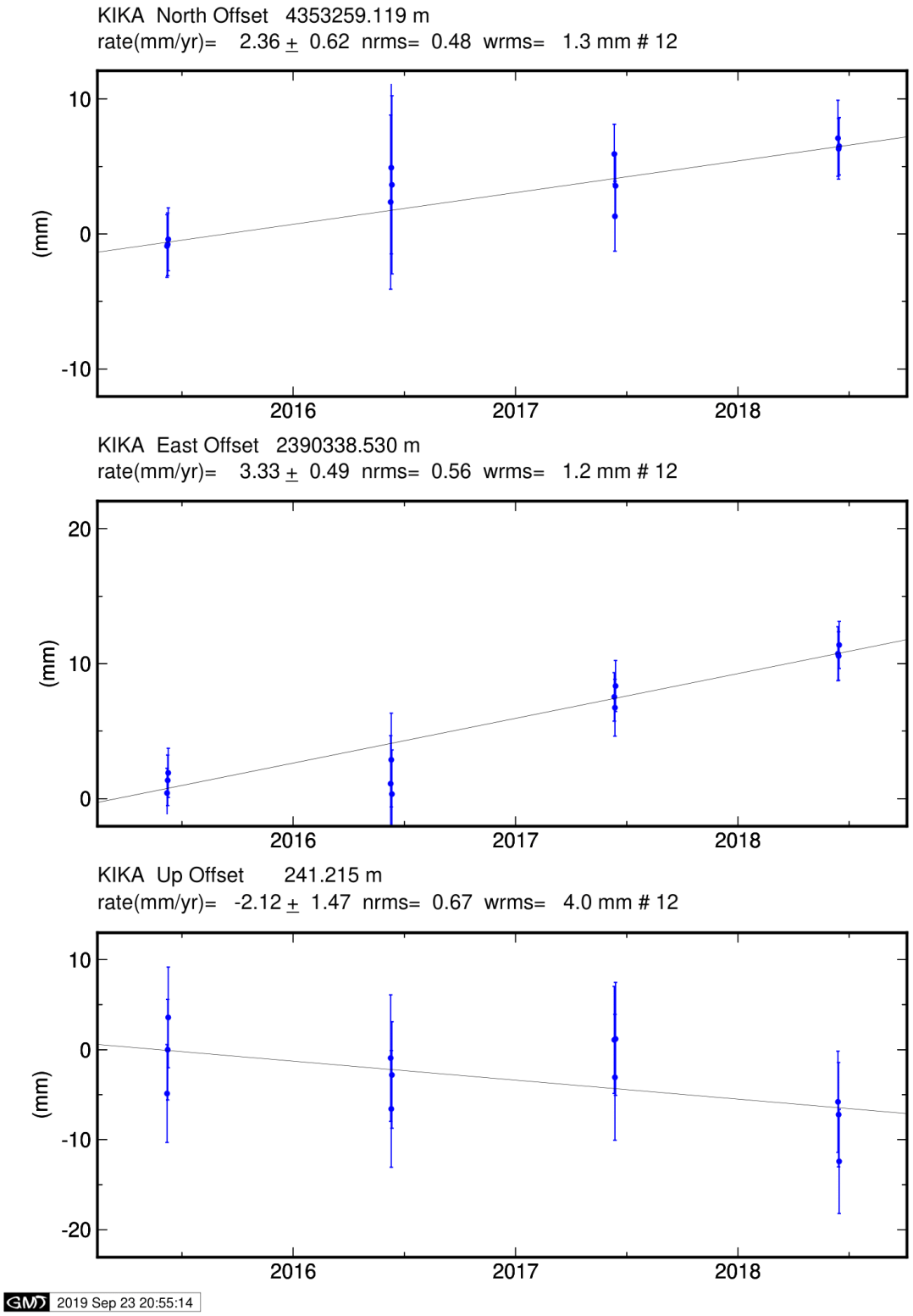


Figure D.13. KIKA station coordinate-time series.

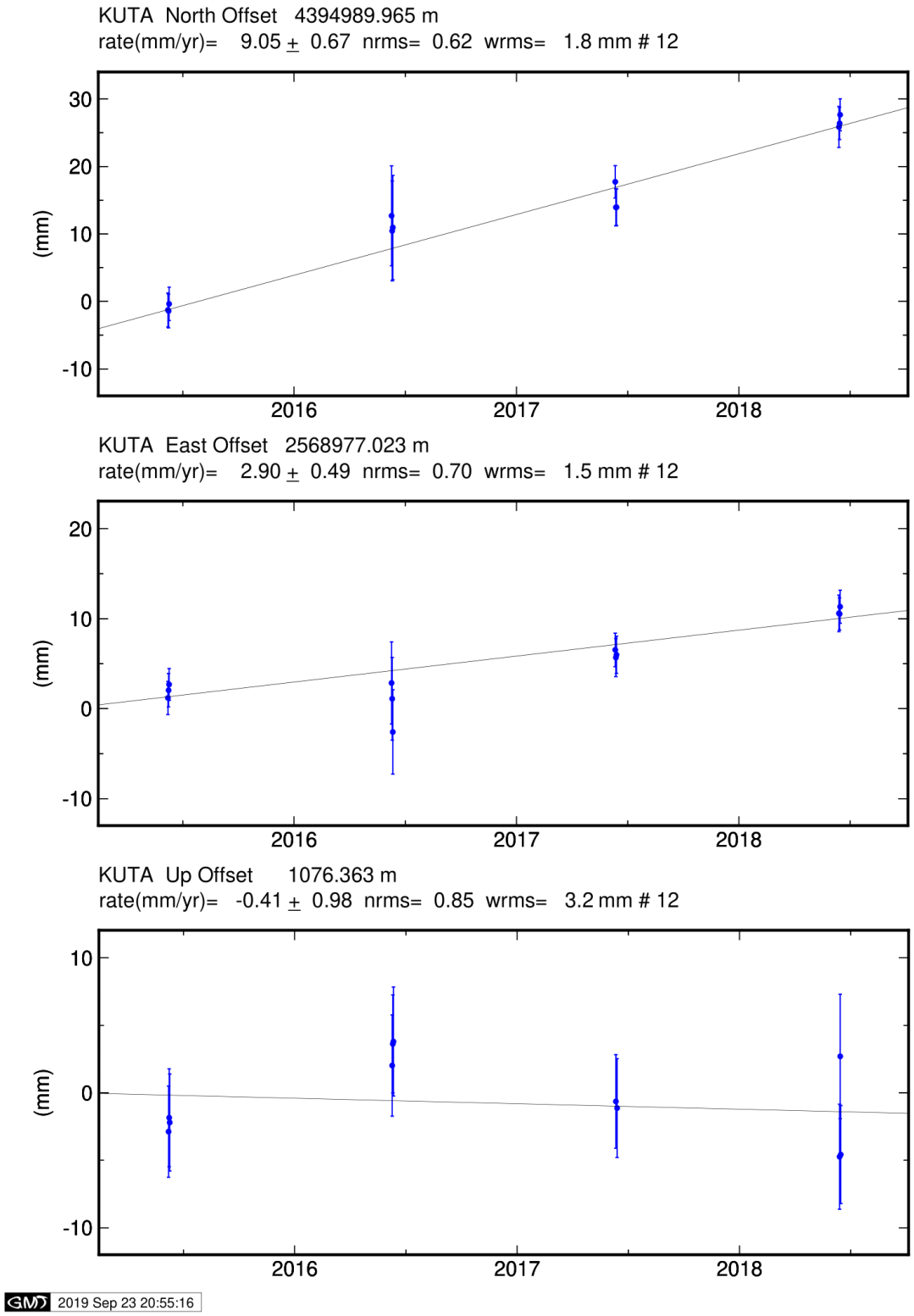


Figure D.14. KUTA station coordinate-time series.

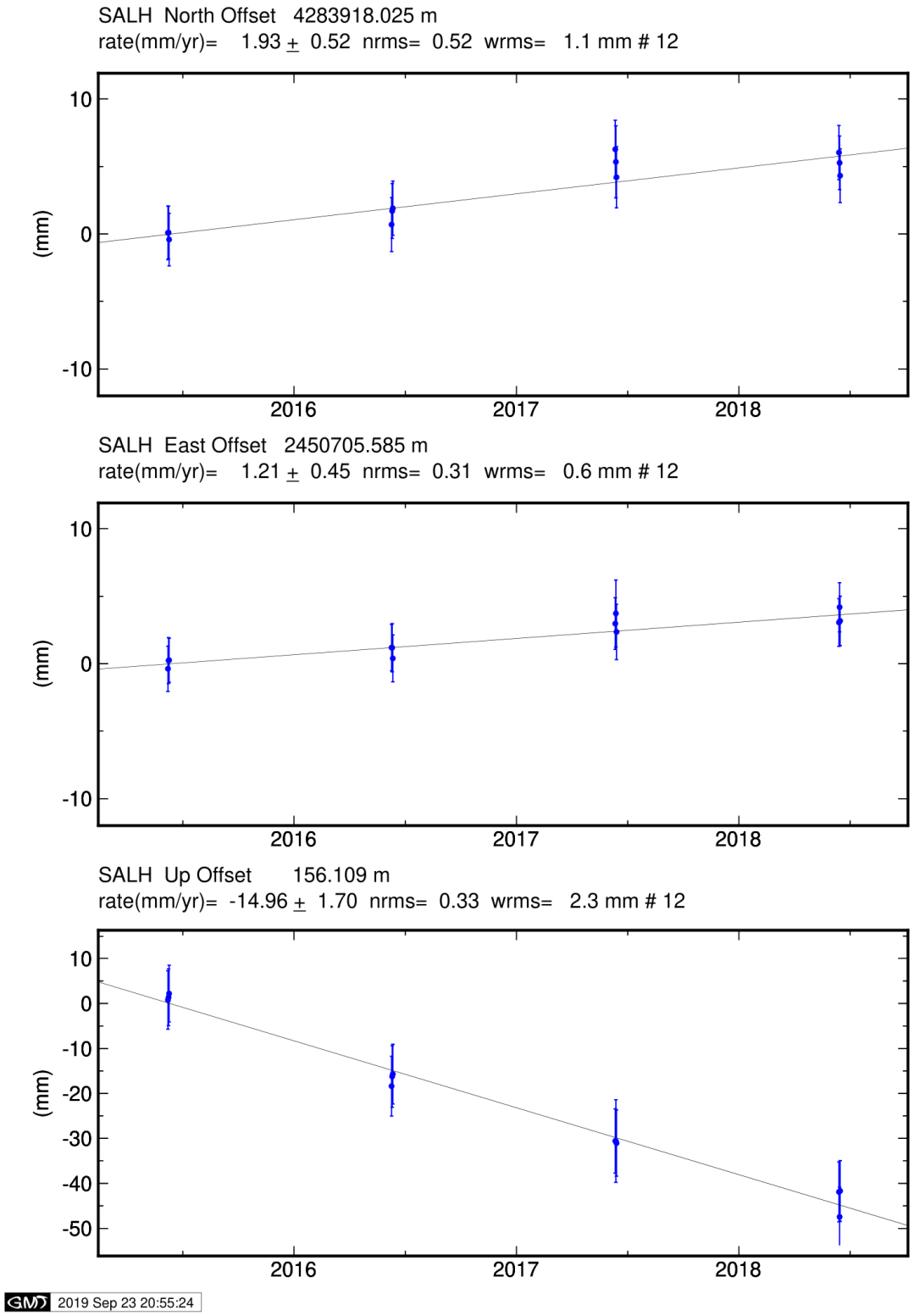


Figure D.15. SALH station coordinate-time series.

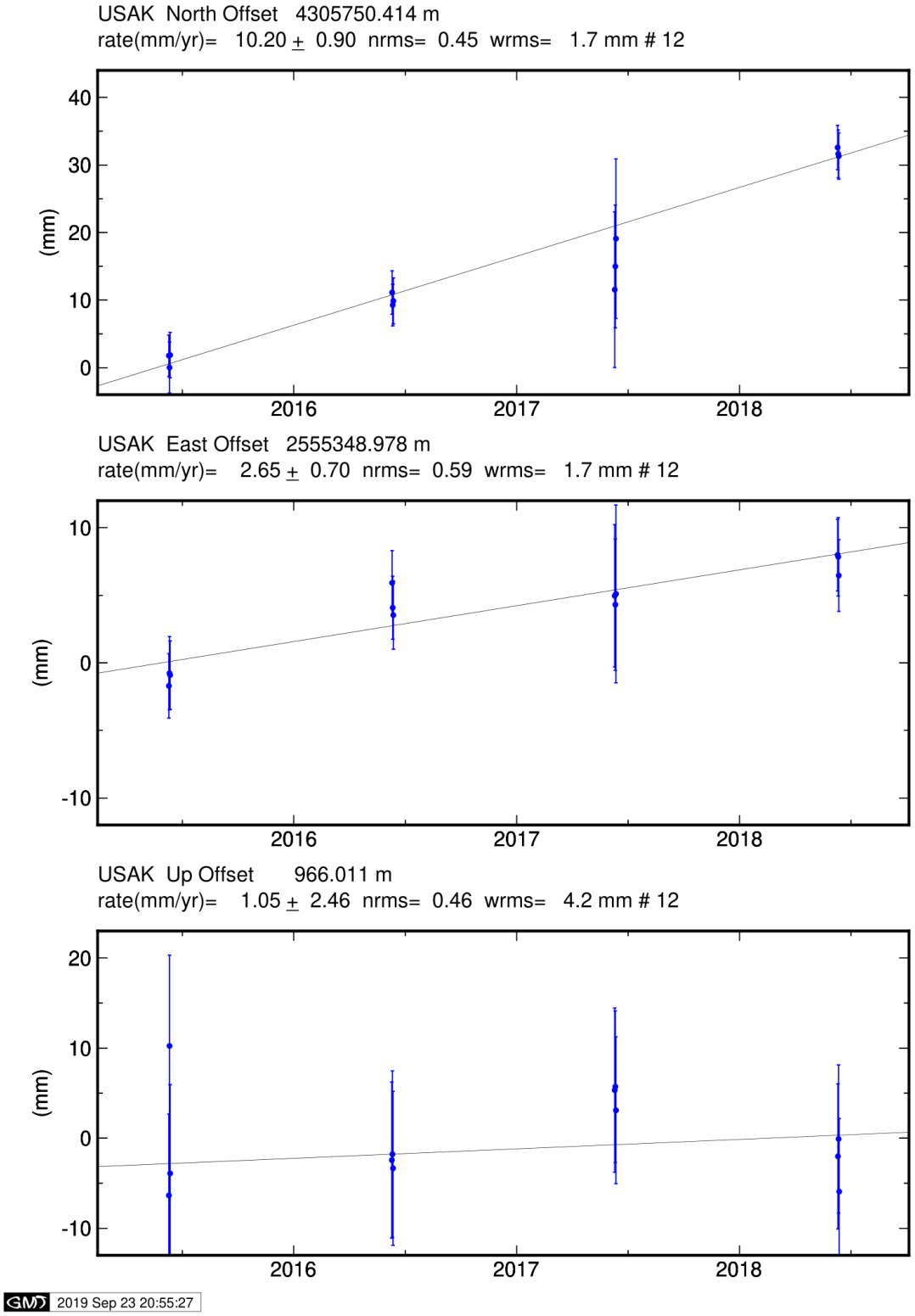


Figure D.16. USAK station coordinate-time series.